

Stochastic Processes with Modified Lognormal Distribution Featuring Flexible Upper Tail

Dionissios T. Hristopoulos *Senior Member, IEEE* and Anastassia Baxevani and Giorgio Kaniadakis

Abstract

Asymmetric, non-Gaussian probability distributions are often observed in the analysis of natural and engineering datasets. The lognormal distribution is a standard model for data with skewed frequency histograms and fat tails. However, the lognormal law severely restricts the asymptotic dependence of the probability density and the hazard function for high values. Herein we present a family of three-parameter non-Gaussian probability density functions that are based on generalized κ -exponential and κ -logarithm functions and investigate its mathematical properties. These κ -lognormal densities represent continuous deformations of the lognormal with lighter right tails, controlled by the parameter κ . In addition, bimodal distributions are obtained for certain parameter combinations. We derive closed-form analytic expressions for the main statistical functions of the κ -lognormal distribution. For the moments, we derive bounds that are based on hypergeometric functions as well as series expansions. Explicit expressions for the gradient and Hessian of the negative log-likelihood are obtained to facilitate numerical maximum-likelihood estimates of the κ -lognormal parameters from data. We also formulate a joint probability density function for κ -lognormal stochastic processes by applying Jacobi's multivariate theorem to a latent Gaussian process. Estimation of the κ -lognormal distribution based on synthetic and real data is explored. Furthermore, we investigate applications of κ -lognormal processes with different covariance kernels in time series forecasting and spatial interpolation using warped Gaussian process regression. Our results are of practical interest for modeling skewed distributions in various scientific and engineering fields.

Index Terms

stochastic processes, asymmetric probability distribution, hazard function, Gaussian process regression, warped Gaussian process, stochastic oscillator kernel

I. INTRODUCTION

THE Gaussian (normal) distribution is one of the most popular models in science. It is used for point-like random variables, for stochastic processes that exhibit temporal dependence [1], and for spatially extended processes [2], [5]. It is also widely used in machine learning, as for example in the Gaussian process regression framework [4], [5]. Despite the dominant role of the Gaussian model, data often display skewed probability distributions with heavy tails [6]. Such distributions can assign considerably higher probabilities than the Gaussian law for large deviations from the mean. A paradigmatic heavy-tailed distribution is the lognormal model [7].

The lognormal distribution is ubiquitous in natural and engineered processes. It is used to model intermittent energy dissipation in fluid turbulence [8]–[11] and the distribution of local stiffness in living cells [12]; it finds applications in mining [13]–[16], geology [17], hydrology [18], [19], geochemistry [20], lifetime analysis of electronic components [21] and wireless communications [22]–[24]. The lognormal is used to model the distribution of permeability [25]–[29] and fluid velocity [30] in porous media, particle size distributions in coagulation-free vapor growth processes [31], and the distribution of matter in the universe [32]–[34]. It is also a candidate distribution for earthquake recurrence times [35]–[38], and it is employed in pharmacokinetics due to its ability to model asymmetry and positive skewness [39]. As emphasized in [40], the lognormal distribution is crucial in the description of brain processes, reflecting the fact that in highly interconnected systems operations tend to be multiplicative rather than additive. Finally, the lognormal is used to model heteroskedastic stochastic processes, because it captures variance changes over time, as for example, in the well-known Black-Scholes-Merton model [41], [42]. Theoretical generative models for the lognormal distribution are reviewed in [7], [43]–[45]. The impact of the lognormal's upper (right) tail on extreme events is discussed in [46].

The upper tail of the lognormal may be too “heavy” for certain applications. This happens if the tail assigns unrealistically high probabilities to large values of the process. In such cases, truncated lognormal models are used [47], [48]. For example, the Kolmogorov-Avrami-Mehl-Johnson crystallization model of random nucleation and growth exhibits a grain size distribution which evolves into a truncated lognormal form for specific nucleation and growth rates [49]. A shorter-than-lognormal tail was also observed in ecological population abundance data [50], [51]. The pore size distribution of hydrated cement paste exhibits a lighter-than-lognormal right tail, due to an upper limit of the particle size [52]. Geochemical data also show evidence of a lighter-than-lognormal tail [20]. Finally, the lognormal model has an asymptotically declining hazard rate which is a potential shortcoming for failure time analysis.

D. T. Hristopoulos is with the School of Electrical and Computer Engineering, Technical University of Crete, Chania 73100, Greece (e-mail: dchristopoulos@tuc.gr).

Anastassia Baxevani is with the Department of Mathematics and Statistics, University of Cyprus, Nicosia, Cyprus (e-mail: baxevani@ucy.ac.cy)

Giorgio Kaniadakis is with the Department of Applied Science and Technology, Politecnico di Torino, 10129 Turin, Italy (e-mail: giorgio.kaniadakis@polito.it)

The above considerations motivate the need for asymmetric, right-skewed probability distributions with a flexible right tail which is lighter than the lognormal tail. Such a distribution model optimally should continuously deform into the natural lognormal model by controlling a deformation parameter. This paper pursues this quest by exploiting the Kaniadakis deformation of the exponential and logarithmic functions to introduce the κ -lognormal probability model. The latter is shown to incorporate the natural lognormal as well as asymmetric distributions with lighter tails; it also closely approximates the normal distribution for certain parameter combinations, while in certain regions of the parametric space it leads to bimodal distributions. We discuss the mathematical properties of the κ -lognormal marginal distribution (including the statistical moments and the hazard rate) and their dependence on the parameter κ . We formulate κ -lognormal stochastic processes based on Jacobi's multivariate theorem and the κ -exponential transformation. Predictive equations in the framework of *warped Gaussian processes*, suitable for κ -lognormal processes, are also formulated; these are used for time series forecasting and spatial interpolation.

The remainder of this paper has the following structure: Section II presents necessary notation and definitions, the main properties of modified exponential and logarithm functions, as well as a short review of the lognormal distribution and associated stochastic process. In Section III we derive the κ -lognormal distribution and its main statistical functions. We also present bounds and a power-series expansion for the statistical moments. In addition, we derive the hazard rate of the κ -lognormal and investigate its asymptotic behavior. In Section IV we introduce the κ -lognormal stochastic process in terms of the joint probability density function. We also formulate predictive equations by focusing on warped Gaussian process regression. We formulate maximum likelihood estimation for the κ -lognormal distribution in Section V. In Section VI we study applications related to the estimation of the probability model, time series forecasting, and spatial regression using simulated and real datasets. Finally, Section VII presents a brief discussion of the results and some open questions. Longer proofs are relegated to the Appendix, and additional information is presented in the Supplement.

II. METHODOLOGICAL BACKGROUND

In this section, we introduce notation and review the main mathematical properties of lognormal stochastic processes, as well as the κ -exponential and κ -logarithmic functions. We also present new results regarding the dependence of the κ -modified functions on κ (cf. Propositions 1, 2, and 3). Certain useful properties of the κ -exponential and κ -logarithm that are not used herein are given in the Supplement (Section 1).

A. Notation

- 1) Vector and matrix quantities will be denoted by boldface font, e.g., \mathbf{A} . The superscript \top , e.g., \mathbf{A}^\top , denotes the transpose of the vector or matrix \mathbf{A} .
- 2) \mathbb{R} denotes the set of real numbers and \mathbb{N} the set of positive integers; $\mathbf{s} \in \mathcal{D} \subset \mathbb{R}^d$ denotes a vector in a d -dimensional feature space where $d \in \mathbb{N}$.
- 3) $\mathcal{N}(\mu, \sigma^2)$ denotes the normal distribution with mean μ and variance σ^2 ; $Y(\vartheta) \stackrel{d}{=} \mathcal{N}(\mu, \sigma^2)$ means that the random variable $Y(\vartheta)$ follows the normal distribution with mean μ and variance σ^2 . $\phi(\cdot)$ and $\Phi(\cdot)$ denote the probability density and the cumulative distribution functions of a standard normal distribution respectively.
- 4) $\text{LN}(\mu, \sigma)$ denotes the lognormal distribution with parameters $\mu \in \mathbb{R}$ and $\sigma > 0$, and $\kappa\text{LN}(\mu, \sigma, \kappa)$, where $\kappa \geq 0$, the κ -lognormal distribution.
- 5) The symbol \triangleq is used to define mathematical entities.
- 6) $X(\mathbf{s}; \vartheta)$, $Y(\mathbf{s}; \vartheta)$ represent random variables defined over a probability space (Ω, \mathcal{F}, P) indexed by \mathbf{s} , where $\vartheta \in \Omega$ is the state index in the sample space Ω , \mathcal{F} is a σ -algebra of events, and P is the probability measure for these events [1], [6], [53].
- 7) $\mathcal{X} = \{X(\mathbf{s}; \vartheta), \mathbf{s} \in \mathcal{D}, \vartheta \in \Omega\}$ and $\mathcal{Y} = \{Y(\mathbf{s}; \vartheta), \mathbf{s} \in \mathcal{D}, \vartheta \in \Omega\}$ represent stochastic processes with the index $\mathbf{s} \in \mathcal{D}$. In the following, we will use for brevity $X(\mathbf{s}; \vartheta)$ and $Y(\mathbf{s}; \vartheta)$ to refer to the stochastic processes \mathcal{X} and \mathcal{Y} respectively as well as the corresponding random variables.
- 8) The expectation operator over the probability space is denoted by $\mathbb{E}[\cdot]$.
- 9) The vector $\mathbf{x}_S \triangleq (x_1, \dots, x_N)^\top$ denotes sample values of $X(\mathbf{s}; \vartheta)$ for the respective sampled features $\mathbb{S}_N = \{\mathbf{s}_1, \dots, \mathbf{s}_N\}$, where $\mathbf{s}_i \in \mathcal{D} \subset \mathbb{R}^d$, $i = 1, \dots, N$. In real-world scenarios, the sampled values involve a noise term. For simplicity, we will assume Gaussian white noise $\epsilon_i \stackrel{d}{=} \mathcal{N}(0, \sigma_\epsilon^2)$.
- 10) The symbol $\ln(\cdot)$ denotes the natural logarithm, while $\text{erf}(\cdot)$ is the error function defined as $\text{erf}(z) = \frac{2}{\sqrt{\pi}} \int_0^z e^{-t^2} dt$.
- 11) The symbols $\exp_\kappa(\cdot)$ and $\ln_\kappa(\cdot)$ will be used for the modified exponential and logarithmic functions respectively. If the deformation factor κ is viewed as a parameter, the total derivative $d\exp_\kappa(x)/dx$ will be used. To study the dependence of κ -modified functions on κ , partial derivatives, namely, $\partial \exp_\kappa(x)/\partial x$ and $\partial \exp_\kappa(x)/\partial \kappa$ will be used.
- 12) Sample-based averages will be denoted by the overline symbol, for example, \bar{x} is the sample mean. Sample-based estimates of a distribution parameter θ will be denoted by $\hat{\theta}$.

The following two sections focus on the definitions and most relevant properties of the κ -exponential and the κ -logarithm. The mathematical properties of the κ -exponential and the κ -logarithm are thoroughly studied in [55].

B. The κ -Exponential Function

The base of the exponential function is the Euler number e which can be defined as the limit

$$e = \lim_{n \rightarrow \infty} \left(1 + \frac{1}{n}\right)^n.$$

Therefore, the natural exponential function $\exp(y)$, $y \in \mathbb{R}$, corresponds to the limit

$$\exp(y) = \lim_{n \rightarrow \infty} \left(1 + \frac{y}{n}\right)^n, \text{ where } n \in \mathbb{N}. \quad (1)$$

The Kaniadakis κ -exponential is defined by means of the expression [56], [57]

$$\exp_\kappa(y) \triangleq \left(\sqrt{1 + \kappa^2 y^2} + y\kappa\right)^{1/\kappa}, \quad (2)$$

with $0 \leq \kappa < 1$ and $y \in \mathbb{R}$. The function (2) emerges naturally within the framework of special relativity, where the deformation factor κ is proportional to the reciprocal light speed [58]. In that context, $\exp_\kappa(y)$ is the relativistic generalization of $\exp(y)$. Herein we take an agnostic viewpoint and consider (2) as a mathematical generalization of $\exp(y)$.

By replacing $1/\kappa$ with n and realizing that at the limit $\kappa \rightarrow 0$ ($n \rightarrow \infty$), $1 + \kappa^2 y^2 \approx 1$, it follows that the $\kappa \rightarrow 0$ limit of the modified exponential (2) is the same as the $n \rightarrow \infty$ limit in (1). The κ -exponential function is visually compared to the natural exponential in Fig. 1. While in the relativistic theory the constraint $0 \leq \kappa < 1$ makes sense (strictly speaking, $-1 < \kappa < 1$), mathematically the κ -exponential (2) and other κ -modified functions can be defined for $\kappa > 1$. Herein, we thus focus on $\kappa \geq 0$. A Taylor series expansion of $\exp_\kappa(y)$ around $y = 0$ is available [1]. We elaborate on this expansion in the Supplement (Section 1).

a) Asymptotic behavior: The function $\exp_\kappa(y)$ exhibits *power-law* asymptotic behavior as $y \rightarrow \infty$ [1], [57]:

$$\exp_\kappa(y) \sim |2\kappa y|^{\pm 1/\kappa}, \text{ as } y \rightarrow \pm\infty. \quad (3)$$

In light of the above, the κ -exponential $\exp_\kappa(-y)$ exhibits a *heavy right tail* for $y \rightarrow +\infty$, i.e.

$$\exp_\kappa(-y) \sim (2\kappa y)^{-1/\kappa}, \text{ as } y \rightarrow \infty. \quad (4)$$

Hence, $\exp_\kappa(-y)$ can be used to model probability distributions with high probability density (power law) in the tail.

b) Monotonicity and convexity: The κ -exponential is continuously differentiable with respect to y . Its derivatives are proportional to $\exp_\kappa(y)$, but they also involve a modifying factor that depends on κ and y and vanishes at $\kappa = 0$. The first two derivatives are given by the following expressions

$$\frac{d \exp_\kappa(y)}{d y} = \frac{\exp_\kappa(y)}{\sqrt{1 + (\kappa y)^2}}, \quad (5)$$

$$\frac{d^2 \exp_\kappa(y)}{d y^2} = \exp_\kappa(y) \frac{\sqrt{1 + \kappa^2 y^2} - \kappa^2 y}{(1 + \kappa^2 y^2)^{3/2}}. \quad (6)$$

It follows from (5) that the first derivative is nonnegative for all $y \in \mathbb{R}$. Hence, the κ -exponential is a monotonically increasing function of y for fixed κ . Since $\exp_\kappa(y)$ and the denominator in (6) are nonnegative for all $y \in \mathbb{R}$, it is easy to see that the κ -exponential is a convex function of y for all $\kappa \in [0, 1]$. The numerator $\sqrt{1 + \kappa^2 y^2} - \kappa^2 y$ is clearly positive for $y < 0$, while for $y > 0$ it is enough to observe that $1 + (\kappa y)^2 - \kappa^4 y^2 = 1 + \kappa^2 y^2(1 - \kappa^2) > 0$ for all $\kappa \in [0, 1]$.

Proposition 1 (Bounds of κ -exponential): The κ -exponential decreases monotonically as a function of $\kappa \geq 0$ for $y \geq 0$ and increases monotonically as function of $\kappa \geq 0$ for $y < 0$. Thus, $\exp(y) \leq \exp_\kappa(y)$ for $y < 0$ and $\exp(y) \geq \exp_\kappa(y)$ for $y \geq 0$ for all $\kappa \geq 0$.

Proof: Viewing $\exp_\kappa(y)$ as a function of both y and κ , its partial derivative with respect to κ is given by

$$\frac{\partial \exp_\kappa(y)}{\partial \kappa} = \frac{g(\kappa y) \exp_\kappa(y)}{\kappa^2 \sqrt{1 + \kappa^2 y^2}}, \quad (7)$$

$$g(\kappa y) = -\sqrt{1 + \kappa^2 y^2} \ln \left(\sqrt{1 + \kappa^2 y^2} + y\kappa \right) + \kappa y. \quad (8)$$

The denominator of the κ -exponential's partial derivative is positive for all $y \in \mathbb{R}$ and $\kappa > 0$. The sign of the partial derivative $\partial \exp_\kappa(y)/\partial \kappa$ is determined by the sign of $g(\kappa y)$. To find the latter, consider that $\partial g(\kappa y)/\partial y$ is given by

$$\frac{\partial g(\kappa y)}{\partial y} = -\frac{\ln(\sqrt{1 + \kappa^2 y^2} + y\kappa) y \kappa^2}{\sqrt{1 + \kappa^2 y^2}}.$$

For $y > 0$ it holds that $\sqrt{1 + \kappa^2 y^2} + \kappa y > 1$, the logarithm of the above is positive, and thus $\partial g(\kappa y)/\partial y$ is negative for $y > 0$. For $y < 0$, since $\sqrt{1 + \kappa^2 y^2} < 1 + |y|\kappa$, it also holds that $y \ln(\sqrt{1 + \kappa^2 y^2} + \kappa y) > 0$ since the argument of the logarithm is less than one. Hence, $\frac{\partial g(\kappa y)}{\partial y} < 0$ for $y < 0$ as well. Finally, for $y = 0$ it holds that $\frac{\partial g(\kappa y)}{\partial y} = 0$. Therefore, $g(\kappa y)$ is a monotonically decreasing function for all $y \in \mathbb{R}$ and $\kappa > 0$.

The monotonic decline of $g(\cdot)$, together with the fact that $g(0) = 0$, implies that $g(\cdot)$ takes negative (positive) values for $y > 0$ ($y < 0$). Since the sign of $\partial \exp_\kappa(y)/\partial \kappa$ is controlled by $g(\kappa y)$ according to (7), it holds that $\partial \exp_\kappa(y)/\partial \kappa < 0$ for any $y \geq 0$ and $\kappa > 0$ while $\partial \exp_\kappa(y)/\partial \kappa > 0$ for any $y < 0$ and $\kappa > 0$.

At $\kappa = 0$, the derivative (7) vanishes—as can be shown by applying de l'Hospital's rule and noticing that the leading-order term of the Taylor expansion for $g(\kappa y)$ around $\kappa = 0$ is proportional to κ^3 . Thus, $\exp(y)$ provides an upper bound of the κ -exponential for $y \geq 0$. For $y < 0$ the fact that $g(\kappa y) > 0$ implies that $\exp_\kappa(y)$ is an increasing function of κ ; thus, $\exp(y) \leq \exp_\kappa(y)$ for $y < 0$ and the exponential provides a lower bound of $\exp_\kappa(y)$. ■

The exponential upper bound of the κ -exponential is illustrated in Fig. 1.

C. The κ -Logarithm Function

The inverse of the κ -exponential is the κ -logarithm [1], defined by the following function for $x > 0$:

$$\ln_\kappa(x) \triangleq \frac{x^\kappa - x^{-\kappa}}{2\kappa}, \quad \kappa > 0. \quad (9)$$

The κ -logarithm function is compared to the natural logarithm in Fig. 2.

The κ -logarithm can be used to normalize skewed, non-negative data by means of the transformation $x \mapsto y \triangleq \ln_\kappa(x)$. The κ -logarithm transform is similar to the well-known Box-Cox transform $x \mapsto y \triangleq (x^\lambda - 1)/\lambda$ [60]. Both the Box-Cox and the κ logarithm yield the logarithmic transformation at the respective limits $\lambda \rightarrow 0$ and $\kappa \rightarrow 0$. However, the inverse of the κ -logarithm is the κ -exponential $y \mapsto x \triangleq \exp_\kappa(y)$ which is stable even for $y < 0$ as evidenced in (2). In contrast, the inverse Box-Cox transform $y \mapsto x \triangleq (\lambda y + 1)^{1/\lambda}$ fails for $\lambda y + 1 < 0$ [61].

a) Taylor expansion: It follows from (9) that as $x \rightarrow 0$, $\ln_\kappa(x) \rightarrow -\infty$ just as the natural logarithm. It is also straightforward to see—by writing $x^\kappa = \exp(\kappa \ln(x))$ and using the Taylor series expansion of the exponential—that $\lim_{\kappa \rightarrow 0} \ln_\kappa(x) = \ln(x)$. In particular, the small- κ expansion of (9) yields

$$\ln_\kappa(x) = \ln(x) + \frac{1}{6} \kappa^2 \ln(x)^3 + \frac{1}{120} \kappa^4 \ln(x)^5 + \mathcal{O}(\kappa^6). \quad (10)$$

Hence, the above expansion recovers the natural logarithm for $\kappa = 0$. According to expansion (10), $\ln_\kappa(x) \leq \ln(x)$ for $x \leq 1$ and $\ln_\kappa(x) > \ln(x)$ for $x > 1$. Hence, the difference $\ln_\kappa(x) - \ln(x)$ changes sign at $x = 1$ as evidenced in Fig. 2.

b) Asymptotic behavior: For $\kappa > 0$, it follows that

$$\ln_\kappa(x) \sim x^\kappa/(2\kappa), \text{ as } x \rightarrow \pm\infty. \quad (11)$$

c) Monotonicity of κ -logarithm with respect to κ : Partial derivatives are introduced here to consider variations of $\ln_\kappa(x)$ with respect to both x and κ . The derivative of $\ln_\kappa(x)$ with respect to κ is given by

$$\frac{\partial \ln_\kappa(x)}{\partial \kappa} = \ln(x) \frac{x^\kappa + x^{-\kappa}}{2\kappa} - \frac{\ln_\kappa(x)}{\kappa}. \quad (12)$$

$$\frac{\partial \ln_\kappa(x)}{\partial x} = \frac{1}{2x} (x^\kappa + x^{-\kappa}), \quad (13)$$

$$\frac{\partial^2 \ln_\kappa(x)}{\partial x^2} = \frac{(\kappa - 1)x^\kappa - (\kappa + 1)x^{-\kappa}}{2x^2}. \quad (14)$$

Note that $\partial \ln_\kappa(x)/\partial x > 0$ for all $x \geq 0$ and $\kappa > 0$, and thus the κ -logarithm is a monotonically increasing function.

Proposition 2 (κ -logarithm increases faster than the natural logarithm): (i) The κ -logarithm defined by (9) increases faster than the natural logarithm for all $x > 0$. (ii) The rate difference $d_{\ln}(x, \kappa) \triangleq \frac{\partial \ln_\kappa(x)}{\partial x} - \frac{d \ln(x)}{dx}$ increases with increasing κ , indicating a faster increase of the κ -logarithm with x for higher κ .

Proof: (i) We need to show that $\frac{\partial \ln_\kappa(x)}{\partial x} > \frac{d \ln(x)}{dx}$ for all $x > 0$. Since $d \ln(x)/dx = 1/x$, the above is equivalent to $x^\kappa + x^{-\kappa} > 2$ for $x > 0$. Defining $z \triangleq x^\kappa$, it suffices to show that $z + 1/z > 2$; since $z > 0$, this is equivalent to $z^2 - 2z + 1 = (z - 1)^2 > 0$ which is true for all $z \in \mathbb{R}$ (and thus for $z > 0$).

(ii) The κ -derivative of the rate difference, $\frac{\partial d_{\ln}(x, \kappa)}{\partial \kappa} = \frac{\partial^2 \ln_\kappa(x)}{\partial x \partial \kappa} = \frac{\ln(x)}{2x} (x^\kappa - x^{-\kappa})$, is nonnegative for all $x > 0$: for $0 < x < 1$ both $\ln(x)$ and $x^\kappa - x^{-\kappa}$ are negative, while both functions are positive for $x > 1$. ■

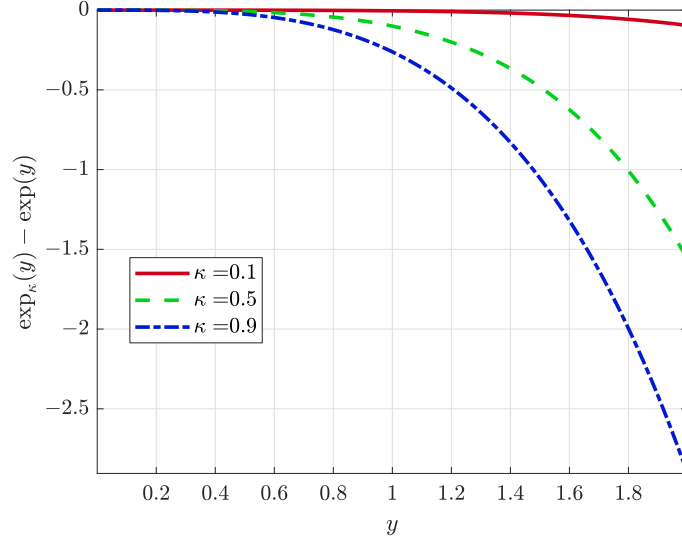


Fig. 1. Plots of the difference $\exp_\kappa(x) - \exp(x)$ for $\kappa = 0.1, 0.5, 0.9$ based on the κ -exponential definition (2) for $x \geq 0$, which confirm that the natural exponential is the upper bound of the κ -exponential, namely $\exp(x) \geq \exp_\kappa(x)$, for $x \geq 0$ (cf. Proposition 1). For $x < 0$ (not shown) the sign of the difference is reversed, that is, $\exp_\kappa(x) \geq \exp(x)$, and the natural exponential is a lower bound of the κ -exponential.

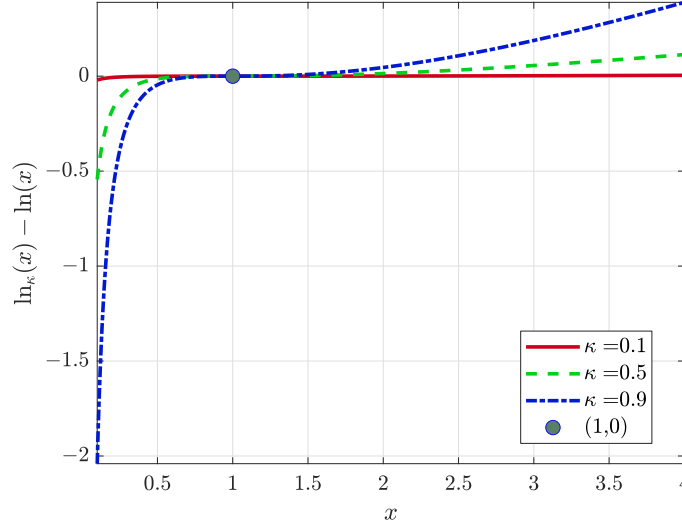


Fig. 2. Plots of the difference $\exp_\kappa(y) - \exp(y)$ for $\kappa = 0.1, 0.5, 0.9$ based on the κ -exponential definition (2) for $y \geq 0$, which confirm that the natural exponential is the upper bound of the κ -exponential, namely $\exp(y) \geq \exp_\kappa(y)$, for $y \geq 0$ (cf. Proposition 1). For $y < 0$ (not shown) the sign of the difference is reversed, that is, $\exp_\kappa(y) \geq \exp(y)$, and the natural exponential is a lower bound of the κ -exponential.

Proposition 3 (κ -logarithm convexity): (i) For $0 \leq \kappa \leq 1$, the κ -logarithm is concave for all $x > 0$. (ii) For $\kappa > 1$ the κ -logarithm is concave for $0 < x < x_+$ and convex for $x > x_+$ where $x_+ \triangleq \left(\frac{\kappa+1}{\kappa-1}\right)^{1/2\kappa}$ is a κ -dependent *inflection point*.

Proof: (i) By inspection of (14), it follows that the second derivative $\frac{\partial^2 \ln_\kappa(x)}{\partial x^2}$ is negative for $\kappa \in [0, 1]$ and $x > 0$, which implies that $\ln_\kappa(x)$ is *concave*.

(ii) For $\kappa > 1$, the zeros of the second-order derivative (14) are determined by the zeros of the function $g(z) \triangleq (\kappa - 1)z - (\kappa + 1)z^{-1}$ which represents the numerator of the fraction, where $z \triangleq x^\kappa > 0$. The zeros of $g(z)$ are the same as the two non-zero roots of $z g(z) = 0$, namely $z_\pm = \pm x_+^\kappa$. In addition, the sign of $z g(z)$ is the same as that of $g(z)$ for $z > 0$. Hence, since $z g(z) = (\kappa - 1)(z - z_+)(z - z_-)$, the sign of $z g(z)$ is negative for $0 < z < z_+$ and positive for $z > z_+$; consequently, the sign of the second-order derivative of $\ln_\kappa(x)$ is negative for $0 \leq x < x_+$ and positive for $x > x_+$ where $x_+ \triangleq \left(\frac{\kappa+1}{\kappa-1}\right)^{1/2\kappa}$. Therefore, x_+ is an inflection point, where the behavior of $\ln_\kappa(x)$ changes from concave to convex. ■

D. Review of Lognormal Stochastic Processes

Definition 1 (Lognormal stochastic process): Given a probability space (Ω, \mathcal{F}, P) , the collection of real-valued, scalar random variables $\{Y(\mathbf{s}, \vartheta) : \mathbf{s} \in \mathcal{D}, \vartheta \in \Omega\}$ is a scalar, real-valued *stochastic process* $Y : \mathcal{D} \times \Omega \mapsto \mathbb{R}$. Let $\{Y(\mathbf{s}; \vartheta)\}$ represent a *stationary Gaussian stochastic process* with mean μ , variance σ^2 and covariance kernel $C_Y(\mathbf{r})$, where \mathbf{r} is the lag between any two points $\mathbf{s}, \mathbf{s}' \in \mathcal{D}$. Then, the stochastic process defined by $X(\mathbf{s}; \vartheta) = \exp[Y(\mathbf{s}; \vartheta)] : \mathcal{D} \times \Omega \mapsto \mathbb{R}_+$ is a *stationary lognormal stochastic process*.

The main statistics and probability functions of a lognormal stochastic process are given below.

1) Marginal probability density function (PDF)

$$f_X(x) = \frac{1}{\sqrt{2\pi}\sigma x} e^{-(\ln(x)-\mu)^2/2\sigma^2} = \frac{1}{x\sigma} \phi\left(\frac{\ln(x)-\mu}{\sigma}\right), \quad x \in (0, +\infty), \quad (15)$$

where $\phi(\cdot)$ is the PDF of the standard normal distribution.

2) Median ($\mu_{0.5}$), mode (x_*), and mean (μ_X):

$$\mu_{0.5} = e^\mu, \quad x_* = e^{\mu-\sigma^2}, \quad \mu_X = e^{\mu+\sigma^2/2}. \quad (16)$$

The median of the lognormal is also known as the *geometric mean* of $X(\mathbf{s}; \vartheta)$.

3) Variance (σ_X^2) and skewness (s_X):

$$\sigma_X^2 = \mu_X^2 [\exp(\sigma^2) - 1], \quad s_X = [\exp(\sigma^2) + 2] \sqrt{\exp(\sigma^2) - 1}. \quad (17)$$

4) The marginal cumulative distribution function (CDF) is defined as $F_X(x) = P(X(\vartheta) \leq x)$, where $x > 0$:

$$F_X(x) = \frac{1}{2} \left[1 + \operatorname{erf}\left(\frac{\ln(x)-\mu}{\sigma\sqrt{2}}\right) \right] = \Phi\left(\frac{\ln(x)-\mu}{\sigma}\right), \quad (18)$$

where $\Phi(\cdot)$ is the CDF of the standard normal distribution.

5) The quantile function $x_p = Q_X(p)$ is defined so that $P(X(\vartheta) \leq x_p) = p$, where $0 \leq p \leq 1$:

$$Q_X(p) = \exp\left[\mu + \sqrt{2\sigma^2} \operatorname{erf}^{-1}(2p - 1)\right]. \quad (19)$$

6) Covariance kernel

$$C_X(\mathbf{r}) = \mu_X^2 \left(e^{C_Y(\mathbf{r})} - 1 \right). \quad (20)$$

III. MODIFIED LOGNORMAL DISTRIBUTION

Definition 2 (κ -lognormal distribution): If $Y(\vartheta) : \vartheta \in \Omega$ represents a scalar, real-valued Gaussian random variable in the probability space (Ω, \mathcal{F}, P) with mean μ , and variance σ^2 , the random variable $X(\vartheta)$ defined by means of the κ -exponential transformation

$$X(\vartheta) \triangleq \exp_\kappa[Y(\vartheta)] = \left[\sqrt{1 + Y^2(\vartheta)\kappa^2} + Y(\vartheta)\kappa \right]^{1/\kappa}, \quad \kappa \geq 0, \quad (21a)$$

follows the κ -lognormal distribution, $\kappa\text{LN}(\mu, \sigma, \kappa)$. The inverse transformation is given by the κ -logarithm, that is,

$$Y(\vartheta) \triangleq \ln_\kappa[X(\vartheta)] = \frac{X^\kappa(\vartheta) - X^{-\kappa}(\vartheta)}{2\kappa}. \quad (21b)$$

The marginal probability functions for the κ -lognormal distribution are defined below.

A. Probability Functions of κ -Lognormal Distribution

1) Marginal probability density function (PDF)

By defining the nonlinear monotone transformation $x = g(y)$, where $g(\cdot) = \exp_\kappa(\cdot)$, and $y = g^{-1}(x)$ where $g^{-1}(\cdot) = \ln_\kappa(\cdot)$, the random variable $X = g(Y)$ follows the κ -lognormal distribution, if Y is normally distributed. The respective PDF is given by the following function

$$f_X(x) = \frac{1}{2\sqrt{2\pi}\sigma} e^{-(\ln_\kappa(x)-\mu)^2/2\sigma^2} (x^{\kappa-1} + x^{-\kappa-1}), \quad x > 0, \quad \kappa \geq 0. \quad (22)$$

The κ -lognormal PDF is obtained using the conservation of probability under the monotone variable transformation by means of the PDF of a normal $\mathcal{N}(\mu, \sigma^2)$ and the derivative of κ -logarithm which is given by (13). This PDF decays faster (has a shorter right tail) than the lognormal, because the function $\ln_\kappa(y)$ increases with y faster than the natural logarithm $\ln(y)$.

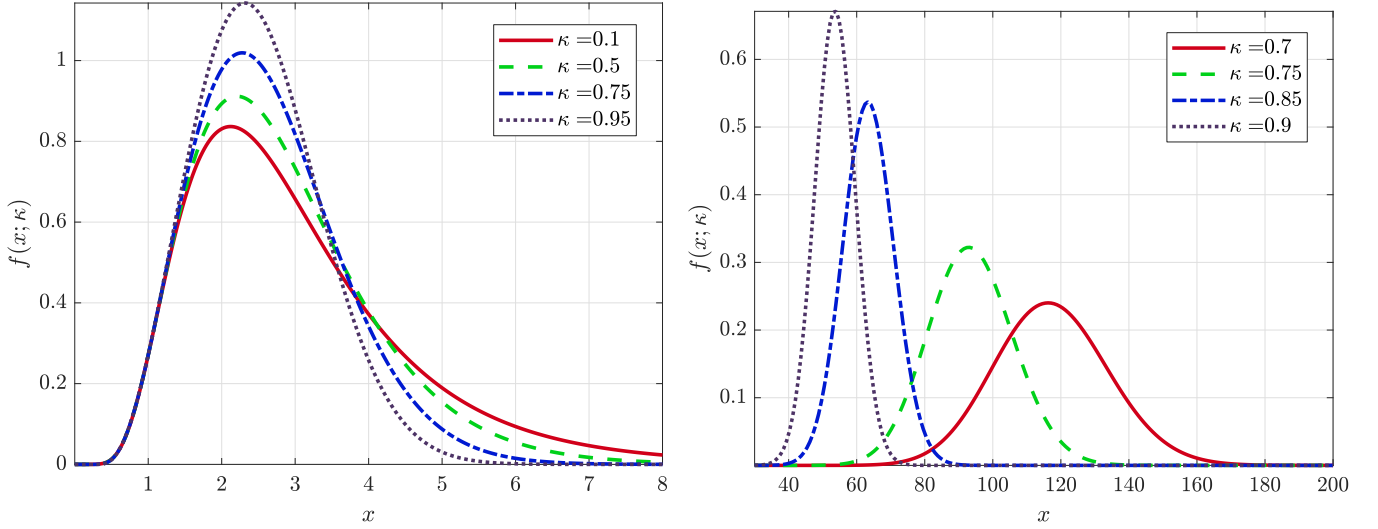


Fig. 3. **Left:** Unimodal probability density functions of κ -lognormal distributions defined by (22) with parameters $\mu = 1$ and $\sigma = 0.5$. The lognormal probability density is recaptured at the limit $\kappa = 0$. **Right:** Approximately Gaussian κ -lognormal PDFs with parameters $\mu = 20$ and $\sigma = 2$ for $0.7 \leq \kappa \leq 0.9$.

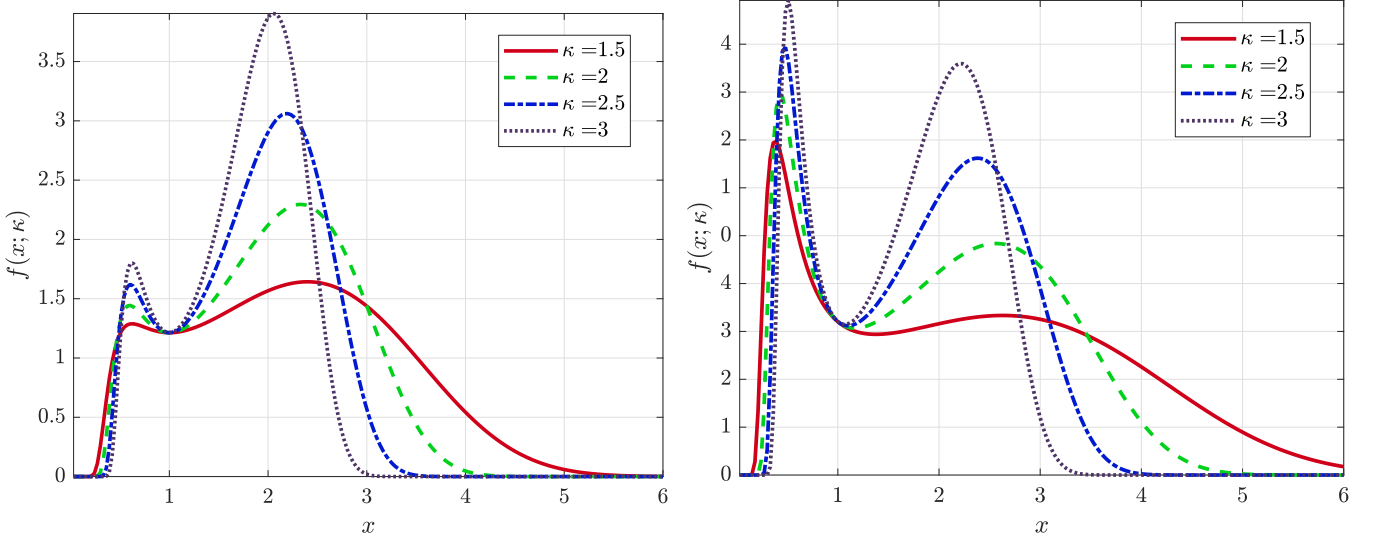


Fig. 4. **Left:** Bimodal probability density functions of κ -lognormal distributions defined by (22) with parameters $\mu = 1$ and $\sigma = 1$ for $1.5 \leq \kappa \leq 3$. **Right:** Bimodal κ -lognormal PDFs with parameters $\mu = 1$ and $\sigma = 1.5$ for $1.5 \leq \kappa \leq 3$.

A comparison of the κ -lognormal with the lognormal PDF for $\kappa < 1$ is shown in the left frame of Fig. 3. In this case the κ -lognormal is similar to the lognormal PDF. For all values of κ , the right tail of the κ -lognormal density is shorter than that of the lognormal, while it approaches the lognormal tail in the limit $\kappa \rightarrow 0$. On the other hand, the κ -lognormal density has more weight than the lognormal over an intermediate range of values that depends on κ (as well as μ and σ) a property which is useful in applications.

Remark 1 (On the asymmetry of κ -lognormal PDF): The asymmetry of the κ -lognormal PDF is controlled by the combination of μ , σ and κ . For example, assume $\kappa = 1$, then $\ln_\kappa(x) = (x - x^{-1})/2$ so that for $x \gg 1$ it holds $\ln_\kappa(x) \approx x/2$. At the same time, $x^{\kappa-1} + x^{-\kappa-1} = 1 + x^{-2} \approx 1$ for $x \gg 1$. Hence, the right tail of the PDF (22) is approximately normal. Moreover, if $\mu \gg 1$, the PDF (22) is approximately a normal PDF with mean 2μ and standard deviation equal to 2σ —because most of the mass is concentrated around 2μ where the condition $x \gg 1$ holds. This behavior is illustrated by the PDFs obtained for $\mu = 20$ and $\sigma = 2$ shown in Fig. 3 (right frame).

Figure 4 presents PDF plots that exhibit bimodality for $\kappa > 1$. For the cases shown, PDFs with higher κ display more pronounced peaks. For the same values of $\kappa \in [1.5, 3]$ and $\mu = 1$, the relative position of the highest peak depends on σ . Hence, for $\sigma = 1$ (left frame of Fig. 4) the most prominent peaks occur for larger x , while for $\sigma = 1.5$ (right frame), the tallest peaks appear at the lower peak locations.

Remark 2 (On bimodality): The plots shown in Figs. 3-4 should not lead readers to the erroneous conclusion that values $0 < \kappa < 1$ give unimodal and $\kappa \geq 1$ bimodal distributions. In fact, for the κ values shown in Fig. 4, unimodal distributions are obtained for $\mu = -1$ and $\sigma = 0.5$ (not shown). Vice versa, $\kappa < 1$ leads to bimodal distributions for certain combinations of μ and σ (e.g., for $\mu = 4, \sigma = 3, \kappa = 0.8$). The shape of the κ -lognormal PDF implicitly depends on the triplet μ, σ, κ and the boundaries between different regimes are nonlinear (as per the arguments in the proof of Theorem 1 in Appendix A).

2) Median

$$\mu_{0.5} = \exp_{\kappa}(\mu). \quad (23)$$

The principle of *quantile invariance* states that the quantiles of a probability distribution remain invariant under a monotonic transformation. Hence, since μ is the median of Y , quantile invariance requires that $\exp_{\kappa}(\mu)$ be the median of $X = \exp_{\kappa}(Y)$.

3) Marginal cumulative distribution function (CDF)

Using the same justification as for (22), the conservation of probability under the transform implies that $F_X(x) = \Phi(g^{-1}(x))$, leading to the following CDF for $x > 0$:

$$F_X(x) = \frac{1}{2} \left[1 + \operatorname{erf} \left(\frac{\ln_{\kappa}(x) - \mu}{\sigma\sqrt{2}} \right) \right] = \Phi \left(\frac{\ln_{\kappa}(x) - \mu}{\sigma} \right). \quad (24)$$

4) Quantile function (defined for $0 \leq p \leq 1$)

$$Q_X(p) = \exp_{\kappa} \left[\mu + \sqrt{2\sigma^2} \operatorname{erf}^{-1}(2p - 1) \right]. \quad (25)$$

Theorem 1 (Modes of κ -lognormal PDF): The κ -lognormal PDF defined by (22) is unimodal or bimodal depending on the values of $\mu, \sigma \geq 0$ and $\kappa \geq 0$. For $\kappa = 0$ (lognormal distribution) the PDF has a single mode at $x_{\text{mode}} = \exp(\mu - \sigma^2)$. For $\kappa > 0$ the PDF can sustain up to three modes. For $0 < \kappa \leq 1$ the modes (at least one) are in the interval $(0, \mu_{0.5})$. For $\kappa > 1$, if $\mu_{0.5} < x_+$, where $x_+ = [(\kappa + 1)/(\kappa - 1)]^{1/2\kappa}$ as defined in Proposition 3, there is at least one mode in $(0, \mu_{0.5})$ while a mode can potentially emerge in (x_+, ∞) . For $\kappa > 1$ and $\mu_{0.5} > x_+$, the mode(s) are located inside the intervals $(0, x_+)$ or $(\mu_{0.5}, \infty)$.

For $\kappa > 0$ the locations of the mode(s) are determined from the zeros of the *characteristic polynomial*

$$p_1(z) = z^6 - a z^5 + b z^4 - 2a z^3 + c z^2 - a z - 1, \quad (26)$$

where $a = 2\mu\kappa$, $b = 1 - 4\kappa\sigma^2(\kappa - 1)$ and $c = 4\kappa\sigma^2(\kappa + 1) - 1$. If we denote by z_r the positive real root(s) of $p_1(z)$, then the stationary points of the PDF are given by $x_{*,r} = z_r^{1/\kappa}$, $r = 1, \dots, R$, with $R \in \{1, 3\}$.

- 1) For $R = 1$, there is a unique mode given by $x_{\text{mode}} = x_{*,1}$.
- 2) For $R = 3$ there are two modes located at $x_{\text{mode};1} = x_{*,1}$ and $x_{\text{mode};2} = x_{*,3}$ (the ordering $x_{*,1} < x_{*,2} < x_{*,3}$ is assumed).
- 3) If at most one of the coefficients a, b, c is non-zero, then $R = 1$ and the PDF is unimodal. The converse is generally not true, unless one of the following conditions holds: $\mu = 0, \kappa = 0, \sigma^2 = \frac{1}{4\kappa(\kappa-1)}$ or $\sigma^2 = \frac{1}{4\kappa(\kappa+1)}$.
- 4) Finally, while $R = 5$ (implying three modes) is not excluded by Descartes' rule if $a, b, c > 0$, five positive roots have not been detected in numerical investigations.

Proof: The proof of Theorem 1 is given in Appendix A. ■

Remark 3 (Number of Modes of κ -Lognormal PDF): Descartes' rule of signs allows but does not require multiple (3 or 5) positive roots of the polynomial $p_1(z)$ (26). Numerical evaluation of roots is necessary for a given combination of μ, σ, κ (except for the combinations that lead to single positive roots, see Table IX in Appendix A). We conducted a small numerical study of the real positive roots of $p_1(z)$ for a rectangular grid comprising 10^6 parameters with 100 nodes per side and parameters in the range $\mu \in [-5, 5]$, $\sigma \in [0, 3]$ and $\kappa \in [0, 5]$. About 39% of the parameter combinations admit three positive roots (corresponding to a bimodal PDF) with the remaining 61% admitting a single positive root (corresponding to a unimodal PDF). The numerical investigation did not identify a combination of (μ, σ, κ) that admits five roots, even though parameter vectors $(a, b, c) \in (0, \infty)^3$ —which according to Descartes' rule is the only admissible sign combination that allows up to five positive roots—were included among the cases studied. The numerical calculation of the roots of $p_1(z)$ was performed using the Matlab® function `roots`.

B. Marginal Moments of κ -Lognormal Distribution

Theorem 2 (Statistical moments of integer order): Let $m_{X;\ell}(\kappa; \mu, \sigma) = \mathbb{E}[X^{\ell}(\vartheta)]$, where $\ell \in \mathbb{N}$, denote the moment of order ℓ of a κ -lognormal variable $X(\vartheta)$ such that $Y(\vartheta) = \ln_{\kappa}[X(\vartheta)] \stackrel{d}{=} \mathcal{N}(\mu, \sigma^2)$. The κ -lognormal moments can be obtained from the following integral

$$m_{X;\ell}(\kappa; \mu, \sigma) = \int_{-\infty}^{\infty} \exp_{\kappa/\ell}(\ell y) f_Y(y; \mu, \sigma^2) dy, \quad (27)$$

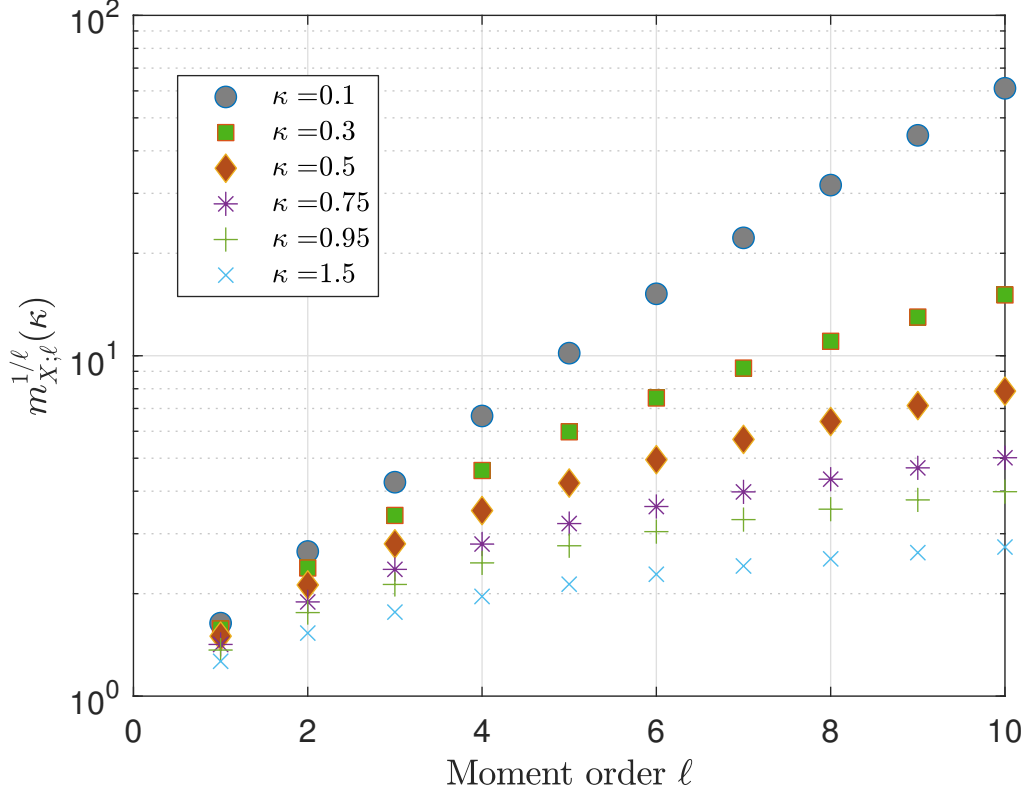


Fig. 5. Moments of order $\ell \in \{1, 2, \dots, 10\}$ for the κ -lognormal distribution with different κ values. All curves are obtained by numerical evaluation of the integral (27) for $\mu = 0$ and $\sigma = 1$. The horizontal axis shows the moment order ℓ . The vertical axis uses a logarithmic scale to display $m_{X;\ell}^{1/\ell}(\kappa)$ where $m_{X;\ell}(\kappa) \triangleq m_{X;\ell}(\kappa; 0, 1)$; the ℓ -th root of the order- ℓ moments is used in order to maintain a common scale for different ℓ .

where $f_Y(y; \mu, \sigma^2) = \frac{1}{\sigma} \phi\left(\frac{y-\mu}{\sigma}\right)$ is the PDF of a $\mathcal{N}(\mu, \sigma^2)$. Moreover, the moments satisfy the following scaling relation

$$m_{X;\ell}(\kappa; \mu, \sigma) = m_{X;1}(\kappa/\ell; \ell\mu, \ell\sigma). \quad (28)$$

Proof: The proof is given in Appendix B. ■

Remark 4 (On moment scaling): The scaling relation (28) implies that if a closed-form expression is available for the first-order moment of the κ -lognormal (for all possible values of μ, σ , and κ), this expression can be used to calculate the moments of order $\ell \in \mathbb{N}$. Another implication of (28) is that the κ -lognormal moments of any order $\ell \gg 1$ (so that $\kappa/\ell \rightarrow 0$) are essentially equal to the expectation of the lognormal with parameters $\ell\mu$ and $\ell\sigma$.

In the following, if $\mu = 0$ and $\sigma = 1$ we use the shorthand notation $m_{X;\ell}(\kappa) \triangleq m_{X;\ell}(\kappa; 0, 1)$ for the moments of order ℓ . We evaluate the moments $m_{X;\ell}(\kappa)$ for $\ell = 1, 2, \dots, 10$ by numerical integration of (27). The functions $m_{X;\ell}^{1/\ell}(\kappa)$ that are plotted in Fig. 5 represent the ℓ -th roots of the ℓ -order moments—thus all $m_{X;\ell}^{1/\ell}(\kappa)$ have the same units as X . As evidenced in Fig. 5, the ℓ -th roots of the moments increase faster with ℓ for κ values closer to zero. This pattern is due to the increased weight in the tail of the κ -lognormal PDF as $\kappa \rightarrow 0$.

C. Moment Bounds

The moments $m_{X;\ell}(\kappa; \mu, \sigma)$ in (27) are bounded from below by zero, since $\exp_\kappa(y) \geq 0$. The upper bounds depend on the values of μ and σ : if the latter are such that $f_Y(y; \mu, \sigma^2)$ is practically zero for $y < 0$, then it becomes evident from the defining integral, that a moment of order ℓ for $\kappa > 0$ is bounded from above by the same-order lognormal moment (with the same μ and σ as the κ -lognormal), because $[\exp_\kappa(y)]^\ell \leq [\exp(y)]^\ell$ for $y > 0$. In fact, given the monotonic dependence of κ -exponential on κ the ordering $m_{X;\ell}(\kappa'; \mu, \sigma) < m_{X;\ell}(\kappa; \mu, \sigma)$ if $\kappa' > \kappa$ holds. On the other hand, the above argument cannot be extended if $f_Y(y; \mu, \sigma^2)$ is non-negligible for $y < 0$, because $\exp_\kappa(y) > \exp(y)$ for $y < 0$. In the following, we derive stricter bounds on the moments of the κ -lognormal distribution.

Theorem 3 (Moment bounds): Let X denote a κ -lognormal process so that $\ln_\kappa [X(\vartheta)] \stackrel{d}{=} \mathcal{N}(\mu, \sigma^2)$ with $\mu > 0$. Then, the moments $m_{X;\ell}(\kappa; \mu, \sigma)$ of order ℓ respect the following inequalities

$$UB_{X;\ell}(\kappa; \mu, \sigma) \geq m_{X;\ell}(\kappa; \mu, \sigma) \geq LB_{X;\ell}(\kappa; \mu, \sigma), \quad (29a)$$

where $LB_{X;\ell}(\kappa; \mu, \sigma)$ and $UB_{X;\ell}(\kappa; \mu, \sigma)$ represent, respectively, lower and upper bounds of $m_{X;\ell}(\kappa; \mu, \sigma)$ given by

$$LB_{X;\ell}(\kappa; \mu, \sigma) = \frac{(2\kappa)^{\ell/\kappa} 2^{\frac{\ell-\kappa}{2\kappa}} \sigma^{\ell/\kappa}}{\sqrt{2\pi}} e^{-\frac{\mu^2}{2\sigma^2}} \left[\Gamma\left(\frac{\ell+\kappa}{2\kappa}\right) {}_1F_1\left(\frac{\ell+\kappa}{2\kappa}, \frac{1}{2}; \frac{\mu^2}{2\sigma^2}\right) + \Gamma\left(\frac{\ell+2\kappa}{2\kappa}\right) \frac{\mu\sqrt{2}}{\sigma} {}_1F_1\left(\frac{\ell+2\kappa}{2\kappa}, \frac{3}{2}; \frac{\mu^2}{2\sigma^2}\right) \right] + \frac{e^{\ell\mu+\ell^2\sigma^2/2}}{2} \left[1 - \operatorname{erf}\left(\frac{\mu+\ell\sigma^2}{\sqrt{2}\sigma}\right) \right], \quad (29b)$$

$$UB_{X;\ell}(\kappa; \mu, \sigma) = \frac{1}{2} \left[1 - \operatorname{erf}\left(\frac{\mu}{\sqrt{2}\sigma}\right) \right] + \frac{2^{\ell/\kappa-1} e^{-\mu^2/2\sigma^2}}{\sqrt{\pi}} \sum_{m=0}^{n_*} \frac{n_*!}{m!(n_*-m)!} (2\kappa^2\sigma^2)^m \times \left[\Gamma\left(m+\frac{1}{2}\right) {}_1F_1\left(m+\frac{1}{2}, \frac{1}{2}; \frac{\mu^2}{2\sigma^2}\right) + \Gamma(m+1) \frac{\mu\sqrt{2}}{\sigma} {}_1F_1\left(m+1, \frac{3}{2}; \frac{\mu^2}{2\sigma^2}\right) \right]. \quad (29c)$$

$\Gamma(\cdot)$ is the Gamma function, ${}_1F_1(a, b; z)$ is the *confluent hypergeometric function* [62, 9.210], $\operatorname{erf}(\cdot)$ is the error function, and $n_* = \lceil \frac{\ell}{2\kappa} \rceil$ is the nearest integer that is not smaller than $\frac{\ell}{2\kappa}$.

Proof: The proof of Theorem 3 is given in Appendix C. ■

Remark 5 (Scaling relation for moment bounds): The moment bounds (29b) and (29c) respect scaling relations analogous to (28) for the moments, i.e.,

$$UB_{X;\ell}(\kappa; \mu, \sigma) = UB_{X;1}\left(\frac{\kappa}{\ell}; \ell\mu, \ell\sigma\right), \quad (30a)$$

$$LB_{X;\ell}(\kappa; \mu, \sigma) = LB_{X;1}\left(\frac{\kappa}{\ell}; \ell\mu, \ell\sigma\right). \quad (30b)$$

The scaling relations follow directly from (29b) and (29c) because the bounds depend on the ratios ℓ/κ and μ/σ ; such terms are invariant under the transformation $\ell \mapsto 1$, $\kappa \mapsto \kappa/\ell$, $\mu \mapsto \ell\mu$, and $\sigma \mapsto \ell\sigma$. The lower bound also includes the term $\exp(\ell\mu + \ell^2\sigma^2/2)$ which is invariant under the transformations $\ell \mapsto 1$, $\mu \mapsto \ell\mu$, $\sigma \mapsto \ell\sigma$. The upper bound contains terms $\kappa^{2m}\sigma^{2m}$ which also remain invariant under $\ell \mapsto 1$, $\kappa \mapsto \kappa/\ell$ and $\sigma \mapsto \ell\sigma$.

Remark 6 (Tightness of the bounds): Tightness of both the lower and upper bounds requires $\sqrt{1 + \kappa^2 y^2} \approx \kappa y$, which is easier to achieve over a wide range of y as κ moves away from zero. For the upper bound, it is also necessary that $\ell/2\kappa$ be equal to an integer value. Both the lower and upper bounds contain terms that involve the error function. These terms become important only if the arguments of the error functions are considerably less than one, namely $\mu/\sigma \ll \sqrt{2}$ (for the upper bound) and $\mu/\sigma + \ell\sigma \ll \sqrt{2}$ (for the lower bound).

Figure 6 compares the moments obtained by means of numerical integration of (27) with the lower bounds (29b) for a κ -lognormal model with $\mu = 5$, $\sigma = 2$ and varying $\kappa \geq 0.4$. The mean $m_{X;1}(\kappa; \mu, \sigma)$ shows excellent agreement for $\kappa \in [0.4, 2]$, while the moments $m_{X;\ell}(\kappa; \mu, \sigma)$ for $\ell \in \{2, \dots, 10\}$ also show very good agreement for $\kappa = 0.4, 0.5, 0.75, 0.95$. Higher $\kappa \in [1.40, 1.50, 1.75, 1.95]$ (not shown) yield even better agreement.

Table I compares the ℓ -th root moments $m_{X;\ell}^{1/\ell}(\kappa; \mu, \sigma)$ evaluated by numerical integration, cf. (27), with both the lower and upper bounds derived from (29b) and (29c). It is evident that the lower bound provides a very accurate approximation (in agreement with Fig. 6), especially for higher values of κ . The upper bound is tight for $\kappa \geq 0.5$ and values such that $\ell/2\kappa \in \mathbb{N}$. This is not surprising since the upper bound is constructed based on $n_* = \lceil \frac{\ell}{2\kappa} \rceil$ (cf. Theorem 3). For $\kappa = 0.4$, the upper bound significantly exceeds the “true” value of the moments except for integer values of $\ell/2\kappa$. For smaller κ , both bounds become less accurate. Figure 7 shows the same plots now obtained for $\mu = -2$ and $\sigma = 2$. We notice that due to the negative μ the value of the mean is in the range $[0.6, 0.8]$ for all κ . The lower bound, on the other hand, is approximately limited to values between 0.4 and 0.5; hence, it underestimates the mean but correctly captures its order of magnitude. For $\ell \in \{1, 2, \dots, 10\}$, the lower bound provides an accurate approximation for $\kappa \in [0.5, 0.95]$.

D. Power Series Expansions of the Moments

Based on the moment integral (27), we can develop a power series expansion for the moment of order ℓ by expanding the κ -exponential. The expansion can be developed around different points. Below, we focus on the Taylor series expansion of the moments around μ .

Theorem 4 (Power series of κ -lognormal moments): Let X be a random variable that follows the κ -lognormal distribution with parameters $\mu \geq 0$, $\sigma \geq 0$, $\kappa \geq 0$ and $\ell \in \mathbb{N}$. Then,

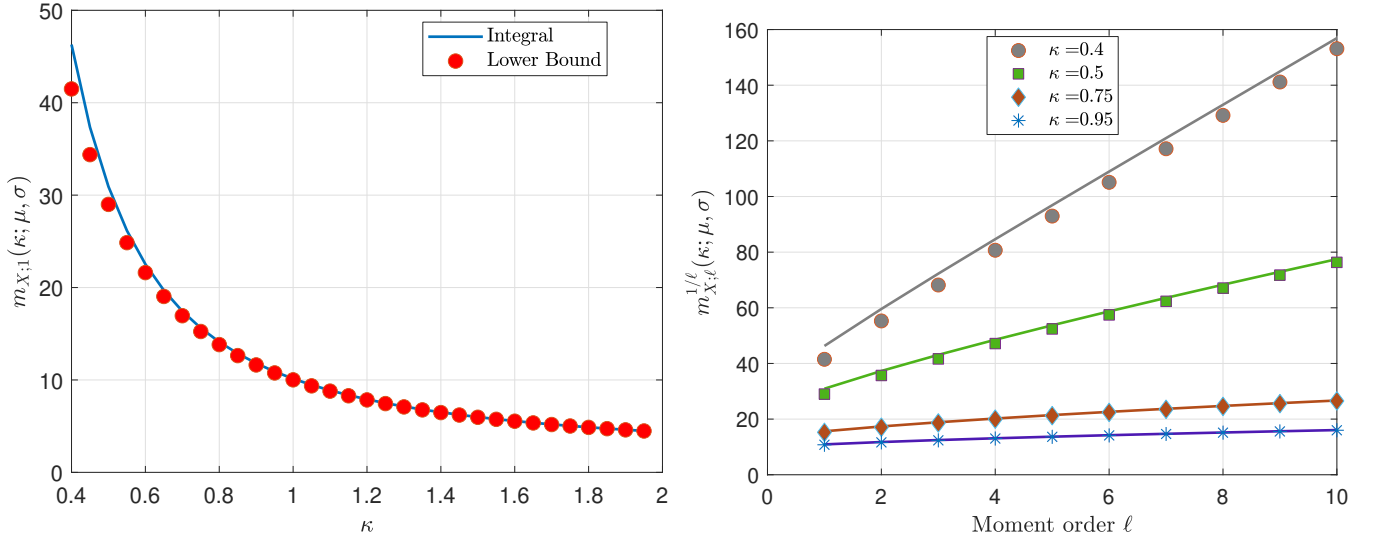


Fig. 6. **Left:** Mean of the lognormal distribution (continuous line, blue online) with $\mu = 5$ and $\sigma = 2$ calculated by means of numerical integration (cf. (27)) and lower bound of the first-order moment based on (29b) (circle markers, red online). **Right:** Root of order ℓ of the expectation $m_{X;\ell}(\kappa; \mu, \sigma)$ versus ℓ for $\mu = 5$ and $\sigma = 2$. Continuous lines represent the numerical integral (27) while markers denote the lower bounds (29b). Four different values of κ are used: $\kappa \in \{0.4, 0.5, 0.75, 0.95\}$.

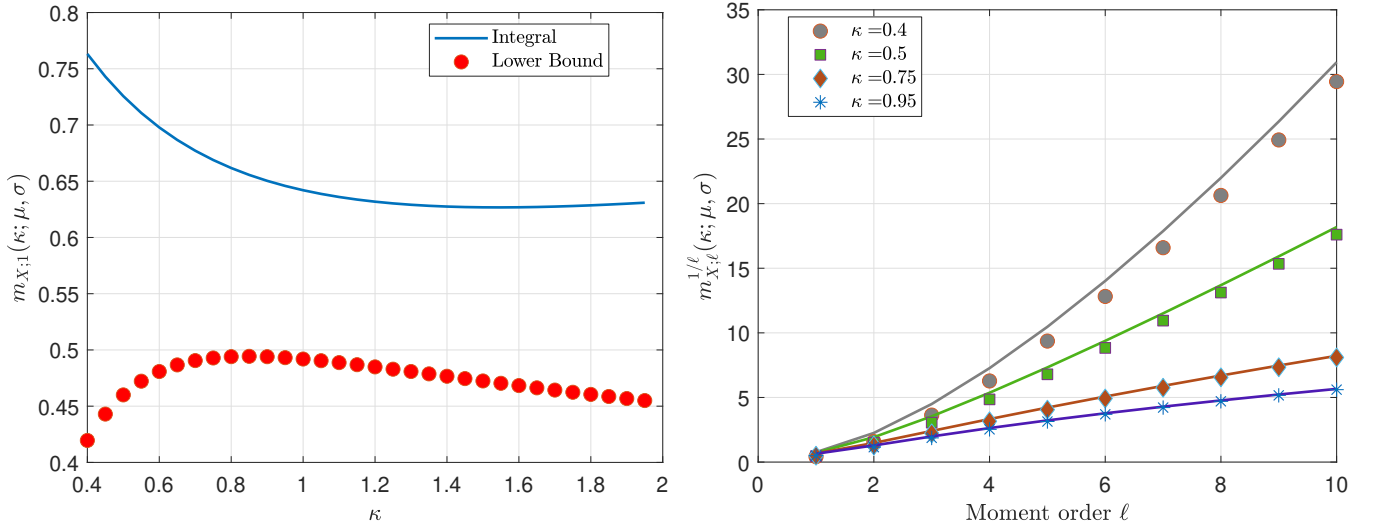


Fig. 7. **Left:** Mean of the κ -lognormal distribution (continuous line) with $\mu = -2$ and $\sigma = 2$ versus κ (continuous line, blue online). The expectation is calculated by means of numerical integration (cf. (27)). The lower bound of the mean as a function of κ , based on (29b), is shown using circle markers (red online). **Right:** Root of order ℓ of the moment $m_{X;\ell}(\kappa; \mu, \sigma)$ versus ℓ for $\mu = -2$ and $\sigma = 2$. Continuous lines represent the numerical integral (27) while markers denote the lower bounds (29b). Four different values of κ are used: $\kappa \in \{0.4, 0.5, 0.75, 0.95\}$.

$$m_{X;\ell}(\kappa; \mu, \sigma) = \exp_{\kappa/\ell}(\ell \mu) \left[1 + \ell \sum_{q=1}^{\infty} \frac{\sigma^{2q}}{q! 2^q} \frac{g_{2q}(\mu; \kappa, \ell)}{(1 + \kappa^2 \mu^2)^{2q-1/2}} \right], \quad (31a)$$

where the functions $g_n(\cdot)$ satisfy the recursive relation

$$g_{n+1}(\mu; \kappa, \ell) = (1 + \kappa^2 \mu^2) \frac{d g_n(\mu; \kappa, \ell)}{d \mu} - \left[(2n-1) \kappa^2 \mu - \ell \sqrt{1 + \kappa^2 \mu^2} \right] g_n(\mu; \kappa, \ell), \quad (31b)$$

with $g_1(\mu; \kappa, \ell) = 1$.

Proof: The proof of Theorem 4 is given in Appendix D. ■

TABLE I

ESTIMATES OF THE κ -LOGNORMAL MOMENTS $m_{X;\ell}^{1/\ell}(\kappa; \mu, \sigma)$ FOR $\kappa = 0.4, 0.5, 0.75, 0.95$ AND $\ell \in \{1, 2, \dots, 10\}$. THE RATIO $\ell/2\kappa$ OF THE MOMENT ORDER ℓ OVER 2κ IS ALSO SHOWN. ALL RESULTS ARE OBTAINED FOR $\mu = 5$ AND $\sigma = 2$. THE FOLLOWING ABBREVIATIONS ARE USED: LB: LOWER BOUND BASED ON (29b). MOM: NUMERICAL MOMENT ESTIMATES BASED ON THE INTEGRAL (27). UB: UPPER BOUND BASED ON (29c). THE BOUNDS PROVIDE TIGHT APPROXIMATION OF THE MOMENTS FOR INTEGER $\ell/2\kappa$.

	ℓ	1	2	3	4	5	6	7	8	9	10
$\kappa = 0.4$	LB	41.49	55.28	68.19	80.69	92.96	105.10	117.16	129.17	141.15	153.12
	MOM	46.29	59.58	72.27	84.66	96.86	108.96	120.99	132.98	144.95	156.91
	UB	242.46	114.25	94.31	88.86	154.15	144.21	139.21	136.92	194.66	189.55
	$\ell/2\kappa$	1.25	2.5	3.75	5	6.25	7.5	8.75	10	11.25	12.5
$\kappa = 0.5$	LB	29.00	35.68	41.62	47.14	52.39	57.44	62.33	67.10	71.76	76.34
	MOM	30.92	37.30	43.09	48.52	53.71	58.71	63.56	68.30	72.93	77.49
	UB	32.98	39.00	44.62	49.95	55.06	60.00	64.82	69.52	74.13	78.66
	$\ell/2\kappa$	1	2	3	4	5	6	7	8	9	10
$\kappa = 0.75$	LB	15.24	17.07	18.61	19.98	21.24	22.41	23.51	24.56	25.56	26.54
	MOM	15.62	17.36	18.86	20.21	21.44	22.60	23.70	24.73	25.73	26.69
	UB	43.61	52.64	19.11	27.45	35.41	22.80	28.70	34.65	25.90	30.77
	$\ell/2\kappa$	0.67	1.33	2	2.67	3.33	4	4.67	5.33	6	6.67
$\kappa = 0.95$	LB	10.76	11.64	12.38	13.02	13.60	14.14	14.65	15.12	15.57	16.00
	MOM	10.91	11.75	12.47	13.10	13.68	14.21	14.71	15.18	15.63	16.06
	UB	56.35	68.49	21.35	31.94	18.48	25.55	17.85	23.30	17.81	22.33
	$\ell/2\kappa$	0.53	1.06	1.58	2.11	2.63	3.16	3.69	4.21	4.74	5.27

Remark 7: The functions $g_n(\mu; \kappa, \ell)$ for $n = 1, 2, 3, 4$ are given by

$$g_1(\mu; \kappa, \ell) = 1, \quad (32a)$$

$$g_2(\mu; \kappa, \ell) = \ell \sqrt{1 + \kappa^2 \mu^2} - \mu \kappa^2, \quad (32b)$$

$$g_3(\mu; \kappa, \ell) = -3\kappa^2 \ell \mu \sqrt{1 + \kappa^2 \mu^2} - \kappa^2 + 2\kappa^4 \mu^2 + \ell^2 (1 + \kappa^2 \mu^2), \quad (32c)$$

$$g_4(\mu; \kappa, \ell) = \ell \kappa^2 \sqrt{1 + \kappa^2 \mu^2} (11\kappa^2 \mu^2 - 4) + 3\kappa^2 \mu (3\kappa^2 - 2\kappa^4 \mu^2 - 2\ell^2 - 2\kappa^2 \mu^2 \ell^2) + \ell^3 \sqrt{1 + \kappa^2 \mu^2} (1 + \kappa^2 \mu^2). \quad (32d)$$

From the above, only the even-order $g_2(\mu; \kappa, \ell)$ and $g_4(\mu; \kappa, \ell)$ contribute to the moment expansion (31a).

At the limit of the lognormal distribution, that is for $\kappa = 0$, the moment series (31a) for fixed ℓ is expressed as

$$m_{X;\ell}(\kappa = 0; \mu, \sigma) = \exp(\ell \mu) \left[1 + \ell \sum_{q=1}^{\infty} \frac{\sigma^{2q}}{q! 2^q} g_{2q}(\mu; 0, \ell) \right], \quad (33a)$$

where the functions $g_n(\cdot)$ satisfy the recursive equation

$$g_{n+1}(\mu; 0, \ell) = \frac{d g_n(\mu; 0, \ell)}{d \mu} + \ell g_n(\mu; 0, \ell), \text{ for } n > 1, \quad (33b)$$

with $g_1(\mu; 0, \ell) = 1$. The above recursive equation is solved by $g_{n+1}(\mu; 0, \ell) = \ell^n$. Hence, the power series (33a) can be explicitly summed yielding the lognormal moments, i.e., $m_{X;\ell}(\kappa = 0; \mu, \sigma) = \exp(\ell \mu + \frac{1}{2} \ell^2 \sigma^2)$.

Figure 8 tests the accuracy of the Taylor series moment expansion (31). In the left frame, the expectation of the κ -lognormal distribution, obtained from the numerical integral (27), is compared with the mean obtained by means of the Taylor series (31) for $\ell = 1$, truncated at second order, that is for $q_* = 2$. The parameters of the κ -lognormal distribution are $\mu = 5$ and $\sigma \in \{0.9, 2\}$. For all $\kappa \in [0.05, 1.95]$ there is very good agreement between the true mean and the approximation; the agreement is better for the lower normal variance, that is for $\sigma = 0.9$, as expected. Furthermore, the agreement between the true mean and the truncated series improves as κ increases. The right frame compares the true order- ℓ moments (continuous lines) with the respective truncated series approximations (markers) for $\kappa \in \{0.15, 0.20, 0.25, 0.30\}$. Excellent agreement is obtained for $\ell = 1, 2, 3, 4$ for all κ examined. The agreement deteriorates for moments of order $\ell \geq 5$ for lower values of κ . The results shown are obtained for $\mu = 5$ and $\sigma = 0.5$. The accuracy of the approximation is reduced as σ increases.

E. Behavior of κ -Lognormal Tail versus the Lognormal Tail

As stated in the Introduction, the tail of the lognormal distribution is too long for certain applications—a comparison presented in the Supplement (Section 2) between the normal and lognormal distributions confirms this behavior.

To intuitively explore this observation, we consider the behavior of lognormal quantiles for probability values $p_* \triangleq 1 - 1/N$ that are close to one. The quantiles $x_{\max} \triangleq Q(p_*)$ can be viewed as typical extremes obtained from $N = 2^L$, where $L \in \mathbb{N}$,

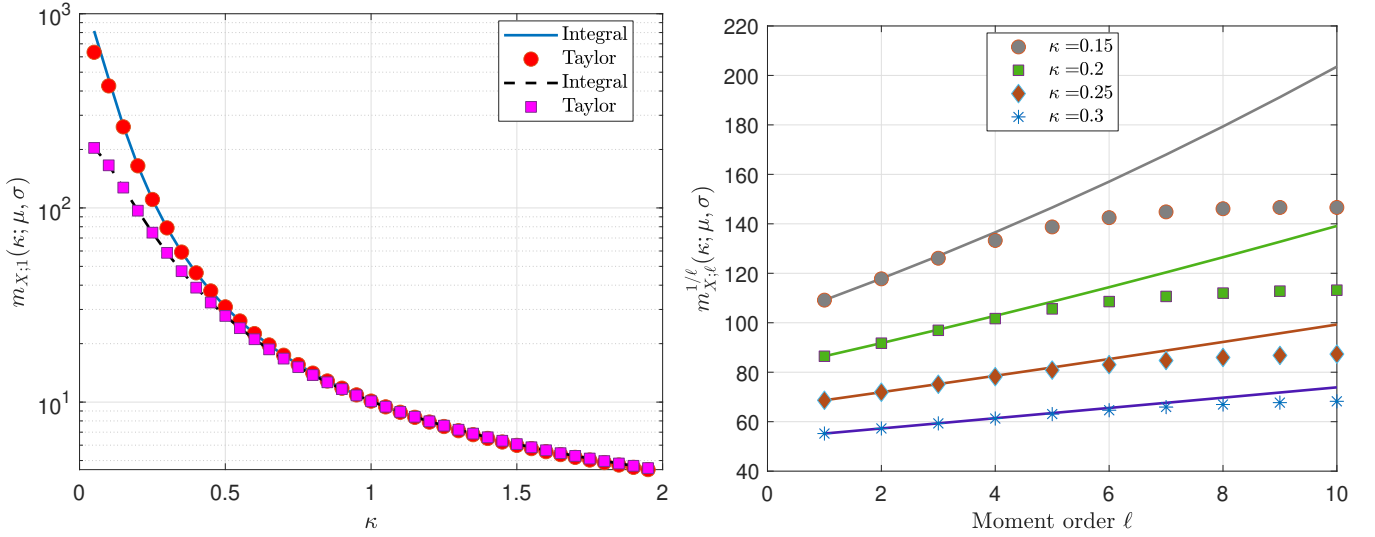


Fig. 8. **Left:** Mean of the κ -lognormal distribution with $\mu = 5$ and $\sigma = 2$ (continuous line) and $\sigma = 0.9$ (dashed line) calculated by means of numerical integration (cf. (27)) for $\kappa \in [0.05, 1.95]$. The Taylor-series moment approximation (31) is also shown (circles for $\sigma = 2$ and square markers for $\sigma = 0.9$). A logarithmic (base 10) scale is used for the vertical axis. **Right:** Root of order ℓ of the moment $m_{X;\ell}(\kappa; \mu, \sigma)$ versus ℓ for $\mu = 5$ and $\sigma = 0.5$. Continuous lines represent the numerical integral (27) while markers denote the Taylor-based expression (31). Four different values of κ are used: $\kappa \in \{0.15, 0.2, 0.25, 0.30\}$. The Taylor series moment approximations include only the low-order terms $g_2(\mu; \kappa, \ell)$ and $g_4(\mu; \kappa, \ell)$.

independent samples of a lognormal variable. We focus on the *dimensionless ratio* $q_*(\kappa) \triangleq x_{\max}/\mu_{0.5}$ of the “typical extreme” value over the median. This ratio represents the *normalized typical extreme*. For the lognormal distribution it is given by

$$q_*(\kappa = 0) \triangleq \frac{Q_{\text{LN}}(p_*)}{Q_{\text{LN}}(0.5)} = \exp \left[\sqrt{2\sigma^2} \operatorname{erf}^{-1}(1 - 2/N) \right], \quad (34)$$

where Q_{LN} is the quantile function of the lognormal distribution. For stochastic processes, normalized typical extremes can be smaller—for given N —because the values at neighboring nodes are not independent. This implies an effective system size $N_{\text{eff}} \approx N/\xi^d$ (instead of N), where ξ is the correlation length of the stochastic process [6, Chap. 13].

To highlight the tail difference between the lognormal and κ -lognormal, we calculate the normalized typical extreme as a function of N assuming that both distributions have the same mean, μ_X , and variance, σ_X^2 . To calculate $q_*(\kappa)$ we use the κ -quantile function given by (25) in (34). We select $\mu = 0$, $\sigma = 1.5$, and estimate the κ -lognormal mean, μ_X , and variance, σ_X^2 , for different κ based on the integral (27). Then, we obtain the lognormal mean, μ' , and variance, σ'^2 , by inverting (16) for the mean and (17) for the variance leading to

$$\sigma'^2 = \ln \left(1 + \frac{\sigma_X^2}{\mu_X^2} \right), \quad \mu' = \ln \mu_X - \ln \left(\sqrt{1 + \frac{\sigma_X^2}{\mu_X^2}} \right). \quad (35)$$

Equations (35) ensure that the lognormal and κ -lognormal distributions share the same mean and variance. The behavior of the κ -lognormal typical extreme values is shown in the parametric plots (left frame of Fig. 9). For $\kappa = 0.05$ the κ -lognormal typical extremes are close to those of the lognormal. However, the values of normalized typical extremes are considerably reduced for $\kappa > 0.25$. Figure 9 (right frame) also focuses on the ratio $q_*(\kappa)/q_*(\kappa = 0)$. This ratio is close to one for $\kappa = 0.05$ since the two distributions have the same mean and variance and $\kappa = 0.05$ is close to the lognormal. As L increases beyond a κ -dependent threshold, the ratio $q_*(\kappa)/q_*(\kappa = 0)$ decreases monotonically. This behavior is more pronounced (smaller threshold and steeper decline) for higher κ .

F. Hazard Rate of the κ -Lognormal

The *hazard rate* (also known as *hazard function* and *failure rate*), $h(x)$, is a key concept in reliability engineering and survival analysis [63], [64]. Its definition involves the survival function, $S_X(x)$, also known as complementary CDF (CCDF): $S_X(x) = 1 - F_X(x)$. The hazard function, $h(x)$, is then defined as

$$h(x) = \frac{f_X(x)}{S_X(x)}. \quad (36)$$

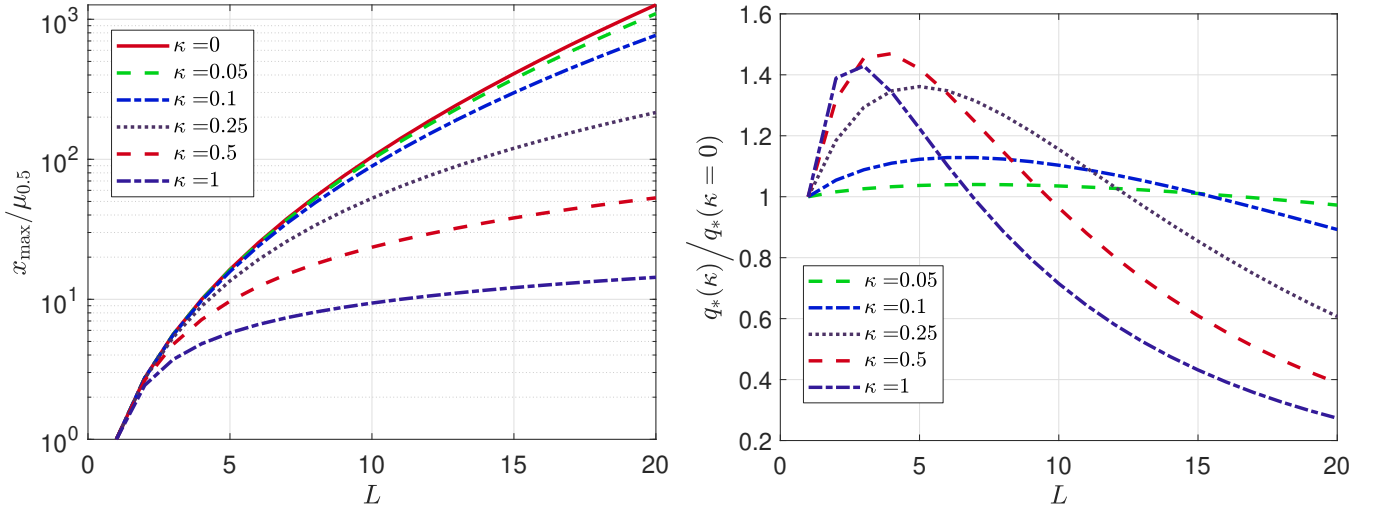


Fig. 9. **Left:** Ratio $q_*(\kappa) \triangleq x_{\max}/\mu_{0.5}$ for the κ -lognormal distribution with different κ including the lognormal limit $\kappa = 0$ based on (34); $x_{\max} = Q(1 - 1/N)$ where $N = 2^L$ and $\mu_{0.5} = Q(0.5)$. The quantile function (25) is used to calculate x_{\max} . Different L values correspond to probability levels between $p_* = 0.5$ for $L = 2$ and $p_* \approx 0.999999046$ for $L = 20$. **Right:** Ratio of $q_*(\kappa)$ for the κ -lognormal with $\kappa > 0$ over $q_*(\kappa = 0)$ for the lognormal distribution. All curves are generated using $\mu = 0$ and $\sigma = 1.5$.

a) *Significance:* For an ensemble of identical systems under “stress, where the latter is denoted by the random variable $X(\vartheta)$, $h(x)$ is the conditional probability that a system fails at stress level $X(\vartheta) = x$ considering that identical systems have survived for $X(\vartheta) \leq x$. Alternatively, $X(\vartheta)$ could represent the time to failure. For example, in lifetime analysis it represents the time to catastrophic failure of a mechanical or electrical component. For systems that can sustain multiple failure events, such as geological faults, it represents the recurrence time to the next event (e.g., an earthquake above a certain threshold magnitude). For random failure events, lifetime and recurrence times follow the exponential distribution with rate parameter λ . The exponential hazard rate equals the constant λ , a result which is anticipated due to the randomness of the failure events.

b) *Asymptotic behavior:* The dependence of $h(x)$ for large x is a matter of interest. If $h(x)$ increases as $x \rightarrow \infty$, the probability of the next failure event increases with the time elapsed since the last event [65]; for non-repairable systems, an increasing $h(x)$ implies that the failure probability increases with elapsed time. Such behavior represents an aging effect [64]. On the other hand, decreasing hazard rates indicate that the probability of new occurrences (or a single failure) is reduced with increasing waiting time; this behavior is often observed in electronic parts and is attributed to a “burn-in” effect [64].

c) *Lognormal hazard rate:* The hazard function of the lognormal distribution is given by

$$h(x) = \frac{\phi\left(\frac{\ln(x)-\mu}{\sigma}\right)}{x\sigma\left[1 - \Phi\left(\frac{\ln(x)-\mu}{\sigma}\right)\right]}, \text{ for } x \geq 0. \quad (37)$$

The hazard rate (37) starts at zero for $x = 0$, rises to a maximum, and then slowly decreases to zero [66]. Hence, the lognormal distribution is not suitable for survival or failure-time data. To determine the asymptotic dependence of $h(x)$ we use $z(x) \triangleq (\ln(x) - \mu)/\sigma$ and subsequently (dropping the dependence of z on x for convenience), $h(z) = \phi(z)e^{-\mu-\sigma z}/\sigma[1 - \Phi(z)]$. As $z \rightarrow \infty$, $\phi(z)$, $e^{-\mu-\sigma z}$, and $1 - \Phi(z)$ tend to zero. To lift the indeterminacy, we use L'Hôpital's rule, that is, $\phi(z)/[1 - \Phi(z)] \sim \phi'(z)/[-\phi(z)] = -[\ln \phi(z)]'$, where $\phi(z) = \exp(-z^2/2)/\sqrt{2\pi}$ and the prime denotes differentiation with respect to z . Since $[\ln \phi(z)]' = -z$, it follows that $h(x) \sim z(x)/x\sigma$, that is,

$$h(x) \sim \frac{\ln(x) - \mu}{x\sigma^2}, \quad x \rightarrow \infty. \quad (38)$$

d) *κ -lognormal hazard rate:* Based on (22) and (24), the κ -lognormal hazard function is given by

$$h_\kappa(x) = \frac{\phi\left(\frac{\ln_\kappa(x)-\mu}{\sigma}\right)(x^{\kappa-1} + x^{-\kappa-1})}{2\sigma\left[1 - \Phi\left(\frac{\ln_\kappa(x)-\mu}{\sigma}\right)\right]}. \quad (39)$$

We investigate the asymptotic behavior of $h_\kappa(x)$ following the same procedure, now setting $z = (\ln_\kappa(x) - \mu)/\sigma$ and using $h_\kappa(x) \sim z(x^{\kappa-1} + x^{-\kappa-1})/(2\sigma)$. Since, according to (11), as $x \rightarrow \infty$ $\ln_\kappa(x) \sim x^\kappa/(2\kappa)$ and $(x^{\kappa-1} + x^{-\kappa-1}) \approx x^{\kappa-1}$, it follows that

$$h_\kappa(x) \sim \frac{x^{2\kappa-1} - 2\kappa\mu x^{\kappa-1}}{4\kappa\sigma^2}, \quad x \rightarrow \infty, \quad (40)$$

which implies that the dominant term is $x^{2\kappa-1}/(4\kappa\sigma^2)$.

It follows from the above analysis that $\kappa = 0.5$ corresponds to a critical point where the hazard rate asymptotically tends to the constant $1/2\sigma^2$. Hence, for $\kappa = 0.5$ the κ -lognormal behaves asymptotically as the exponential hazard rate with $\lambda = 1/2\sigma^2$. On the other hand, $h_\kappa(x)$ is a decreasing function of x for $\kappa < 0.5$ (thus exhibiting “burn-in” effect) and an increasing function for $\kappa > 0.5$ (demonstrating the aging effect). In all three cases, however, $h_\kappa(x=0) = 0$, and thus the κ -lognormal distribution does not support the “infant mortality” (early failures) effect, unlike the Weibull distribution with shape modulus less than one [64]. Nonetheless, the κ -lognormal with $\kappa > 0.5$ is, unlike the lognormal, more suitable for failure-time analysis. Plots of $h_\kappa(x)$ for different values of κ confirming the near-zero and the asymptotic behavior are shown in Fig. 10.

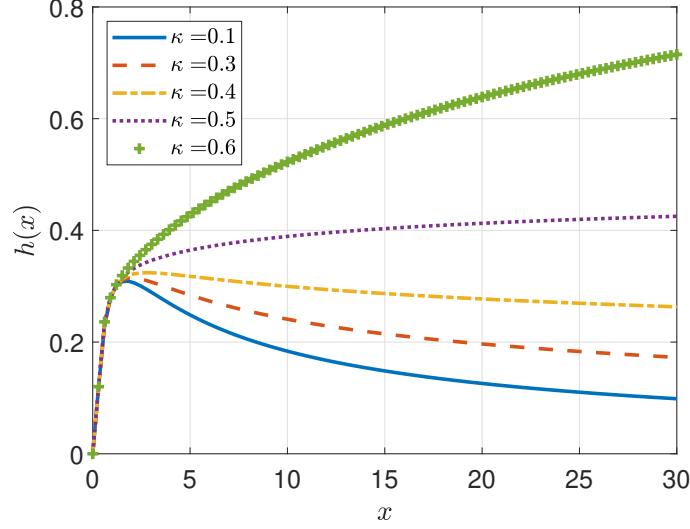


Fig. 10. Hazard function $h_\kappa(x)$ for the κ -lognormal distribution based on (39) for five different values of κ . All curves are obtained with $\mu = \sigma = 1$. The transition from asymptotically declining to increasing $h_\kappa(x)$ at $\kappa = 0.5$ is evident.

G. Failure of Simple Scaling Invariance

The lognormal distribution has a scaling property which ensures the invariance of the CDF under a scaling operation: If $X(\vartheta) \stackrel{d}{=} \text{LN}(\mu, \sigma)$ and $\lambda > 0$ then for $X'(\vartheta) = \lambda X(\vartheta)$ it follows that $X'(\vartheta) \stackrel{d}{=} \text{LN}(\mu', \sigma)$, where $\mu' = \mu + \ln \lambda$. It can easily be shown by replacing $\ln(x)$ in (24) with $\ln(\lambda x)$ and translating $\mu \mapsto \mu' = \mu + \ln \lambda$ that the CDF remains invariant. The κ -lognormal distribution lacks this simple scaling property for $\kappa > 0$.

To study the CDF transformation of $X'(\vartheta) = \lambda X(\vartheta)$, for $\lambda > 0$ we need the κ -logarithm composition law [57]

$$\ln_\kappa(\lambda x) = \ln_\kappa(\lambda) \sqrt{1 + \kappa^2 \ln_\kappa^2(x)} + \ln_\kappa(x) \sqrt{1 + \kappa^2 \ln_\kappa^2(\lambda)}$$

which shows that the mapping $(\ln_\kappa(\lambda x) - \mu)/\sigma \mapsto (\ln_\kappa(x) - \mu')/\sigma'$ is not possible in general for μ', σ' independent of x . There are two cases when such a mapping is approximately possible.

- 1) If $\kappa |\ln_\kappa(x)| \ll 1$ for all x such that the values of $f_X(x)$ in (22) exceed some arbitrary threshold (e.g., 10^{-6}), then the CDF is invariant under the mapping $\mu \mapsto \mu' = \mu \sqrt{1 + \kappa^2 \ln_\kappa^2(\lambda)} + \ln_\kappa(\lambda)$ and $\sigma \mapsto \sigma' = \sigma \sqrt{1 + \kappa^2 \ln_\kappa^2(\lambda)}$. The condition $\kappa |\ln_\kappa(x)| \ll 1$ is equivalent to $1 < x \ll \exp_\kappa(1/\kappa)$ or $1 > x \gg \exp_\kappa(-1/\kappa)$.
- 2) If $\kappa |\ln_\kappa(x)| \gg 1$ for all x such that $f_X(x)$ is not negligible, then the CDF is invariant under the mapping $\mu \mapsto \mu' = \mu \left[\sqrt{1 + \kappa^2 \ln_\kappa^2(\lambda)} + \kappa \ln_\kappa(\lambda) \right] + \ln_\kappa(\lambda)$ and $\sigma \mapsto \sigma' = \sigma \left[\sqrt{1 + \kappa^2 \ln_\kappa^2(\lambda)} + \kappa \ln_\kappa(\lambda) \right]$. The condition $\kappa |\ln_\kappa(x)| \gg 1$ is equivalent to $x \gg \exp_\kappa(1/\kappa)$ or $x \ll \exp_\kappa(-1/\kappa)$.

IV. κ -LOGNORMAL STOCHASTIC PROCESS

Definition 3 (κ -lognormal process): The κ -lognormal stochastic process $\{X(\mathbf{s}; \vartheta) : \mathbf{s} \in \mathbb{R}^d, \vartheta \in \Omega\}$ in the probability space (Ω, \mathcal{F}, P) is defined as the process obtained by applying the κ -exponential transformation on a scalar, real-valued Gaussian stochastic process $\{Y(\mathbf{s}; \vartheta)\}$ as follows

$$X(\mathbf{s}; \vartheta) \triangleq \exp_\kappa[Y(\mathbf{s}; \vartheta)] = \left(\sqrt{1 + \kappa^2 Y^2(\mathbf{s}; \vartheta)} + \kappa Y(\mathbf{s}; \vartheta) \right)^{1/\kappa}, \quad \kappa \geq 0, \quad (41)$$

The finite-dimensional distributions of the κ -lognormal process are given below in (43). The inverse transformation that recovers the latent Gaussian stochastic process is given by the κ -logarithm, that is,

$$Y(\mathbf{s}; \vartheta) \triangleq \ln_{\kappa} [X(\mathbf{s}; \vartheta)] = \frac{X^{\kappa}(\mathbf{s}; \vartheta) - X^{-\kappa}(\mathbf{s}; \vartheta)}{2\kappa}. \quad (42)$$

We focus on *weakly stationary* (also known as second-order stationary) stochastic processes with constant mean μ and covariance kernel $C_Y(\mathbf{s}, \mathbf{s}'; \boldsymbol{\theta})$ that depends on the input vectors purely via the lag $\mathbf{s} - \mathbf{s}'$, where $\mathbf{s}, \mathbf{s}' \in \mathbb{R}^d$ and $\boldsymbol{\theta} \in \mathbb{R}^m$ is the kernel parameter vector.

A. Joint Density of κ -Lognormal Processes

In order to derive the joint density of the κ -lognormal process we use Jacobi's multivariate theorem [1].

Theorem 5 (Jacobi's multivariate theorem): Let $\mathbf{X}(\vartheta) = (X_1(\vartheta), \dots, X_N(\vartheta))^{\top}$ and $\mathbf{Y}(\vartheta) = (Y_1(\vartheta), \dots, Y_N(\vartheta))^{\top}$ denote two N -dimensional continuously-valued random vectors; the index $i = 1, \dots, N$ refers to the input vector \mathbf{s}_i . The vector variable $\mathbf{Y}(\vartheta)$ is obtained by means of the transformation $\mathbf{Y}(\vartheta) = \mathbf{g}(\mathbf{X}(\vartheta))$, where $\mathbf{g}(\cdot)$ is a vector function with elements $Y_l = g_l(\mathbf{X})$, $l = 1, \dots, N$. The functions $g_l(\cdot)$ are assumed to be continuous, possess continuous partial derivatives with respect to all inputs, and define one-to-one mappings. Then, there exist unique inverse functions $g_l^{-1}(\cdot)$ such that $X_l(\vartheta) = g_l^{-1}(\mathbf{Y}(\vartheta))$.

In addition, the joint PDF $f_{\mathbf{Y}}(\mathbf{y})$ is given by means of the following equation

$$f_{\mathbf{X}}(\mathbf{x}) = f_{\mathbf{Y}}(\mathbf{g}(\mathbf{x})) |\det(\mathbb{J})|, \quad (43)$$

where \mathbb{J} is the Jacobian of the transformation $\mathbf{y} \mapsto \mathbf{x}$. \mathbb{J} is given by the following matrix of partial derivatives

$$\mathbb{J} = [J_{i,j}]_{i,j=1}^N, \quad (44a)$$

where

$$J_{i,j} = \frac{\partial g_i(\mathbf{x})}{\partial x_j}, \quad i, j = 1, \dots, N. \quad (44b)$$

For the κ -lognormal process, we apply Jacobi's multivariate theorem with the transformation $y_i = g_i(x_i)$, where $g_i(x_i) \triangleq \ln_{\kappa}(x_i)$. Therefore, $J_{i,j} = \delta_{i,j} \frac{\partial \ln_{\kappa}(x_i)}{\partial x_j}$, where $\delta_{i,j}$ is the Kronecker delta, leading to $J_{i,i} = \frac{1}{2} (x_i^{\kappa-1} + x_i^{-\kappa-1})$, for $i = 1, \dots, N$ and $J_{i,j} = 0$ for $i \neq j$. Hence, assuming that $\mathbf{Y} \stackrel{d}{=} \mathcal{N}(\boldsymbol{\mu}, \mathbf{C}_Y)$, the κ -lognormal joint PDF is given by

$$f_{\mathbf{X}}(\mathbf{x}) = \frac{1}{(2\sqrt{2\pi})^N |\det(\mathbf{C}_Y)|^{1/2}} e^{-\frac{1}{2}(\ln_{\kappa}(\mathbf{x}) - \boldsymbol{\mu})^{\top} \mathbf{C}_Y^{-1}(\ln_{\kappa}(\mathbf{x}) - \boldsymbol{\mu})} \prod_{i=1}^N (x_i^{\kappa-1} + x_i^{-\kappa-1}), \quad (45)$$

where $\ln_{\kappa}(\mathbf{x})$ and $\boldsymbol{\mu}$ are $N \times 1$ vectors with i -th elements $\ln_{\kappa}(x_i)$ and μ respectively for all $i = 1, \dots, N$. Furthermore, the PDF (45) can be extended to non-stationary models by considering proper covariance kernels or by introducing temporal dependence in $\boldsymbol{\mu}$.

B. Predictive Distribution

In this section, we formulate warped Gaussian process regression for the κ -lognormal stochastic process.

a) Warping: Let $\mathbf{x}_S \triangleq (x_1, \dots, x_N)^{\top}$ represent the sample values of the κ -lognormal process $X(\mathbf{s}; \vartheta)$ for respective features $\mathbb{S}_N = \{\mathbf{s}_1, \dots, \mathbf{s}_N\}$. The sampled values may contain a noise term $\{\epsilon_i\}_{i=1}^N$. To keep notation simple, we do not use a different symbol for “noise contaminated” data. However, the presence of noise is accounted for by including a diagonal noise variance term in the covariance kernel. Assume that we aim to estimate $X(\mathbf{s}_*; \vartheta)$ for a new input \mathbf{s}_* . Using the framework of Gaussian process regression [4], the answer involves the marginal conditional distribution of $X(\mathbf{s}_*; \vartheta)$. For processes with asymmetric probability distributions, the concept of warped Gaussian processes (w-GPs) is used [7], [8]. In w-GPs, the observation space is warped by means of a nonlinear monotonic transformation, so that learning and prediction are performed with a *latent Gaussian process*. In spatial statistics this approach is known as Gaussian anamorphosis [5], [6].

b) κ -logarithm warping: Herein, we study a warping transform implemented by means of the κ -logarithm, assuming that the resulting latent process $Y(\mathbf{s}; \vartheta)$ is a stationary Gaussian process with mean μ , variance σ^2 , and covariance kernel $C_Y(\mathbf{s} - \mathbf{s}')$ as in Definition 3. Furthermore, we allow for contamination of the sample by Gaussian white noise with variance σ_{ϵ}^2 .

c) *Prediction in latent space:* The latent-space sample vector $\mathbf{y}_S \triangleq (y_1, \dots, y_N)^\top$ is obtained by applying the κ -logarithm to each element of \mathbf{x}_S . For the latent Gaussian process $Y(\mathbf{s}; \vartheta)$ the marginal predictive distribution function $f_*(y_* | \mathbf{s}_*; \mathbf{y}_S, \mathbb{S}_N)$ becomes the conditional Gaussian $\mathcal{N}(\mu_*, \sigma_*^2)$. The posterior mean, μ_* , which represents the optimal forecast, \hat{y}_* , is given by

$$\mu_* = \mu + \mathbf{C}_Y(\mathbf{s}_*, \mathbb{S}_N) [\mathbf{C}_Y(\mathbb{S}_N, \mathbb{S}_N) + \sigma_\epsilon^2 \mathbf{I}]^{-1} (\mathbf{y}_S - \mu \mathbf{1}), \quad (46)$$

and the posterior variance by

$$\sigma_*^2 = \sigma^2 - \mathbf{C}_Y(\mathbf{s}_*, \mathbb{S}_N) [\mathbf{C}_Y(\mathbb{S}_N, \mathbb{S}_N) + \sigma_\epsilon^2 \mathbf{I}]^{-1} \mathbf{C}_Y^\top(\mathbf{s}_*, \mathbb{S}_N). \quad (47)$$

In the above, the following notation is used:

- $\mathbf{C}_Y(\mathbf{s}_*, \mathbb{S}_N)$ is the $1 \times N$ kernel vector with elements $C_Y(\mathbf{s}_*, \mathbf{s}_i)$, $i = 1, \dots, N$,
- $\mathbf{C}_Y(\mathbb{S}_N, \mathbb{S}_N)$ is the $N \times N$ kernel matrix with elements $C_Y(\mathbf{s}_i, \mathbf{s}_j)$, $i, j = 1, \dots, N$,
- \mathbf{I} is the $N \times N$ identity matrix,
- $\mathbf{1}$ is the $N \times 1$ vector of ones.

d) *Prediction in observation space:* Since the marginal predictive distribution $f(y_* | \mathbf{s}_*; \mathbf{y}_S, \mathbb{S}_N)$ is Gaussian, μ_* represents the mean, median, and mode of $f(y_* | \mathbf{s}_*; \mathbf{y}_S, \mathbb{S}_N)$ and the unequivocal optimal prediction in warped space. The predictive marginal PDF in the observation space is the following κ -lognormal, where $x_* \triangleq \exp_\kappa(y_*)$

$$f_*(x_* | \mathbf{s}_*; \mathbf{x}_S, \mathbb{S}_N) = \frac{1}{2\sqrt{2\pi}\sigma_*} e^{-(\ln_\kappa(x_*) - \mu_*)^2 / 2\sigma_*^2} (x_*^{\kappa-1} + x_*^{-\kappa-1}). \quad (48)$$

The principle of *quantile invariance* affirms that the quantiles of a probability distribution remain invariant under a monotonic transformation. Hence, if we assume that (i) $Y(\vartheta) = g(X(\vartheta)) \stackrel{d}{=} \mathcal{N}(0, 1)$, (ii) y_α is the $\alpha \in [0, 1]$ quantile, that is, $\Phi(y_\alpha) = \alpha$, then $F_X(x_\alpha) = \alpha$ where $x_\alpha = g^{-1}(y_\alpha)$ [6]. For κ -lognormal processes, $g(\cdot) = \ln_\kappa(\cdot)$ and $g^{-1}(\cdot) = \exp_\kappa(\cdot)$. Since $\Phi(\mu_*) = 0.5$, quantile invariance implies that the predictor $\hat{x}_* \triangleq \exp_\kappa(\mu_*)$ corresponds to the median of the predictive distribution (48). In warped space, the *prediction interval* at confidence level $(1 - \alpha) \times 100\%$ for $0 < \alpha < 1$ is $[\mu_* - z_{1-\alpha/2} \sigma_*, \mu_* + z_{1-\alpha/2} \sigma_*]$ where $z_{1-\alpha/2} = \Phi^{-1}(1 - \alpha/2)$ is the $(1 - \alpha/2) \times 100\%$ quantile of the standard normal distribution. For example, if $\alpha = 0.05$, $z_{1-\alpha/2} = \Phi^{-1}(0.975) = 1.96$. Then, based on the principle of quantile invariance, the respective *prediction interval in observation space* is given by

$$[g^{-1}(\mu_* - z_{1-\alpha/2} \sigma_*), g^{-1}(\mu_* + z_{1-\alpha/2} \sigma_*)]. \quad (49)$$

Remark 8 (Mode predictor): Even if $X(\mathbf{s}; \vartheta) \stackrel{d}{=} \kappa\text{LN}(\mu, \sigma, \kappa)$, the predictive distribution could be approximately Gaussian, namely, $f_*(x_* | \mathbf{s}_*; \mathbf{x}_S, \mathbb{S}_N) \stackrel{d}{=} \mathcal{N}(x_*, \sigma_*^2)$. As discussed in Section III-A (see Fig. 3), certain combinations of (μ, σ, κ) lead to nearly Gaussian PDF. In this case, the median predictor X at \mathbf{s}_* , that is, $\hat{x}_* \triangleq \exp_\kappa(\mu_*)$ is adequate. If, on the other hand, $f_*(x_* | \mathbf{s}_*; \mathbf{x}_S, \mathbb{S}_N)$ is significantly skewed, the mode predictor could be of interest

$$\hat{x}_{\text{mode}}(\mathbf{s}_*) = \operatorname{argmax}_{x_* \in \mathbb{R}} f_*(x_* | \mathbf{s}_*; \mathbf{x}_S, \mathbb{S}_N) = \operatorname{argmax}_{\{x_{*,r}\}_{r=1}^R} f_*(x_{*,r} | \mathbf{s}_*; \mathbf{x}_S, \mathbb{S}_N). \quad (50)$$

where $x_{*,r}$ for $r = 1, \dots, R$, represent the κ -th root of the zeros of the characteristic polynomial $p_1(z)$ (cf. Theorem 1).

V. ESTIMATION OF κ -LOGNORMAL PARAMETERS

A. Estimating the Marginal Distribution

a) *Marginal likelihood:* Maximizing the likelihood of the marginal κ -lognormal distribution with respect to the parameters given \mathbf{x}_S is equivalent to minimizing the respective negative log-likelihood (NLL). Based on (22), the NLL (normalized by the sample size N) for the marginal κ -lognormal distribution is given by

$$\text{NLL}(\beta) = \ln(2\sqrt{2\pi}\sigma) + \frac{1}{2N\sigma^2} \sum_{i=1}^N (\ln_\kappa(x_i) - \mu)^2 - \frac{1}{N} \sum_{i=1}^N \ln(x_i^{\kappa-1} + x_i^{-\kappa-1}), \quad (51)$$

where $\beta = (\mu, \sigma, \kappa)^\top$. Respectively, the estimates of the optimal parameters $\hat{\mu}, \hat{\sigma}, \hat{\kappa}$ are given by

$$(\hat{\mu}, \hat{\sigma}, \hat{\kappa}) = \arg \min_{\beta} \text{NLL}(\beta). \quad (52)$$

b) *Gradient of NLL*: The gradient $\nabla_{\beta} \text{NLL}(\beta) = \left(\frac{\partial \text{NLL}(\beta)}{\partial \mu}, \frac{\partial \text{NLL}(\beta)}{\partial \sigma}, \frac{\partial \text{NLL}(\beta)}{\partial \kappa} \right)^\top$ of the NLL (51) involves the following partial derivatives

$$\frac{\partial \text{NLL}(\beta)}{\partial \mu} = -\frac{1}{N\sigma^2} \sum_{i=1}^N (\ln_{\kappa}(x_i) - \mu), \quad (53a)$$

$$\frac{\partial \text{NLL}(\beta)}{\partial \sigma} = \frac{1}{\sigma} - \frac{1}{N\sigma^3} \sum_{i=1}^N (\ln_{\kappa}(x_i) - \mu)^2, \quad (53b)$$

$$\frac{\partial \text{NLL}(\beta)}{\partial \kappa} = \frac{1}{N\sigma^2} \sum_{i=1}^N (\ln_{\kappa}(x_i) - \mu) \left[\frac{\ln(x_i) (x_i^{\kappa} + x_i^{-\kappa})}{2\kappa} - \frac{\ln_{\kappa}(x_i)}{\kappa} \right] - \frac{1}{N} \sum_{i=1}^N \frac{\ln(x_i) (x_i^{\kappa-1} - x_i^{-\kappa-1})}{(x_i^{\kappa-1} + x_i^{-\kappa-1})}. \quad (53c)$$

The system of equations (53) that determines NLL stationary points is not in general analytically solvable. Hence, we are forced to seek numerical solutions by means of optimization methods; the latter rely on initial guesses for the parameters. Finally, the NLL Hessian matrix is evaluated in Appendix E.

Remark 9 (Initialization of parameter vector): Note that the point $\beta_0 \triangleq (\mu_0, \sigma_0, \kappa_0)^\top$ with $\kappa_0 = 0$, $\mu_0 = \frac{1}{N} \sum_{i=1}^N \ln(x_i)$, and $\sigma_0^2 = \frac{1}{N} \sum_{i=1}^N (\ln(x_i) - \mu)^2$ is a stationary point of the NLL. It is straightforward to verify that the NLL partial derivatives with respect to μ and σ vanish at this point according to (53a)-(53b). It also follows from (53c) that the derivative $\partial \text{NLL}(\beta)/\partial \kappa$ also vanishes at $\kappa = 0$: since $\lim_{\kappa \rightarrow 0} x_i^{\kappa} = \lim_{\kappa \rightarrow 0} x_i^{-\kappa} = 1$, it follows that $\lim_{\kappa \rightarrow 0} \frac{1}{2\kappa} [\ln(x_i) (x_i^{\kappa} + x_i^{-\kappa}) - 2 \ln_{\kappa}(x_i)] = 0$ and $\lim_{\kappa \rightarrow 0} (x_i^{\kappa-1} - x_i^{-\kappa-1}) = 0$; thus, both summands participating in $\partial \text{NLL}(\beta)/\partial \kappa$ vanish. Therefore, using β_0 as initial guess in a gradient descent or a naive Newton's algorithm will lead to the lognormal distribution.

B. Estimating Joint Dependence

A κ -lognormal process $X(\mathbf{s}; \vartheta)$, as specified in Definition 3, involves the parameter triplet $\beta = (\mu, \sigma, \kappa)^\top$ of the marginal PDF, and the parameters θ of the covariance kernel $C_Y(\mathbf{r}; \theta)$ associated with $Y(\mathbf{s}; \vartheta) = \ln_{\kappa}[X(\mathbf{s}; \vartheta)]$. MLE requires optimization of the following NLL function

$$\begin{aligned} \text{NLL}(\beta, \theta) = & \frac{1}{2} \ln [\sigma^2{}^N \det \rho(\theta)] + \frac{1}{2\sigma^2 N} (\mathbf{y}_S - \mu \mathbf{I})^\top \rho^{-1}(\theta) (\mathbf{y}_S - \mu \mathbf{I}) \\ & + \frac{N}{2} \ln 2\pi - \sum_{i=1}^N \ln (x_i^{\kappa-1} + x_i^{-\kappa-1}), \end{aligned} \quad (54)$$

where $\mathbf{y}_S = \ln_{\kappa}(\mathbf{x}_S)$, \mathbf{I} is an $N \times 1$ vector of ones and $\rho(\theta)$ is the $N \times N$ correlation matrix such that $\rho_{i,j} \triangleq C_Y(\mathbf{s}_i - \mathbf{s}_j)/\sigma^2$. Based on numerical experiments, we observed that optimization of the parameter vector $\zeta = (\theta^\top, \beta^\top)^\top$ by means of local optimization methods can lead to sub-optimal results. For certain problems (e.g., when estimating parameters for an ensemble of many realizations), global optimization methods may be prohibitively expensive. The estimation procedure that we propose employs profile likelihood and involves the following steps:

- 1) Determine the parameters $\beta \triangleq (\mu, \sigma, \kappa)^\top$ using maximum likelihood estimation (MLE) to fit the data to the marginal κ -lognormal distribution (cf. Section V-A). This step is sufficient if only the marginal dependence is of interest.
- 2) Generate the transformed dataset $\hat{\mathbf{y}}_S \triangleq (\ln_{\kappa}(x_1), \dots, \ln_{\kappa}(x_N))^\top$ by means of the κ -logarithm transformation with $\kappa = \hat{\kappa}$.
- 3) Finally, keep $\hat{\kappa}$ fixed and apply MLE to estimate optimal parameters μ, σ, θ using $\hat{\mathbf{y}}_S$.

VI. APPLICATIONS

In this section we apply the formalism developed above to simulated and real data. In the Supplement (Section 3), we provide additional comparisons between the lognormal and κ -lognormal distributions.

A. Estimation of Marginal Distribution from Simulated Data

To generate independent $\kappa\text{LN}(\mu, \sigma, \kappa)$ variates, we generate a $N \times 1$ random vector \mathbf{y} drawn from $\mathcal{N}(0, 1)$ and then apply the κ -exponential as follows to generate synthetic data

$$\mathbf{x} = \exp_{\kappa}(\mu + \sigma \mathbf{y}).$$

We then estimate the $\kappa\text{LN}(\mu, \sigma, \kappa)$ parameters from the samples using MLE and the simpler quantile fitting (described below).

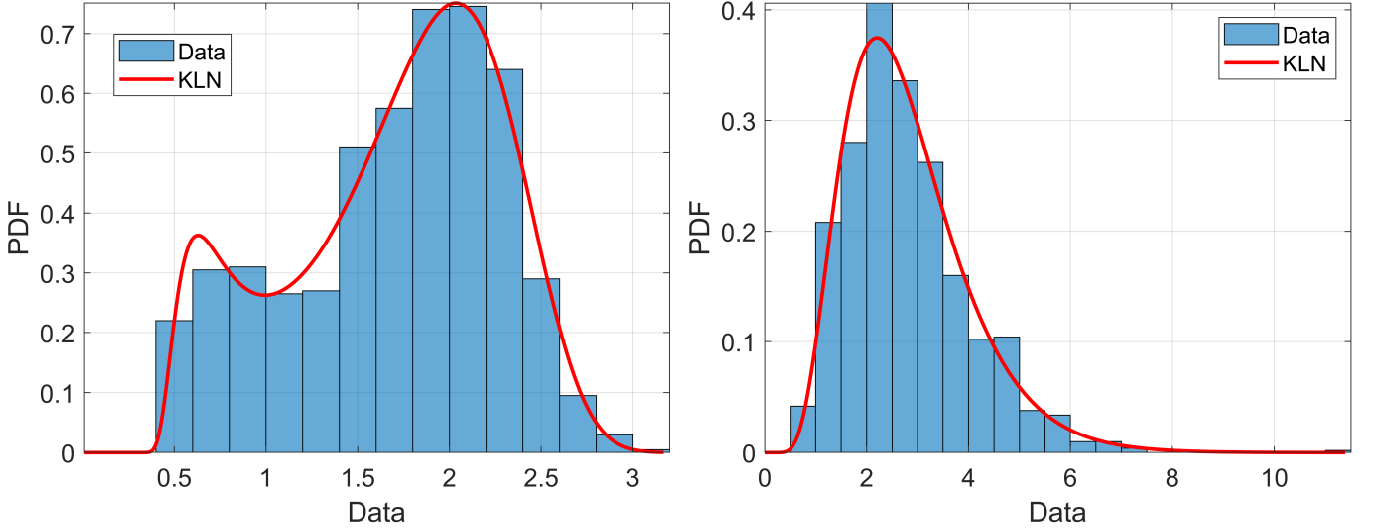


Fig. 11. Histograms and ML-estimated PDFs obtained from samples comprising 1000 random numbers from the $\kappa\text{LN}(\mu, \sigma, \kappa)$ distribution. **Left.** Model A: $\mu = 1, \sigma = 1, \kappa = 3$. The MLE parameter vector for Model A is $(0.92, 0.94, 2.89)$. **Right.** Model B: $\kappa\text{LN}(\mu, \sigma, \kappa)$ with $\mu = 1, \sigma = 0.5, \kappa = 0.5$. The MLE parameter vector for Model B is $(1.00, 0.51, 0.52)$.

a) *MLE*: We propose the following strategy to determine initial guesses for the parameters: (i) First, we select an initial κ_0 ; if the histogram shows signs of bimodality, we set $\kappa_0 > 1$. (ii) Then, we calculate the sample-based median, $\hat{\mu}_{0.5}$, and estimate μ_0 by inverting (23), which yields $\mu_0 = \ln_{\kappa}(\hat{\mu}_{0.5}, \kappa)$. (iii) Finally, we estimate σ_0 by taking advantage of (25) which connects σ to the quantiles of the distribution, assuming μ and κ are known. The initial guess becomes

$$\sigma_0 = \frac{1}{M} \sum_{m=1}^M \frac{\ln_{\kappa}(\hat{Q}(p_m), \kappa_0) - \mu_0}{\sqrt{2} \operatorname{erf}^{-1}(2p_m - 1)}, \quad (55)$$

where $\hat{Q}(p_m)$ are sample-based quantiles for M arbitrarily selected probability levels p_m . Herein, we use $N = 10^3$ and $p_m = 0.01m$, where $m = 1, \dots, M = 99$.

The MLE solution is derived using the multistart global optimization method [69] (in the Matlab `GlobalSearch` function). In deriving the results shown in Fig. 11 and Table II, we use as initial guess $\kappa_0 = 1.5$, while μ_0 and σ_0 are calculated as described above.

b) *Quantile Fitting*: This procedure aims to estimate the $\kappa\text{LN}(\mu, \sigma, \kappa)$ parameters by matching the empirical and model-based quantiles. It provides a computationally easier optimization problem than MLE. We estimate the optimal parameters by minimizing the following univariate cost function

$$u(\kappa) = \sqrt{\sum_{m=1}^M [\hat{Q}(p_m) - Q(p_m; \hat{\mu}(\kappa), \hat{\sigma}(\kappa), \kappa)]^2}, \quad \kappa \in [0, \kappa_{\max}], \quad (56)$$

where $\hat{\mu}(\kappa) = \ln_{\kappa}(\hat{\mu}_{0.5}, \kappa)$ and $\hat{\sigma}(\kappa)$ is obtained by means of $\hat{\sigma}(\kappa) = [\ln_{\kappa}(\hat{Q}(0.95), \kappa) - \hat{\mu}(\kappa)] / \sqrt{2} \operatorname{erf}^{-1}(0.9)$, that is from (25) using the empirical 95% quantile. The optimal parameter vector is then given by $\hat{\kappa} = \arg \min_{\kappa \in [0, \kappa_{\max}]} u(\kappa)$, while $\hat{\mu}, \hat{\sigma}$ are obtained by means of $\hat{\mu} = \ln_{\kappa}(\hat{\mu}_{0.5}, \hat{\kappa})$ and by replacing κ_0 with $\hat{\kappa}$ and μ_0 with $\hat{\mu}$ in (55) to obtain $\hat{\sigma}$.

Table II provides statistics (averages and standard deviations) of the $(\hat{\mu}, \hat{\sigma}, \hat{\kappa})$ estimates based on an ensemble of $N_{\text{sim}} = 100$ realizations for the κ -lognormal distribution models A and B. The estimates are obtained by means of MLE and quantile fitting as described above. The ensemble-averaged parameter estimates obtained by means of both methods are quite similar and very close to the population parameters. On the other hand, the MLE-derived parameters have smaller standard deviations than those obtained by quantile fitting.

Figure 11 shows the histograms obtained from single realizations of two $\kappa\text{LN}(\mu, \sigma, \kappa)$ distributions: Model A with parameters $\mu = 1, \sigma = 1, \kappa = 3$ and Model B with $\mu = 1, \sigma = 0.5, \kappa = 0.5$. The plots also show the PDF curves obtained from (22) using ML estimates $(\hat{\mu}, \hat{\sigma}, \hat{\kappa})$ of the distribution parameters. Excellent agreement is observed between the sample histograms and the PDF curves, including faithful representation of the bimodality for Model A.

B. Estimation of Marginal Distribution for Berea Sandstone Permeability

We analyze a Berea sandstone permeability data set that contains 1600 mini-permeameter measurements sampled on a 40cm×40cm square grid with a 1-cm grid step. The summary statistics of the dataset are given in Table III.

TABLE II

STATISTICS OF ESTIMATES $(\hat{\mu}, \hat{\sigma}, \hat{\kappa})$ DERIVED BY MAXIMUM LIKELIHOOD ESTIMATION (MLE) AND QUANTILE FITTING (QF). THE AVERAGES, $\langle \cdot \rangle$ AND STANDARD DEVIATIONS, $\text{std}(\cdot)$ ARE BASED ON ENSEMBLES OF $N_{\text{sim}} = 100$ REALIZATIONS EACH OF WHICH COMPRISES 1000 RANDOM NUMBERS SIMULATED FROM $\kappa\text{LN}(\mu, \sigma, \kappa)$. TWO DIFFERENT EXPERIMENTS ARE CONDUCTED THAT SIMULATE THE PDFS SHOWN IN FIG. 11.

Parameter estimates	$\langle \hat{\mu} \rangle$	$\langle \hat{\sigma} \rangle$	$\langle \hat{\kappa} \rangle$	$\text{std}(\hat{\mu})$	$\text{std}(\hat{\sigma})$	$\text{std}(\hat{\kappa})$
First simulation experiment: $\mu = 1, \sigma = 1, \kappa = 3$						
MLE	1.0010	1.0011	2.9998	0.0561	0.0567	0.0976
QF	1.0007	1.0006	2.9990	0.0748	0.0814	0.1382
Second simulation experiment: $\mu = 1, \sigma = 0.5, \kappa = 0.5$						
MLE	1.0013	0.4975	0.4933	0.0208	0.0206	0.0668
QF	1.0013	0.4980	0.4880	0.0274	0.0266	0.0913

TABLE III

STATISTICS OF BEREA SANDSTONE PERMEABILITY MEASUREMENTS. THE UNITS ARE IN MILLIDARCIES (MD).

Mean (md)	Median (md)	Min (md)	Max (md)	Standard deviation (md)	Skewness	Kurtosis
52.53	55.00	19.50	111.50	15.78	0.38	3.13

a) *Profile likelihood*: We study the dependence of the optimized NLL obtained for selected values of $\kappa \in \{\kappa_1, \dots, \kappa_\ell\}$. For each $\kappa_i, i = 1, \dots, \ell$, we calculate the κ -deformed dataset $\mathbf{y}_S^{(i)} = (\ln_\kappa(x_1), \dots, \ln_\kappa(x_N))$, where $\kappa = \kappa_i$. We then determine $\hat{\mu}_i$ and $\hat{\sigma}_i$ by maximizing the likelihood of the normal distribution for $\mathbf{y}_S^{(i)}$. The $\hat{\mu}_i$ and $\hat{\sigma}_i$ are inserted in (51) to obtain the respective NLL($\hat{\mu}_i, \hat{\sigma}_i \mid \kappa_i$). This leads to the profile NLL curve shown in Fig. 12, which features a minimum of NLL at $\hat{\kappa} \approx 0.556$, that is, $\hat{\kappa} = \min_\kappa \{\min_{\mu, \sigma} \text{NLL}(\mu, \sigma \mid \kappa)\}$. ML estimation for $\kappa = 0$ (lognormal distribution) returns $\hat{\mu}_0 \approx 3.97$ and $\hat{\sigma}_0 \approx 0.30$. For $\hat{\kappa} \approx 0.556$ it follows that $\hat{\mu} \approx 8.2$ and $\hat{\sigma} \approx 1.35$. The κ -lognormal distribution corresponding to $(\hat{\mu}, \hat{\sigma}, \hat{\kappa})$ is unimodal with its mode located at $x_{\text{mode}} \approx 54.33$. Figure 13 presents NLL streamlines (lines that are tangential to the local gradient) for the Berea data in the (μ, σ) plane for $\kappa = 0.556$. The stationary point in this plane is $(8.20, 1.35)$, in agreement with the profile likelihood result; the streamlines radiate away from the stationary point indicating increasing gradient.

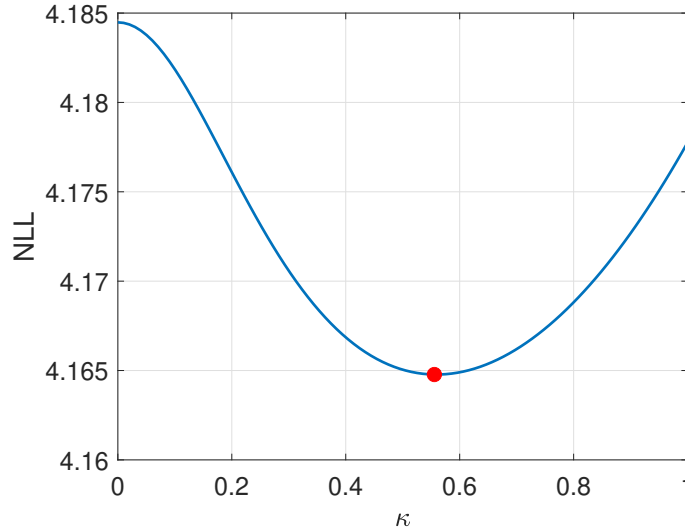


Fig. 12. Profile NLL curve (NLL per site) as a function of κ for the Berea permeability data, obtained from (51). The parameters $\hat{\mu}_i$ and $\hat{\sigma}_i$ for a given κ_i are determined by maximizing the likelihood of the normal distribution for the κ -deformed dataset $\mathbf{y}_S = \ln_\kappa(\mathbf{x}_S)$.

Table IV lists the optimal parameters based on ML estimates of the κ -lognormal and lognormal distributions to the Berea dataset. MLE was conducted in the full parameter space (μ, σ, κ) using global optimization to avoid potential local traps. The table also contains the optimal NLL per site and values of Akaike and Bayesian information criteria (AIC and BIC). Both criteria favor the κ -lognormal distribution. The globally-optimized MLE parameter estimates are very close to those obtained by means of profile likelihood.

b) *Comparison of lognormal and κ -lognormal models*: The histogram of Berea permeability is shown in Fig. 14 (left frame) with superimposed PDF curves for the optimal lognormal and κ -lognormal distributions. As evidenced in the plot, the mode of the κ -lognormal model is closer to the peak of the histogram than that of the lognormal; in addition, the κ -lognormal right tail decays faster than the lognormal, also in agreement with the histogram. The comparison of the PDF tails is more compelling in terms of the quantile-quantile (Q-Q) plot (right frame of Fig. 14). The Q-Q plots are generated by the set of

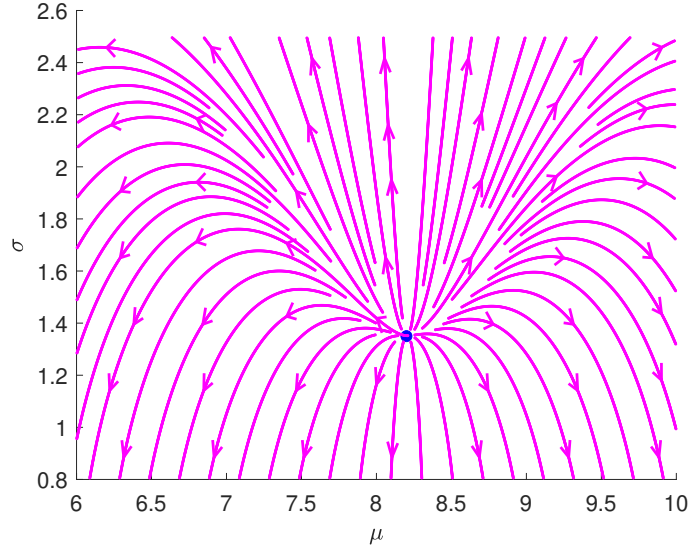


Fig. 13. NLL Streamlines for the Berea permeability data on the (μ, σ) plane obtained using the NLL gradient (53) for $\kappa = 0.556$.

TABLE IV

STATISTICS OF THE BEREA PERMEABILITY DATASET. COLUMNS 2-4 CONTAIN THE OPTIMAL κ -LOGNORMAL PARAMETERS DERIVED BY MLE. COLUMNS 5-7 DISPLAY RESPECTIVELY THE NEGATIVE LOG-LIKELIHOOD (NLL) PER SAMPLING LOCATION, AS WELL AS THE AIC AND BIC SELECTION CRITERIA. COLUMNS 8-9 CONTAIN THE OPTIMAL LOGNORMAL PARAMETERS, AND COLUMNS 10-12 THE NLL PER SITE, THE AIC AND BIC RESPECTIVELY. BOLD FONT INDICATES THE MODEL WITH THE LOWEST AIC AND BIC.

κ -Lognormal						Lognormal				
μ	σ	κ	NLL	AIC	BIC	μ_0	σ_0	NLL ₀	AIC ₀	BIC ₀
8.26	1.37	0.56	4.16	13333.28	13349.41	3.97	0.30	4.18	13394.34	13405.09

N_Q points $(Q_{LN}(p_i), Q_{KLN}(p_i))$, $i = 0, \dots, N_Q - 1$, where $p_i = 0.01 + 0.98i/(N_Q - 1)$ for $i = 0, 1, \dots, N_Q - 1$. We use $N_Q = 500$ herein leading to 500 probability levels in the interval $[0.1, 0.99]$. The quantiles $Q_{LN}(p_i)$, $Q_{KLN}(p_i)$ are given by (19) and (25) respectively using the ML estimates for the respective μ and σ . This plot highlights the fact that the right-tail quantiles of the lognormal exceed those of the κ -lognormal distribution.

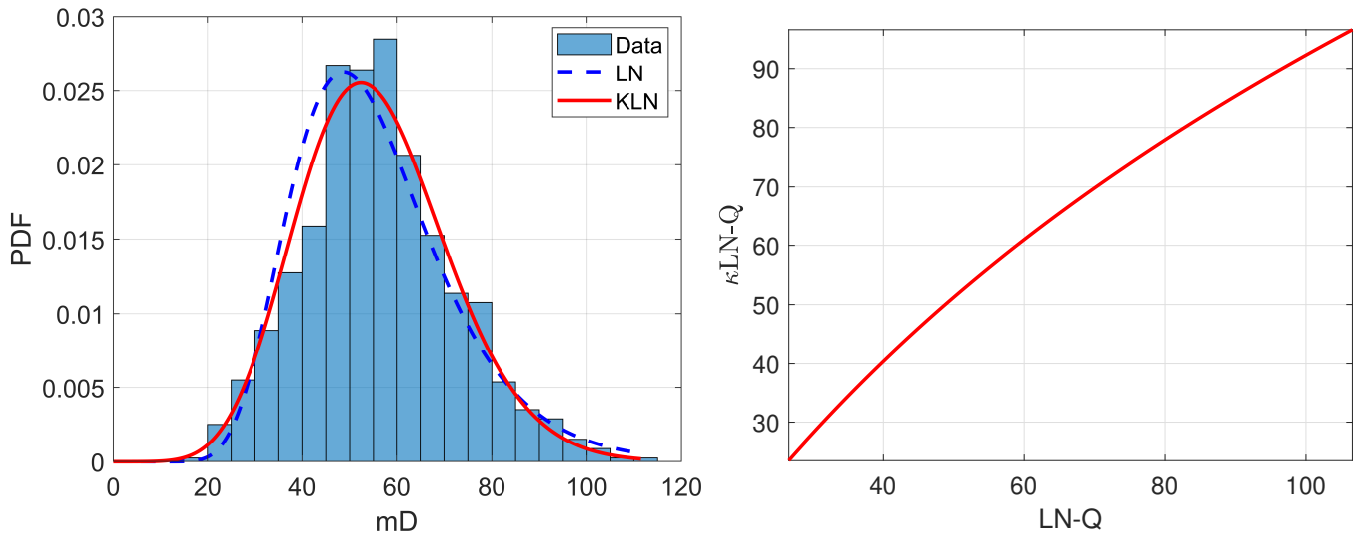


Fig. 14. **Left:** Histogram of Berea permeability data and MLE fits of the lognormal PDF (blue broken line) and the κ -lognormal PDF (continuous line). The horizontal axis measures permeability and the units used are millidarcy (mD). **Right:** Q-Q plot of the lognormal quantiles (horizontal axis) versus the respective κ -lognormal quantiles (vertical axis). The quantiles are obtained from the best-fit distributions for the Berea data. The units of both axes are in millidarcy.

C. Time series forecasting using κ -lognormal processes

This section investigates forecasting for stochastic processes $\{X(t; \vartheta)\}$ defined by means of $X(t; \vartheta) = \exp_{\kappa}[Y(t; \vartheta)]$, where $\{Y(t; \vartheta)\}$ is a scalar, real-valued Gaussian stochastic process with mean μ , variance σ^2 and correlation kernel $\rho_Y(\tau; \theta)$; t is the time index and $\tau = t - t'$ is the time lag. The covariance kernel is given by $C_Y = \sigma^2 \rho_Y$. Then, according to Definition 3, $\{X(t; \vartheta)\}$ is a κ -lognormal stationary stochastic process. We conduct forecasting in the framework of warped Gaussian process regression (cf. Section IV-B).

a) *Simulation method*: We use the multivariate normal (MVN) simulation method [70, p. 50] to generate samples of $\{X(t; \vartheta)\}$, namely time series comprising N times $t_k \in [0, T]$, for $k = 1, \dots, N$. The temporal dependence is determined by the $N \times N$ covariance matrix \mathbf{C}_Y with elements $[\mathbf{C}_Y]_{k,l} = C_Y(t_k - t_l)$, for $k, l = 1, \dots, N$, where $C_Y(\tau)$ is the covariance kernel. If $\mathbf{C}_Y = \mathbf{A}\mathbf{A}^T$ is a factorization of \mathbf{C}_Y , and \mathbf{z} is an $N \times 1$ vector of independent random numbers from $\mathcal{N}(0, 1)$, the $N \times 1$ vector $\mathbf{y} = \mathbf{A}\mathbf{z}$ is a realization of a zero-mean normal stochastic process with covariance kernel $C_Y(\cdot)$. Then, $\mathbf{x} = \exp_{\kappa}(\mu + \sigma\mathbf{y})$ provides a realization of the $\kappa\text{LN}(\mu, \mathbf{C}_Y, \kappa)$ stochastic process with joint PDF given by (45). We use the principal square root factorization of \mathbf{C}_Y for numerical stability [71].

b) *Study design*: We follow the procedure described below.

- 1) $N_{\text{sim}} = 500$ realizations are generated using the MVN method. Each realization represents a correlated sequence sampled at times $t_n = n$ where $n = 1, \dots, N$ and $N = 2^{10}$. The κ -lognormal marginal is determined by the parameter vector $\beta = (\mu, \sigma, \kappa)$, where $\mu = 1$, $\sigma = 1$, $\kappa = 3$. As shown in Figs. 4 and 11, this combination of parameters generates a bimodal distribution, which is clearly non-Gaussian. $C_Y(\tau; \theta, \sigma)$ is given by the linear damped harmonic oscillator (LDHO) kernel [72] in the underdamped regime

$$C_Y(\tau; \theta, \sigma) = \sigma^2 e^{-|\tau|/(2\tau_c)} \left[\cos(\omega_d \tau) + \frac{1}{2\omega_d \tau_c} \sin(\omega_d |\tau|) \right], \quad (57)$$

where $\theta = (\tau_c, \omega_d)^T$, $\tau_c = 30$ is the relaxation (damping) time and $\omega_d = 2\pi/50 \approx 0.126$ is the natural frequency of the damped oscillations.

- 2) Each realization is split into a training set containing $N_{\text{tr}} = 973$ data points, $N_{\text{tr}} = \lfloor 0.95 N \rfloor$, and a test set that comprises the remaining $N_{\text{te}} = 51$ points.
- 3) The model parameter vector $\zeta \triangleq (\beta^T, \theta^T)^T$ is estimated over the training set using MLE as outlined in Section V-B.
- 4) The optimal model, specified by $\hat{\zeta} = (\hat{\mu}, \hat{\sigma}, \hat{\kappa}, \hat{\omega}_d, \hat{\tau}_c)$ is used to forecast the series at the test-set times $t_{N_{\text{tr}}+k}$, $k = 1, \dots, N_{\text{te}}$. We employ the multi-step (multiple output) forecasting strategy (without recursive feedback of predictions into the training set). Both median-based and mode-based predictions are used, respectively, given by the median of the predictive marginal PDF (48) and the mode predictor (50).
- 5) We quantify the forecasting performance using different cross validation measures calculated by comparing the forecasts to the true test values. Finally, we average the cross-validation measures over the N_{sim} realizations.

c) *Parameter estimation*: We apply MLE as described in Section V-B to estimate β, θ . As initial estimates for μ and σ we use the values obtained from the marginal NLL minimization, while $\hat{\tau}_{c;0} = T/2$ and $\hat{\omega}_{d;0} = 2\pi/(T/10)$ are used for θ . The distribution of the ML parameter estimates for the ensemble of 500 realizations is summarized in the violin plots of Fig. 15. Each plot shows the distribution of the ratio $\hat{\theta}_{i;n}/\theta_i$, where $\hat{\theta}_{i;n}$ is the estimate of the i -th parameter from the set $(\mu, \sigma, \kappa, \tau_c, \omega_d)$ based on the n -th realization ($n = 1, \dots, 500$), and θ_i is the true value. We excluded 31 realizations that produce unrealistic cyclical frequency estimates $\hat{\omega}_d > 1$. As evidenced in these plots, the medians of $\hat{\sigma}$ and $\hat{\omega}_d$, respectively, underestimate the true standard deviation and relaxation time. We suspect that this is due to the fact that the persistence of correlations, as expressed by the ratios $N/\tau_c \approx 34$ and $N/T_d = N\omega_d/2\pi \approx 20.5$, does not allow fully resolving the variability of $X(t; \vartheta)$. For computational reasons, NLL optimization is conducted using local search with the interior-point algorithm. Hence, such large $\hat{\omega}_d$ are likely due to local optima of the NLL function.

d) *Forecasting*: Multi-step forecasts are generated using both the median and mode predictors. The median predictor is based on $\hat{\mu}_{0.5} \triangleq \exp_{\kappa}(\mu_*)$, where μ_* is the conditional mean of the latent Gaussian process at s_* given by (46). The mode predictor is based on (50). The *cross-validation* (CV) measures involve the following: Mean error (ME); mean absolute error (MAE); mean absolute relative error (MARE); root mean square error (RMSE); relative RMSE (RRMSE); Pearson correlation coefficient (R). Violin plots of the CV measures obtained from $N_{\text{sim}} = 500$ realizations are shown in Fig. 16. The plots present kernel density estimates of the PDF for each CV measure. Two notable features are: (i) the long RRMSE tail, which is due to high error values for low process values and (ii) the long lower tail of R that extends into negative values for a small number of realizations, indicating poor correlation of the forecasts with the true values. We believe that such results are due to trapping of the NLL optimization in local minima, and they could be avoided if a global optimization method is used.

Average CV measures over the N_{sim} -state ensemble are listed in Table V. The median-based predictor $\hat{\mu}_{0.5}$ outperforms the mode-based predictor with respect to all the measures. We also calculate CV measures by omitting 31 realizations of the process that lead to unreasonably high frequency estimates $\hat{\omega}_d > 1$ (recall that $\omega_d \approx 0.126$). Somewhat surprisingly, this does not seem to improve the forecasting performance.

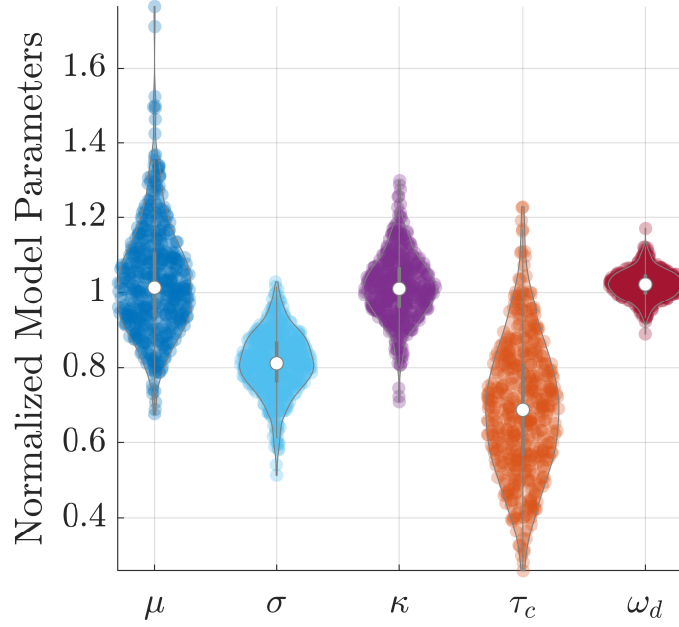


Fig. 15. Violin plots displaying the distribution of the estimated model parameter estimates based on 500 realizations of the κ -lognormal process with harmonic oscillator kernel (57). The estimates are normalized by dividing with the true model parameter values, namely $\mu = 1$, $\sigma = 1$, $\kappa = 3$, $\tau_c = 30$ and $\omega_d = 2\pi/50$. The open circles in the middle of the violins mark the median of the distribution. The estimates from 31 realizations that yield $\hat{\omega}_d > 1$ are not presented in this plot.

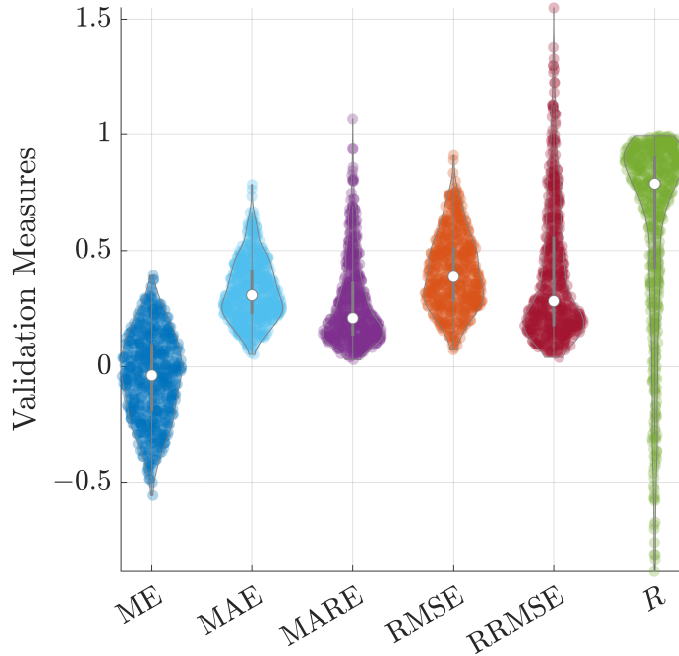


Fig. 16. Violin plots displaying the distribution of cross-validation measures based on 500 realizations of the κ -lognormal process with harmonic oscillator kernel (57) and the following parameters: $\mu = 1$, $\sigma = 1$, $\kappa = 3$, $\tau_c = 30$ and $\omega_d = 2\pi/50$. The open circles in the middle of the violins mark the median.

e) Single realization analysis: We focus on the first realization of the ensemble, namely the time series shown in Fig. 17. The ML estimated parameter vector is $\hat{\zeta} = (\hat{\mu}, \hat{\sigma}, \hat{\kappa}, \hat{\tau}_c, \hat{\omega}_d) \approx (0.82, 0.79, 2.82, 23.63, 0.13)$ —using precision of two decimal places. The optimal NLL for this solution is $\text{NLL} \approx -2.3 \times 10^{-3}$. The left frame of Fig. 18 displays the sample histogram (bars), the κ -lognormal PDF for the population parameter vector $\zeta = (1, 1, 3, 30, 0.13)^\top$ (dash-dot line), the κ -lognormal PDF obtained for the MLE $\hat{\zeta}$ (broken line), and the best-fit lognormal PDF, also derived by means of MLE (continuous line). The lognormal PDF is not a good fit for the bimodality of the underlying process, while the MLE κ -lognormal PDF provides a better match with the sample histogram and the model PDF. The right frame of Fig. 18 confirms the agreement between the model LDHO kernel $C_Y(\tau)$ (continuous line) based on σ , τ_c , and ω_d with the LDHO kernel obtained by means of $\hat{\sigma}$, $\hat{\tau}_c$, and

TABLE V

AVERAGE CROSS-VALIDATION MEASURES OVER THE 51-STEP FORECASTING HORIZON. THE REPORTED VALUES REPRESENT AVERAGES OVER 500 REALIZATIONS OF THE LDHO STOCHASTIC PROCESS WITH PARAMETERS $\mu = 1$, $\sigma = 1$, $\kappa = 3$, $\tau_c = 30$ AND $\omega_d = 2\pi/50$. THE MEDIAN PREDICTOR IS BASED ON $\exp_\kappa(\mu_*)$ WHERE μ_* IS GIVEN BY (46), WHILE THE MODE PREDICTOR IS BASED ON (50). THE “NO-OUTLIERS” FORECASTS EXCLUDE REALIZATIONS WITH VERY HIGH ESTIMATES OF ω_d .

Prediction Method	ME	MAE	MARE	RMSE	RRMSE	R
Median predictor	-0.0472	0.3254	0.2732	0.4079	0.3987	0.6055
Mode predictor	-0.1011	0.3475	0.2954	0.4569	0.4520	0.5628
Median (no outliers)	-0.0508	0.3292	0.2785	0.4125	0.4074	0.5936
Mode (no outliers)	-0.1078	0.3528	0.3023	0.4644	0.4640	0.5483

$\hat{\omega}_d$ (broken line). Figure 19 (left frame) shows the forecasts over the test set (51 points) using both the median-based and mode-based (50) predictors as well as the 95% prediction intervals (49). The mode-based predictor yields forecasts that track the true test values better than the median-based predictor. This performance is confirmed by the CV measures reported in Table VI. However, the superior performance of the mode-based predictor is not universal as shown by Table V, which reveals better overall performance of the median predictor over the 500 realizations. The right frame of Fig. 19 displays the evolution of the predictive marginal PDF (48) (increasing mean and standard deviation) for the first 15 test points.

For short-term forecasts, the one-step-ahead strategy is more suitable. In this case, the model which is determined from the training data is used without updating as in multi-step forecasting. However, the one-step-ahead forecasts are generated in a recursive manner, by extending the training data through inclusion of the test values from earlier times. For one-step-ahead forecasting (not shown), all the predictions are in excellent agreement with the true test values.

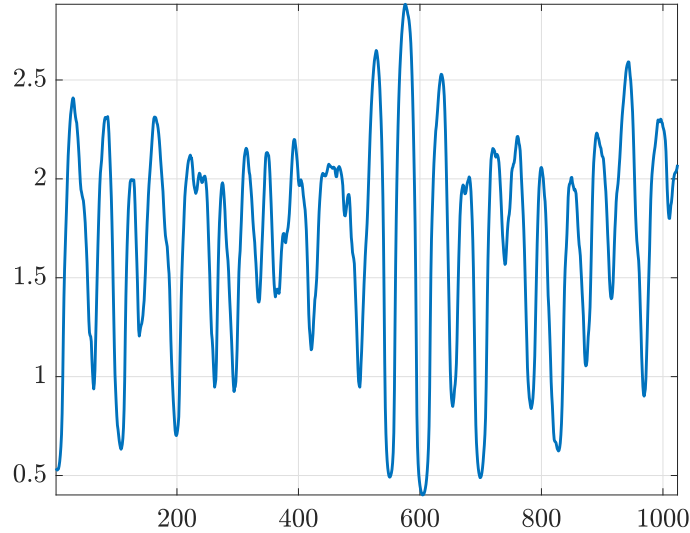


Fig. 17. Time series generated from the κ -LN process with joint PDF (45) and LDHO covariance kernel (57) with parameter set $\zeta = (\mu, \sigma, \kappa, \tau_c, \omega_d) = (1, 1, 3, 30, 0.13)$.

TABLE VI

CROSS-VALIDATION MEASURES OVER THE 51-STEP FORECASTING HORIZON BASED ON A SINGLE RANDOM REALIZATION (CF. FIG. 17) OF THE STOCHASTIC PROCESS WITH LDHO KERNEL (57) AND PARAMETERS $\mu = 1$, $\sigma = 1$, $\kappa = 3$, $\tau_c = 30$ AND $\omega_d = 2\pi/50$. THE MEDIAN PREDICTOR IS BASED ON $\exp_\kappa(\mu_*)$ WHERE μ_* IS GIVEN BY (46), WHILE THE MODE PREDICTOR IS BASED ON (50).

Prediction Method	ME	MAE	MARE	RMSE	RRMSE	R
Median predictor	0.2612	0.2642	0.1296	0.3251	0.1606	0.7471
Mode predictor	0.1278	0.1344	0.0651	0.1692	0.0814	0.9006

Remark 10 (Using variable κ): If we optimize the κ -lognormal model allowing κ to vary, global optimization yields essentially a lognormal solution with $\hat{\zeta} = (\hat{\mu}, \hat{\sigma}, \hat{\kappa}, \hat{\tau}_c, \hat{\omega}_d) \approx (0.44, 0.21, 1.65 \cdot 10^{-4}, 169, 339)$. These estimates, however, differ significantly from the true parameter values and lead to higher NLL $\approx -1.82 \times 10^{-3}$ than the fixed- κ solution. Moreover, the lognormal solution yields poor representation of the temporal correlation structure and inferior CV measures. We believe that the failure of the global optimization in this case is due, at least partly, to the non-convexity of the likelihood for Gaussian processes with quasi-periodic kernels [73].

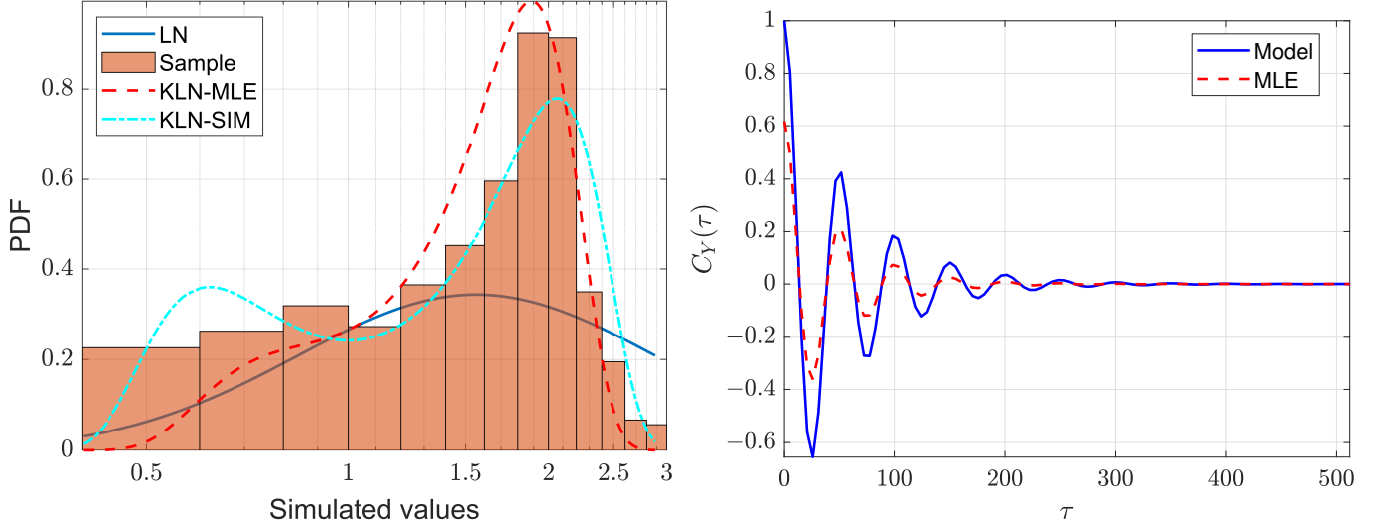


Fig. 18. **Left:** Sample histogram of κ -lognormal process (bars), κ -lognormal PDF corresponding to the parameter set $\zeta = (\mu, \sigma, \kappa, \tau_c, \omega_d) = (1, 1, 3, 30, 0.13)$ (dash-dot line), κ -lognormal PDF obtained for the MLE $\hat{\zeta} = (\hat{\mu}, \hat{\sigma}, \hat{\kappa}, \hat{\tau}_c, \hat{\omega}_d) \approx (0.82, 0.79, 2.82, 23.63, 0.13)$ (broken line), and best-fit lognormal PDF (continuous line). **Right:** Model LDHO kernel $C_Y(\tau)$ (continuous line) based on σ, τ_c , and ω_d with the LDHO kernel based on $\hat{\sigma}, \hat{\tau}_c$, and $\hat{\omega}_d$ (broken line).

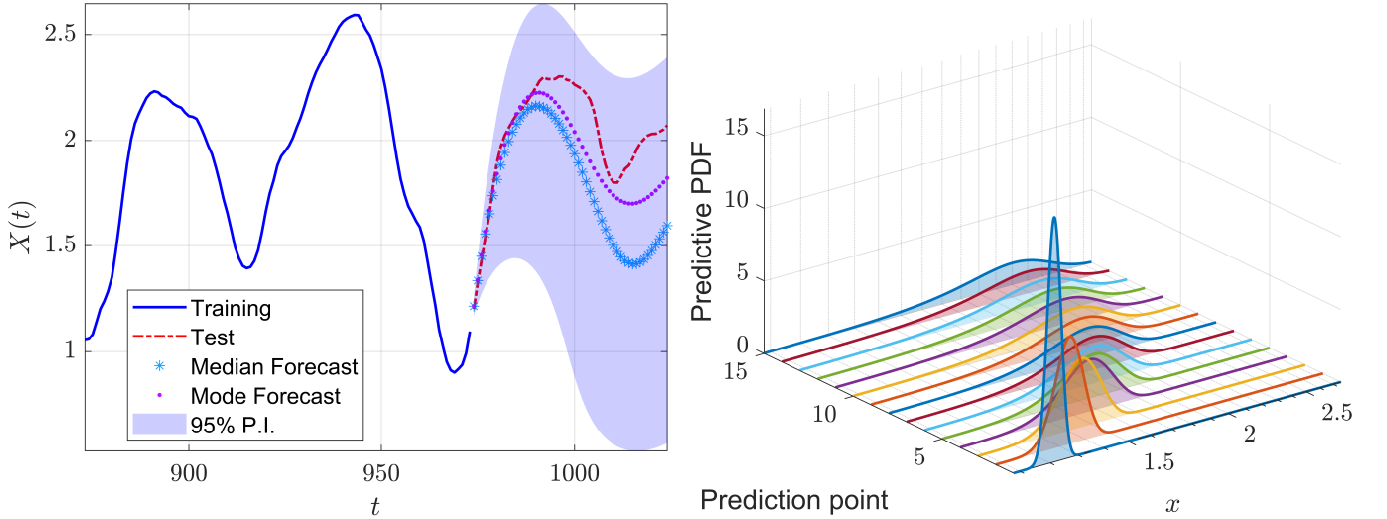


Fig. 19. Multi-step forecast for the time series shown in Fig. 17. **Left:** Diagram showing the last 100 points of the training set (continuous line, blue online), the values of the test set (dash-dot line, red online), the median-based forecasts (stars, cyan online), and the mode-based forecasts (dots, purple online). The shaded area denotes the 95% prediction interval. **Right:** Predictive PDFs for the first 15 points in the test set based on (48).

D. Spatial Regression using κ -lognormal Warping

As an example of spatial regression, we apply κ -lognormal processes to the Berea permeability dataset. We use a randomly selected training set with $N_{tr} = 500, 1100$ points and predict the permeability values over the test set that includes $N_{te} = 1100, 500$ points. The permeability field, shown in Fig. 20, is assumed to follow the stochastic process $P(\mathbf{s}) = X(\mathbf{s}) + \epsilon(\mathbf{s})$, where $\epsilon(\mathbf{s})$ is a Gaussian random noise field with variance σ_ϵ^2 . The prevailing spatial patterns indicate roughness and anisotropic dependence. Accordingly, the permeability correlations are modeled in terms of a latent Gaussian process with exponential kernel and elliptical anisotropy [74]. The anisotropy parameters are the ratio of the principal correlation lengths ρ and the rotation angle φ of the principal anisotropy axes with respect to the coordinate system. The anisotropic exponential correlation kernel is given by

$$\rho_Y(\mathbf{r}) = \exp\left(-\sqrt{\mathbf{r}^\top \mathbf{M}^{-1} \mathbf{r}}/\xi\right), \quad (58a)$$

where $\mathbf{r} = \mathbf{s} - \mathbf{s}'$ is the spatial lag, \mathbf{M}^{-1} is the combined rotation and length rescaling matrix from the grid axes to the principal anisotropy system given by [74]

$$\mathbf{M}^{-1} = \begin{bmatrix} \cos^2 \varphi + \frac{1}{\rho^2} \sin^2 \varphi & \cos \varphi \sin \varphi \left(1 - \frac{1}{\rho^2}\right) \\ \cos \varphi \sin \varphi \left(1 - \frac{1}{\rho^2}\right) & \sin^2 \varphi + \frac{1}{\rho^2} \cos^2 \varphi \end{bmatrix}. \quad (58b)$$

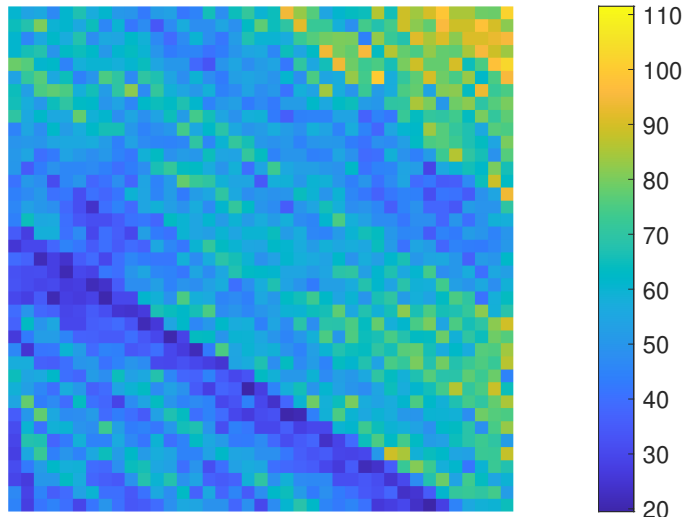


Fig. 20. Spatial configuration of the gridded Berea permeability dataset. The colorbar measures permeability in mD.

The value of κ is set to the estimate $\hat{\kappa} = 0.556$ obtained in Section VI-B. The remaining model parameters, which include $\mu, \sigma, \xi, \rho, \varphi$, are estimated by MLE as described in Section V-B.

TABLE VII

ML PARAMETER ESTIMATES AND CROSS-VALIDATION MEASURES FOR THE BEREA PERMEABILITY DATASET. THE ML ESTIMATES ARE BASED ON TWO RANDOMLY SELECTED TRAINING SETS WITH $N_{\text{tr}} = 500, 1100$. THE CROSS-VALIDATION MEASURES ARE CALCULATED OVER THE RESPECTIVE TEST SETS CONTAINING $N_{\text{tr}} = 1100, 500$ SITES. THE MEDIAN PREDICTOR IS BASED ON $\exp_{\kappa}(\mu_*)$ WHERE μ_* IS GIVEN BY (46), WHILE THE MODE PREDICTOR IS BASED ON (50). THE EXPONENTIAL SPATIAL COVARIANCE KERNEL (58) IS USED. THE ROTATION ANGLE IS GIVEN IN BOTH RADIAN AND DEGREES.

MLE estimates	κ	μ	σ_{ϵ}^2	σ^2	ξ	ρ, φ
$N_{\text{tr}} = 500$	0.88	20.81	2.60	40.31	5.42	16.53, 0.97 (55.58°)
Prediction Method	ME	MAE	MARE	RMSE	RRMSE	R
Median predictor	0.55	6.65	0.13	8.67	0.16	0.83
Mode predictor	0.62	6.66	0.12	8.68	0.16	0.83
MLE estimates	κ	μ	σ_{ϵ}^2	σ^2	ξ	ρ, φ
$N_{\text{tr}} = 1100$	0.88	21.24	1.84	34.64	3.39	10.3, 0.95 (54.43°)
Prediction Method	ME	MAE	MARE	RMSE	RRMSE	R
Median predictor	0.21	5.59	0.11	7.18	0.14	0.89
Mode predictor	0.28	5.59	0.11	7.18	0.14	0.89

The parameter estimates and the cross-validation measures for the two training data sets ($N_{\text{tr}} = 500, 1100$) are shown in Table VII. For both training sets, significant anisotropy is detected (in agreement with the visual assessment of the permeability plot) indicating a principal axes system oriented at $\approx 55^\circ$ with a correlation length ratio > 10 .

The differences between the median-based and mode-based predictors are minimal in the first case and non-existent in the latter (except for the mean error which is in both cases smaller for the median-based predictor). The relative RMSE is 16% for $N_{\text{tr}} = 500$ and 14% for $N_{\text{te}} = 1100$ which underlines the difficulty in predicting the rough permeability profile shown in Fig. 20. We also conducted the same numerical experiment as above using a Matérn covariance kernel for the latent Gaussian process. The cross-validation results are essentially identical to those obtained with the exponential kernel (see Section 4 in the Supplement). This is not surprising since the Matérn kernel with $\nu = 1/2$ is equivalent to the exponential kernel [6].

VII. CONCLUSION

This paper investigates the statistical properties and the estimation of the κ -lognormal probability distribution, where $\kappa > 0$ is a parameter that controls the shape and the asymptotic behavior of the distribution's right tail. This work also presents a κ -lognormal stochastic process. We show that in the limit $\kappa = 0$ the standard lognormal distribution is recovered. For $\kappa > 0$, we obtain probability distributions with flexible, lighter-than-lognormal right tails. Hence, the κ -lognormal family provides a

unifying model which includes the standard lognormal as well as bimodal distributions, and it also approximates quite closely the normal distribution. Such versatility can be useful in practice. For example, simulation-based gene expression studies find both lognormal and normal protein number distributions, which switch to bimodality by introducing a DNA looping mechanism [75]. The κ -lognormal is a candidate model for such applications. On the other hand, bimodal distributions are characterized by the location, height and width of the two peaks as well as the overall asymmetry of the distribution. It is unlikely that the three-parameter κ -lognormal distribution can adequately adapt to all of these features, but it provides a starting point for further investigation.

We present closed-form expressions for the main statistical functions (PDF, CDF, quantile function, hazard rate) of the κ -lognormal distribution and for the median. The presence of bimodality in regions of the parameter space (μ, σ, κ) is established using theoretical analysis and numerical calculations. We obtain the hazard rate for the κ -lognormal distribution, and we show that for $(\kappa < 1)$ $\kappa > 1$ it is an asymptotically (decreasing) increasing function. This adaptability of the κ -lognormal renders it more suitable than the lognormal for failure-time analysis. We also derive (i) lower and upper bounds for the statistical moments in terms of the error function and hypergeometric functions and (ii) power series expansions for the moments which involve a recursive equation for the coefficients. Finally, we prove the scaling relation (28) which implies that moments of any positive order are obtained from the first-order moment, if the latter is known for all (μ, σ, κ) .

We define κ -lognormal stochastic processes and focus on practical aspects such as model parameter estimation and simulation (generation of states). We also show how to exploit the κ -lognormal distribution in the framework of warped Gaussian process regression. We develop predictors based on both the median and the mode of the conditional κ -lognormal distribution, and we present case studies that involve time series forecasting and interpolation of spatial data.

Even though we addressed the main goal set forth at the beginning of the paper, namely to develop a deformed lognormal probability distribution with flexible upper tail for asymmetric data, the advances presented herein raise additional questions for future exploration. Some of these challenges are briefly described below.

a) Lognormal deformations: Besides the PDF (22), other deformations of the lognormal distribution are in principle possible; the resulting modified distributions do not necessarily exhibit shorter-than-lognormal tails. For example, the exponential term that appears in the standard lognormal PDF (22) could be replaced by $\left[1 - \frac{1}{\kappa'} (\ln(x) - \mu)^2 / 2\sigma^2\right]^{\kappa'}$; this function recovers the natural exponential term in the lognormal PDF at the limit $\kappa' \rightarrow \infty$. Using suitable normalization, the above leads to the so-called log-kappa distribution [76]. The latter tends to the standard lognormal for $\kappa \rightarrow \infty$ but presents heavier-than-lognormal tails for finite κ . The log-kappa model describes the observed distributions of magnetic field and plasma fluctuations in the solar wind more accurately than the lognormal.

A PDF with two deformation parameters can be obtained by applying both the κ -exponential and κ -logarithm deformations leading to

$$f_X(x) = \frac{1}{Z} \exp_{\kappa'} \left[-\frac{1}{2\sigma^2} (\ln_{\kappa}(x) - \mu)^2 \right] \quad (59)$$

where $\kappa, \kappa' > 0$ are two deformation parameters that satisfy $\kappa' < 2\kappa$ and $Z > 0$ is the normalization factor. The right tail of this distribution behaves as a power-law, that is,

$$f_X(x) \sim \frac{(2\sigma^2)^{1/\kappa'}}{Z} \left(\frac{2\kappa}{\kappa'} \right)^{1/\kappa'} x^{-2\kappa/\kappa'}, \text{ for } x \rightarrow \infty. \quad (60)$$

In the special case $\kappa' \rightarrow 0$, the deformed PDF (59) has some interesting properties: (1) For $\kappa = 0$, the PDF (59) becomes the lognormal. (2) For $\kappa > 0$ and $x \sim 0$, the PDF is approximately lognormal, because $\ln_{\kappa}(x) \approx \ln(x)$ for $x \approx 0$. (3) For $\kappa > 0$ and $\ln_{\kappa}(x) - \mu \gg \sigma$, it follows from (11) that $f_X(x) \sim \frac{1}{Z} \exp\left(-\frac{x^{2\kappa}}{8\sigma^2\kappa^2}\right)$ if $\kappa > 0$. (3a) If $0 < 2\kappa < 1$, the PDF exhibits stretched exponential upper tail; (3b) for $\kappa = 1$, the upper tail of the PDF is the same as for the normal PDF with zero mean and variance $4\sigma^2$.

Note, however, that the above deformations are not obtained by means of a closed-form transformation function $g(\cdot)$ such that the transformed variable $Y(\vartheta) = g(X(\vartheta))$ is normally distributed. Hence, in contrast with the κ -lognormal distribution presented herein, PDFs such as (60) and the log-kappa PDF do not allow straightforward extension to respective joint densities by means of Jacobi's multivariate theorem (cf. Theorem 5). Such lognormal deformations are therefore more suitable for single-point characterization of the underlying variables but not easily extended to a stochastic process framework.

b) Joint κ -lognormal densities: In addition to the joint lognormal PDF derived from the respective normal PDF and Jacobi's multivariate theorem, several other multivariate lognormal distributions have been proposed. Such distributions do not possess a lognormal marginal but have applications in the analysis of insurance data [77]. Could the deformed exponential and logarithm functions be used to derive generalizations of such distributions?

c) Relation with Central limit theorem?: It is well known that by virtue of the Central limit theorem (applied in the domain of logarithms), the lognormal model represents the asymptotic distribution for multiplicative averaging, namely for the N -th root of the product of N independent, identically distributed random variables. One can then ask whether the κ -lognormal distribution appears as a pre-asymptotic form of multiplicative averaging for finite N or as a fixed point if the aggregated processes have long-range correlations.

APPENDIX A

DETERMINING THE MODES OF κ -LOGNORMAL PDF

This section presents the proof of Theorem 1.

Proof: If $\kappa = 0$ the corresponding PDF is the lognormal which is known to be unimodal with the mode given by $x_{\text{mode}} = \exp(\mu - \sigma^2)$. Therefore, the rest of the proof focuses on $\kappa > 0$.

The PDF (22) can be expressed as $f_X(x) = c f_1(x) f_2(x)$, where $c = 1/(\sqrt{2\pi}\sigma)$, and

$$f_1(x) = \exp\left[-(\ln_\kappa(x) - \mu)^2/(2\sigma^2)\right], \quad f_2(x) = \frac{1}{2} (x^{\kappa-1} + x^{-\kappa-1}), \quad (61)$$

are continuously differentiable, positive-valued functions for $x > 0$. Let us denote the first derivative by a prime for brevity. Then, the first derivative of the PDF is

$$f'_X(x) = c [f'_1(x) f_2(x) + f_1(x) f'_2(x)]. \quad (62)$$

The function $f_1(x)$ has a maximum at $\ln_\kappa(x) = \mu$ where the exponent becomes zero. Hence, $f'_1(\mu_{0.5}) = 0$. Moreover, it follows from (13) that $f_2(x) = d \ln_\kappa(x) / dx$. The following lemmas will be useful in the proof.

Lemma 1 (Derivative of f_2 for $\kappa \leq 1$): If $\kappa \leq 1$, according to Proposition 3 the κ -logarithm is an increasing concave function. Therefore, $f_2(x)$, the κ -logarithm derivative, is a positive, monotonically decreasing function, and thus $f'_2(x) < 0$ for all $x \in \mathbb{R}_{0,+}$.

Lemma 2 (Derivative of f_2 for $\kappa > 1$): For $\kappa > 1$, according to Proposition 3 the κ -logarithm is a concave function for $0 < x \leq x_+$ and convex for $x > x_+$, where according to the analysis following (14),

$$x_+ \triangleq \left(\frac{\kappa + 1}{\kappa - 1} \right)^{1/2\kappa} \quad (63)$$

is the inflection point. Therefore, $f_2(x)$ is monotonically decreasing for $x < x_+$ and monotonically increasing for $x > x_+$.

Lemma 3: Taking into account (62) the following statements are true: (i) For all $\kappa > 0$, it holds that $f'_X(\mu_{0.5}) = f'_2(\mu_{0.5}) f_1(\mu_{0.5})$ since $f'_1(\mu_{0.5}) = 0$; thus the sign of $f'_X(\mu_{0.5})$ is the same as the sign of $f'_2(\mu_{0.5})$. (ii) For $\kappa > 1$, since $f'_2(x_+) = 0$, it holds that $f'_X(x_+) = f'_2(x_+) f_1(x_+)$; thus the sign of $f'_X(x_+)$ is the same as the sign of $f'_1(x_+)$.

We consider the cases $0 < \kappa \leq 1$ and $\kappa > 1$ separately. Recall that $\mu_{0.5} = \exp_\kappa(\mu)$ is the median of the κ -lognormal distribution.

a) $0 < \kappa \leq 1$: We will establish the existence of at least one mode of $f_X(\cdot)$ in $(0, \mu_{0.5})$ by showing that the continuous function $f'_X(x)$ changes sign at least once in $(0, \mu_{0.5})$. We also show that the PDF has no modes for $x > \mu_{0.5}$.

- 1) Since $f_2(x)$ decreases monotonically (according to Lemma 1) and $f_1(x)$ is positive everywhere, $f_1(x) f'_2(x) < 0$ for all $x > 0$. On the other hand, $f'_1(x) f_2(x) \leq 0$ for $x \geq \mu_{0.5}$. Hence critical points x_* of $f_X(x)$ where $f'_X(x_*) = 0$, if they exist, are found inside the interval $(0, \mu_{0.5})$ where the two summands of $f'_X(x)$ have opposite signs.
- 2) In addition, $f'_2(\mu_{0.5}) < 0$, $f_1(\mu_{0.5}) = 1$ and $f'_1(\mu_{0.5}) = 0$. Hence, it follows from Lemma 3 that $f'_X(\mu_{0.5}) = f'_2(\mu_{0.5}) < 0$.
- 3) Since $f_X(x)$ is a continuous, non-negative function and $f_X(0) = 0$, there exists at least some range of values between zero and $\mu_{0.5}$ where $f'_X(x) > 0$.
- 4) Based on statements (2)-(3) above, f'_X changes sign at least once in $(0, \mu_{0.5})$. Since f'_X is differentiable, by Bolzano's theorem it has at least one root $x_* \in (0, \mu_{0.5})$ corresponding to (at least) one peak of $f_X(x)$. Furthermore, for $x > \mu_{0.5}$ both $f'_1 f_2 < 0$ and $f'_2 f_1 < 0$ (the latter according to Lemma 1) leading to $f'_X < 0$; therefore, the PDF does not have critical points for $x > \mu_{0.5}$.

b) $\kappa > 1$: We establish the existence of at least one mode of $f_X(\cdot)$ by determining intervals where the continuous function $f'_X(x)$ changes sign.

- 1) The function $f'_1(x) f_2(x)$ is negative for $x > \mu_{0.5}$ and positive for $x < \mu_{0.5}$ (due to the maximum of f_1 at $\mu_{0.5}$).
- 2) The function $f_1(x) f'_2(x)$ changes sign around x_+ according to Lemma 2; thus, $f_1(x) f'_2(x) < 0$ for $x < x_+$ while $f_1(x) f'_2(x) > 0$ for $x > x_+$.
- 3) First we consider the case $\mu_{0.5} < x_+$. If $\mu < 0$ the condition is automatically satisfied since $x_+ > 0$. If $\mu > 0$, the condition requires $\mu < (\kappa \sqrt{\kappa^2 - 1})^{-1}$. According to Table VIII (Rows 1-4), the critical points x_* of $f_X(x)$ should be sought within the intervals $(0, \mu_{0.5})$ and (x_+, ∞) where the summands of $f'_X(x)$ have opposite signs.
 - (i) According to Lemma 3, $f'_X(\mu_{0.5}) = f'_2(\mu_{0.5}) < 0$. Since $f_X(x)$ is a continuous nonnegative function and $f_X(0) = 0$, there exists at least some range of values between zero and $\mu_{0.5}$ where $f'_X(x) > 0$. Based on the above, f'_X changes sign at least once in $(0, \mu_{0.5})$. Therefore, by Bolzano's theorem, f'_X has at least one root $x_* \in (0, \mu_{0.5})$ corresponding to (at least) one peak of $f_X(x)$.
 - (ii) It also holds that $f'_X < 0$ for $x \in (\mu_{0.5}, x_+)$, since both summands of f'_X are negative (see 1 and 2 above and Table VIII). Furthermore, using Lemma 3 again, $f'_X(x_+) = f'_1(x_+) f_2(x_+) < 0$. If there exist points in (x_+, ∞) where f'_X changes sign (since in this interval the two summands have opposite signs according to 1 and 2), one (or more) peak(s) are possible for $x > x_+$.

- 4) Next, we consider the case $\mu_{0.5} > x_+$. The critical points x_* are now found inside the intervals $(0, x_+)$ and $(\mu_{0.5}, \infty)$. In this case, $f'_1(x_+) > 0$ because f_1 has not reached its maximum at $x_+ < \mu_{0.5}$. Therefore, from Lemma 3 it follows that $f'_X(x_+) > 0$. In addition, $f'_X(\mu_{0.5}) > 0$ as well because $f'_2(\mu_{0.5}) > 0$ (cf. Lemma 2). According to Table VIII (Rows 5-8), f'_X is positive inside $(x_+, \mu_{0.5})$, and it may change sign within the intervals $(0, x_+)$ and $(\mu_{0.5}, \infty)$ where the summands have opposite signs. Thus, possible critical points of $f_X(x)$ lie inside these intervals.
- 5) Finally, for the degenerate case $\mu_{0.5} = x_+$ there is a critical point inside $(0, \mu_{0.5})$ (based on the arguments used for $\mu_{0.5} < x_+$), and possibly more for higher values.

TABLE VIII

SIGNS OF THE PDF-DERIVATIVE SUMMANDS (61) AS WELL AS OF THE κ -LOGNORMAL PDF DERIVATIVE (62) PER INTERVAL FOR $\kappa > 1$. THE CASE $x_+ > \mu_{0.5}$ CORRESPONDS TO ROWS 1-4, WHILE THE CASE $x_+ < \mu_{0.5}$ TO ROWS 5-8. $\mu_{0.5}$ IS THE κ -LOGNORMAL MEDIAN DEFINED IN (23) AND x_+ IS THE κ -LOGNORMAL PDF INFLECTION POINT (63). THE SYMBOL $+\rightarrow-$ DENOTES A TRANSITION FROM POSITIVE TO NEGATIVE SIGN, WHILE THE SYMBOL $+/-$ IMPLIES THAT THE SIGN IS UNDETERMINED ($f' = 0$ IS ALSO POSSIBLE). FOR $x_+ > \mu_{0.5}$ THE FOLLOWING BOUNDARY INEQUALITIES HOLD: $f'_X(\mu_{0.5}) < 0$ AND $f'_X(x_+) < 0$. FOR $x_+ < \mu_{0.5}$ THE FOLLOWING BOUNDARY INEQUALITIES HOLD: $f'_X(\mu_{0.5}) > 0$ AND $f'_X(x_+) > 0$.

Intervals	$(0, \mu_{0.5})$	$(\mu_{0.5}, x_+)$	(x_+, ∞)
$f'_1 f_2$	+	-	-
$f_1 f'_2$	-	-	+
f'_X	$+\rightarrow-$	-	$-/+$
Intervals	$(0, x_+)$	$(x_+, \mu_{0.5})$	$(\mu_{0.5}, \infty)$
$f'_1 f_2$	+	+	-
$f_1 f'_2$	-	+	+
f'_X	$+/-$	+	$+/-$

To determine the number of critical points of the κ -lognormal PDF (22), we investigate the behavior of $f'_X(x)$ with respect to x . For $\kappa > 0$ it holds that

$$f'_X(x) = \frac{-1}{8\sqrt{2\pi}\sigma^3\kappa x^2} e^{-(\ln_\kappa(x)-\mu)^2/2\sigma^2} g_0(x),$$

$$g_0(x) = x^{3\kappa} - x^{-3\kappa} + x^\kappa - x^{-\kappa} - 2\mu\kappa x^{2\kappa} - 4\mu\kappa - 2\mu\kappa x^{-2\kappa} - 4x^\kappa \kappa^2 \sigma^2 + 4x^\kappa \sigma^2 \kappa + 4x^{-\kappa} \kappa^2 \sigma^2 + 4x^{-\kappa} \sigma^2 \kappa. \quad (64)$$

At $x = 0$ both the PDF and its first derivative vanish due to the exponential term. Hence, we will seek extrema of the PDF by searching for the roots of $g_0(x)$ in $(0, \infty)$. Since $x > 0$ the roots of $g_0(x)$ coincide with those of $g_1(x) = x^{3\kappa} g_0(x)$. Furthermore, we define $p_1(z) \triangleq g_1(x = z^{1/\kappa})$ which leads to the sixth-degree polynomial (26). According to the fundamental theorem of algebra, the polynomial $p_1(z)$ has exactly six, in general complex, roots which correspond to roots of the κ -lognormal PDF. The real roots of $p_1(z)$ determine the behavior (number and location of peaks) of $f_X(x)$.

Note that for all $\kappa > 0$, $p_1(z)$ is a univariate polynomial with real-valued coefficients. Thus, we can use *Descartes' rule of signs*: if the nonzero terms of $p_1(z)$ are ordered by descending value of the exponent, the number of positive roots of $p_1(z)$ is equal to the number N_\pm of sign changes between consecutive (nonzero) coefficients or is less than N_\pm by an even number. Roots of multiplicity n are counted as n distinct roots.

The coefficients a, b, c in $p_1(z)$ can each be positive, negative, or zero depending on κ, μ, σ —recall that $a = 2\mu\kappa$, $b = 1 - 4\kappa\sigma^2(\kappa - 1)$ and $c = 4\kappa\sigma^2(\kappa + 1) - 1$. Hence, there are $3^3 = 27$ combinations of a, b, c that lead to different sign sequences. We exclude from consideration the case $\kappa = 0$ which leads to the unimodal lognormal distribution. The “critical” values of κ, μ, σ where the coefficients a, b, c change sign are given respectively by $\mu_{\text{crit}} = 0$, $\sigma_{\text{crit};1}^2 = \frac{1}{4\kappa(\kappa-1)}$ (if $\kappa > 1$), and $\sigma_{\text{crit};2}^2 = \frac{1}{4\kappa(\kappa+1)}$.

Table IX lists the possible combinations, sign changes of the $p_1(z)$ polynomial coefficients, and number of positive roots according to Descartes' rule. For $\kappa \leq 1$ it holds that $b > 0$; thus, b can become negative only if $\kappa > 1$. In addition, since $c + b = 8\kappa\sigma^2$, combinations $b \leq 0 \wedge c \leq 0$ are not allowed (even for $\kappa > 1$). This means that 12 out of the 27 combinations are not feasible (as shown in Table IX). For the remaining sign combinations, there are at most n_r roots of $p_1(z)$ where $n_r \in \{1, 3, 5\}$. If z_r corresponds to a root of $p_1(z)$, the respective peak of the κ -lognormal PDF is given by $x_{\text{mode}} = z_r^{1/\kappa}$. ■

APPENDIX B

PROOF OF THE MOMENT SCALING RELATION

This section presents the proof of Theorem 2.

TABLE IX

NUMBER OF POSITIVE ROOTS OF THE POLYNOMIAL $p_1(z)$ GIVEN BY (26) FOR ALL POSSIBLE SIGN COMBINATIONS OF THE COEFFICIENTS $a = 2\mu\kappa$, $b = 1 - 4\kappa^2\sigma^2 + 4\sigma^2\kappa$ AND $c = 4\kappa\sigma^2(\kappa + 1) - 1$. THE SECOND COLUMN LISTS THE SIGN COMBINATIONS FOR a, b, c . THE THIRD COLUMN SHOWS THE NUMBER OF SIGN CHANGES FOR THE COEFFICIENTS OF $p_1(z)$ ARRANGED IN DESCENDING ORDER OF THE EXPONENT. THE FOURTH COLUMN REPRESENTS THE POSSIBLE NUMBER OF POSITIVE ROOTS ACCORDING TO DESCARTES' RULE. ONE ROOT CORRESPONDS TO A UNIMODAL κ -LOGNORMAL PDF, THREE ROOTS TO A BIMODAL κ -LOGNORMAL PDF. ROWS IN GREY CORRESPOND TO NON-PERMISSIBLE COMBINATIONS OF b AND c THAT FAIL TO SATISFY THE CONSTRAINT $b + c > 0$.

Number	Signs of a, b, c	Sign changes of $p_1(z)$ coefficients	Number of positive roots
1	0, 0, 0	+ -	1
2	0, 0, -	+ - -	1
3	0, 0, +	+ + -	1
4	0, -, 0	+ - -	1
5	0, +, 0	+ + -	1
6	-, 0, 0	+ + + + -	1
7	+, 0, 0	+ - - - -	1
8	0, -, -	+ - - -	1
9	-, 0, -	+ + + - + -	1, 3
10	-, -, 0	+ + - + + -	1, 3
11	0, +, +	+ + + -	1
12	+, 0, +	+ + + - + -	1, 3
13	+, +, 0	+ - + - - -	1, 3
14	0, +, -	+ + - -	1
15	0, -, +	+ - + -	1, 3
16	+, 0, -	+ - - - -	1
17	-, 0, +	+ + + + + -	1
18	+, -, 0	+ - - - -	1
19	-, +, 0	+ + + + + -	1
20	-, -, +	+ + - + + + -	1, 3
21	-, +, -	+ + + + - + -	1, 3
22	+, -, -	+ - - - - -	1
23	+, +, -	+ - + - - - -	1, 3
24	+, -, +	+ - - - + - -	1, 3
25	-, +, +	+ + + + + + -	1
26	-, -, -	+ + - + - + -	1, 3, 5
27	+, +, +	+ - + - + - -	1, 3, 5

Proof: The ℓ -th order non-centered moment of a κ -logarithmic distribution is defined by means of (65)

$$m_{X;\ell}(\kappa; \mu, \sigma) = \int_0^\infty dx x^\ell f_X(x), \quad (65)$$

with $f_X(x)$ the PDF of the κ -lognormal distribution given in (22). Using the fact that $Y = \ln_\kappa X \stackrel{d}{=} \mathcal{N}(\mu, \sigma^2)$ and the conservation of probability under the nonlinear, monotone κ -exponential transform $X = \exp_\kappa(Y)$, the integral (65) becomes

$$m_{X;\ell}(\kappa; \mu, \sigma) = \int_{-\infty}^\infty dy g^\ell(y) f_Y(y; \mu, \sigma^2) = \mathbb{E}_Y \left[(\exp_\kappa Y)^\ell \right], \quad (66)$$

where $f_Y(y; \mu, \sigma^2) = \frac{1}{\sigma} \phi(\frac{y-\mu}{\sigma})$ is the PDF of the normally distributed Y . Hence, the moment of order $\ell \in \mathbb{N}$ is given by

$$m_{X;\ell}(\kappa; \mu, \sigma) \triangleq \mathbb{E}_Y \left[(\exp_\kappa Y)^\ell \right] = \mathbb{E}_Y [\exp_{\kappa'}(\ell Y)] . \quad (67)$$

The second equation is a result of the fact that $g^\ell(y) = [\exp_\kappa(y)]^\ell$ and

$$[\exp_\kappa(y)]^\ell = \exp_{\kappa'}(\ell y), \quad \kappa' = \kappa/\ell. \quad (68)$$

Based on (67), the κ -lognormal moments are obtained from the expectation integral (27) which can be easily evaluated by means of numerical integration.

To prove the scaling relation (28), we use (68) and the variable transformation $\ell y \rightarrow \tilde{y}$ in order to transform the moment integral (27) as follows

$$m_{X;\ell}(\kappa; \mu, \sigma) = \int_{-\infty}^\infty dy \exp_{\kappa/\ell}(\ell y) f_Y(y; \mu, \sigma^2) = \int_{-\infty}^\infty d\tilde{y} \exp_{\kappa/\ell}(\tilde{y}) f_Y(\tilde{y}; \ell\mu, \ell^2\sigma^2) = m_{X;1}(\kappa/\ell; \ell\mu, \ell\sigma),$$

where in the above $\tilde{Y} \stackrel{d}{=} \mathcal{N}(\ell\mu, \ell^2\sigma^2)$. This concludes the proof. ■

APPENDIX C
PROOF OF THE MOMENT BOUNDS RELATIONS

This section presents the proof of Theorem 3, that is, the derivation of the κ -lognormal moment bounds.

Proof: We use the integral (27) for the moments and decompose it into two branches over $R_{0,-}$ and $\mathbb{R}_{0,+}$ respectively

$$m_{X;\ell}(\kappa; \mu, \sigma) = \frac{1}{\sqrt{2\pi}\sigma} \int_0^\infty dy e^{-\frac{1}{2\sigma^2}(y-\mu)^2} \exp_{\kappa/\ell}(\ell y) + \frac{1}{\sqrt{2\pi}\sigma} \int_{-\infty}^0 dy e^{-\frac{1}{2\sigma^2}(y-\mu)^2} \exp_{\kappa/\ell}(\ell y). \quad (69)$$

The bounds will be derived by considering each branch separately. The κ -exponential function satisfies the following bounds for any $\kappa' > 0$ (we will replace κ' with κ/ℓ below)

$$2^{1/\kappa'} (1 + \kappa^2 y^2)^{1/2\kappa'} \geq \exp_{\kappa'}(\ell y) \geq (2\kappa y)^{1/\kappa'}, \text{ for } y \geq 0. \quad (70a)$$

$$1 \geq \exp_{\kappa'}(\ell y) \geq \exp(\ell y), \text{ for } y < 0. \quad (70b)$$

Both the upper and lower bounds of inequality (70a) are derived by using $\sqrt{1 + \kappa^2 y^2} > \kappa y$ (the inequality is valid for $y \geq 0$): for the lower bound, $\sqrt{1 + \kappa^2 y^2}$ in $\exp_{\kappa'}(\ell y)$ is bounded from below by κy , while for the upper bound, κy in $\exp_{\kappa'}(\ell y)$ is bounded from above by $\sqrt{1 + \kappa^2 y^2}$. The upper bound in (70b) is due to the monotonic increase of $\exp_{\kappa'}(\ell y)$ with respect to y which ensures that it is bounded from above by $\exp_{\kappa'}(0) = 1$. On the other hand, the lower bound is due to the fact that $\exp_{\kappa'}(\ell y)$ is a decreasing function of κ' bounded from below by $\exp(\ell y)$ for $y < 0$ according to Proposition 1.

a) *Lower moment bound:* Based on (69) and (70), the lower bound $LB_{X;\ell}(\kappa; \mu, \sigma)$ for $m_{X;\ell}(\kappa; \mu, \sigma)$ is given by

$$LB_{X;\ell}(\kappa; \mu, \sigma) = \frac{1}{\sqrt{2\pi}\sigma} \left(\frac{2\kappa}{\ell} \right)^{\ell/\kappa} \int_0^\infty dy e^{-\frac{1}{2\sigma^2}(y-\mu)^2} (\ell y)^{\ell/\kappa} + \frac{1}{\sqrt{2\pi}\sigma} \int_{-\infty}^0 dy e^{-\frac{1}{2\sigma^2}(y-\mu)^2 + \ell y}. \quad (71)$$

The integral over $\mathbb{R}_{0,-}$ (second term in the right-hand side) in the above is given by

$$\frac{1}{\sqrt{2\pi}\sigma} \int_{-\infty}^0 dy e^{-\frac{1}{2\sigma^2}(y-\mu)^2 + \ell y} = e^{\ell\mu + \ell^2\sigma^2/2} \left(\frac{1 - \operatorname{erf}\left(\frac{\mu + \ell\sigma^2}{\sqrt{2}\sigma}\right)}{2} \right).$$

The integral over the positive real line is defined by

$$I_+ \triangleq \left(\frac{2\kappa}{\ell} \right)^{\ell/\kappa} \int_0^\infty \frac{dy}{\sqrt{2\pi}\sigma} e^{-\frac{1}{2\sigma^2}(y-\mu)^2} (\ell y)^{\ell/\kappa}.$$

Evaluating the integral leads to

$$I_+ = \frac{(2\kappa)^{\ell/\kappa} 2^{\frac{\ell-\kappa}{2\kappa}} \sigma^{\ell/\kappa}}{\sqrt{2\pi}} e^{-\frac{\mu^2}{2\sigma^2}} \left[\Gamma\left(\frac{\ell + \kappa}{2\kappa}\right) {}_1F_1\left(\frac{\ell + \kappa}{2\kappa}, \frac{1}{2}; \frac{\mu^2}{2\sigma^2}\right) + \Gamma\left(\frac{\ell + 2\kappa}{2\kappa}\right) \frac{\mu\sqrt{2}}{\sigma} {}_1F_1\left(\frac{\ell + 2\kappa}{2\kappa}, \frac{3}{2}; \frac{\mu^2}{2\sigma^2}\right) \right], \quad (72)$$

where ${}_1F_1(\alpha, \gamma; z)$ is the *confluent hypergeometric function* [62, 9.210].

To prove (72), we express the integral I_+ as follows

$$I_+ = c_+ e^{-\mu^2/(2\sigma^2)} \int_0^\infty dy e^{-\beta y^2 - \gamma y} y^{\ell/\kappa} \triangleq c_+ e^{-\mu^2/(2\sigma^2)} \tilde{I}_+, \quad (73a)$$

$$\tilde{I}_+ = \int_0^\infty dy e^{-\beta y^2 - \gamma y} y^{\ell/\kappa}, \quad (73b)$$

$$c_+ = \frac{(2\kappa)^{\ell/\kappa}}{\sqrt{2\pi}\sigma}, \quad \beta = \frac{1}{2\sigma^2}, \quad \gamma = -\frac{\mu}{\sigma^2}. \quad (73c)$$

Based on [62, Eq. (3.462.1)] the integral \tilde{I}_+ becomes

$$\begin{aligned} \tilde{I}_+ &= (2\beta)^{-\nu/2} \Gamma(\nu) e^{\gamma^2/8\beta} D_{-\nu} \left(\frac{\gamma}{\sqrt{2\beta}} \right), \\ &= \sigma^\nu \Gamma(\nu) e^{\mu^2/(4\sigma^2)} D_{-\nu}(z) \end{aligned} \quad (74)$$

where $D_{-\nu}(z)$ is the *parabolic cylinder function*, $z \triangleq \gamma/\sqrt{2\beta} = -\mu/\sigma$, and $\nu \triangleq \ell/\kappa + 1 = (\ell + \kappa)/\kappa$. $D_{-\nu}(z)$ can be expressed in terms of the confluent hypergeometric function as follows [62, 9.240]

$$D_{-\nu}(z) = 2^{-\nu/2} e^{-z^2/4} \left\{ \frac{\sqrt{\pi}}{\Gamma(\frac{\nu+1}{2})} {}_1F_1\left(\frac{\nu}{2}, \frac{1}{2}; \frac{z^2}{2}\right) - \frac{\sqrt{2\pi}z}{\Gamma(\frac{\nu}{2})} {}_1F_1\left(\frac{\nu+1}{2}, \frac{3}{2}; \frac{z^2}{2}\right) \right\}. \quad (75)$$

Taking into account that $z = -\mu/\sigma$, and plugging (75) in (74), after cancelation of the exponential terms, \tilde{I}_+ becomes

$$\tilde{I}_+ = \left(\frac{\sigma^2}{2}\right)^{\nu/2} \left\{ \frac{\sqrt{\pi}\Gamma(\nu)}{\Gamma(\frac{\nu+1}{2})} {}_1F_1\left(\frac{\nu}{2}, \frac{1}{2}; \frac{\mu^2}{2\sigma^2}\right) + \frac{\mu}{\sigma} \frac{\sqrt{2\pi}\Gamma(\nu)}{\Gamma(\frac{\nu}{2})} {}_1F_1\left(\frac{\nu+1}{2}, \frac{3}{2}; \frac{\mu^2}{2\sigma^2}\right) \right\}. \quad (76)$$

Next, we use Legendre's duplication formula for the Gamma function [78, 6.1.17]

$$\frac{\Gamma(\nu)\sqrt{\pi}}{\Gamma(\frac{\nu+1}{2})} = 2^{\nu-1} \Gamma(\nu/2),$$

based on which \tilde{I}_+ becomes

$$\tilde{I}_+ = \sigma^\nu 2^{\nu/2-1} \left\{ \Gamma\left(\frac{\nu}{2}\right) {}_1F_1\left(\frac{\nu}{2}, \frac{1}{2}; \frac{\mu^2}{2\sigma^2}\right) + \frac{\mu}{\sigma} \sqrt{2} \Gamma\left(\frac{\nu+1}{2}\right) {}_1F_1\left(\frac{\nu+1}{2}, \frac{3}{2}; \frac{\mu^2}{2\sigma^2}\right) \right\}. \quad (77)$$

Finally, recalling c_+ from (73) and replacing ν with $(\ell + \kappa)/\kappa$ in (77), we obtain (72). This concludes the proof for the lower bound.

b) Upper moment bound: The upper bound for the moments is based on the respective bound of the κ -exponential in (70); the latter imply that $m_{X;\ell}(\kappa; \mu, \sigma)$ is bound from above by the expression

$$\widetilde{UB}_{X;\ell}(\kappa; \mu, \sigma) = \tilde{I}_b + \frac{1}{2} \left[1 - \operatorname{erf}\left(\frac{\mu}{\sqrt{2}\sigma}\right) \right], \quad (78)$$

where the term containing $\operatorname{erf}(\cdot)$ is obtained by integrating the normal density over $\mathbb{R}_{0,-}$ and \tilde{I}_b is the integral

$$\tilde{I}_b = \frac{1}{\sqrt{2\pi}\sigma} 2^{\ell/\kappa} \int_0^\infty dy e^{-\frac{1}{2\sigma^2}(y-\mu)^2} (1 + \kappa^2 y^2)^{\ell/2\kappa}.$$

Taking into account that $(1 + y^2)^{\ell/2\kappa} \leq (1 + y^2)^{n_*}$, where $n_* = \lceil \ell/2\kappa \rceil$, and the fact that the integrand in \tilde{I}_b is non-negative for all $y \in \mathbb{R}$, it holds that

$$I_b \triangleq \frac{2^{\ell/\kappa}}{\sqrt{2\pi}\sigma} \int_0^\infty dy e^{-\frac{1}{2\sigma^2}(y-\mu)^2} (1 + \kappa^2 y^2)^{n_*} \geq \tilde{I}_b, \quad (79)$$

Therefore, we obtain the upper bound $UB_{X;\ell}(\kappa; \mu, \sigma)$ such that

$$UB_{X;\ell}(\kappa; \mu, \sigma) \triangleq I_b + \frac{1}{2} \left[1 - \operatorname{erf}\left(\frac{\mu}{\sqrt{2}\sigma}\right) \right] \geq \widetilde{UB}_{X;\ell}(\kappa; \mu, \sigma). \quad (80)$$

To evaluate I_b we use the binomial expansion, and we calculate the exponential integral in terms of the confluent hypergeometric function (as is done above for the lower limit) leading to

$$\begin{aligned} I_b &= 2^{\ell/\kappa} \sum_{m=0}^{n_*} \frac{n_*!}{m!(n_*-m)!} \kappa^{2m} \int_0^\infty \frac{dy}{\sqrt{2\pi}\sigma} e^{-\frac{1}{2\sigma^2}(y-\mu)^2} y^{2m} \\ &= \frac{2^{\ell/\kappa} e^{-\mu^2/2\sigma^2}}{\sqrt{\pi}} \sum_{m=0}^{n_*} \frac{n_*! 2^{m-1}}{m!(n_*-m)!} \kappa^{2m} \sigma^{2m} \left[\Gamma\left(m + \frac{1}{2}\right) {}_1F_1\left(m + \frac{1}{2}, \frac{1}{2}; \frac{\mu^2}{2\sigma^2}\right) \right. \\ &\quad \left. + \Gamma(m+1) \frac{\mu\sqrt{2}}{\sigma} {}_1F_1\left(m+1, \frac{3}{2}; \frac{\mu^2}{2\sigma^2}\right) \right]. \end{aligned}$$

■

APPENDIX D

PROOF OF POWER-SERIES MOMENT EXPANSIONS

This section presents the proof of Theorem 4.

Proof: We use the moment integral relation (27) in combination with the Taylor series expansion of the κ -exponential around μ . Let us denote $Q(y; \kappa, \ell) \triangleq \exp_{\kappa/\ell}(\ell y)$, so that $Q(y; \kappa, \ell) = \left(\sqrt{1 + (\kappa y)^2} + \kappa y \right)^{\ell/\kappa}$. Then the moment integral (27) becomes

$$m_{X;\ell}(\kappa; \mu, \sigma) = \int_{-\infty}^{\infty} Q(y; \kappa, \ell) f_Y(y; \mu, \sigma) dy. \quad (81)$$

The Taylor expansion of $Q(y; \kappa, \ell)$ around μ is given by

$$Q(y; \kappa, \ell) = Q(\mu; \kappa, \ell) + \sum_{n=1}^{\infty} Q^{(n)}(\mu; \kappa, \ell) \frac{(y - \mu)^n}{n!}, \quad (82)$$

where $Q^{(n)}(\mu; \kappa, \ell) = d^n Q(\mu; \kappa, \ell) / d y^n|_{y=\mu}$.

Inserting the Taylor expansion in (81) and interchanging the order between the summation and the integral we obtain the following power series

$$m_{X;\ell}(\kappa; \mu, \sigma) = Q(\mu; \kappa, \ell) + \sum_{n=1}^{\infty} \frac{1}{n!} Q^{(n)}(\mu; \kappa, \ell) \mathbb{E}[(Y - \mu)^n]. \quad (83)$$

The centered moments $\mathbb{E}[(Y - \mu)^n]$ are calculated using the Wick-Isserlis theorem which states that while the odd powers of $\mathbb{E}[(Y - \mu)^n]$ are equal to zero, the even powers equal $\delta_{n,2q} \frac{\sigma^{2q} (2q)!}{q! 2^q}$, where $q \in \mathbb{N}$ [6].

Next we turn to the derivatives $Q^{(n)}(\mu; \kappa, \ell)$. For $n \geq 1$, the derivatives can be computed using the expression

$$Q^{(n)}(\mu; \kappa, \ell) = \frac{\ell g_n(\mu; \kappa, \ell)}{(1 + \kappa^2 \mu^2)^{n-1/2}} Q(\mu; \kappa, \ell), \text{ for } n \geq 1, \quad (84)$$

with the $g_n(\mu; \kappa, \ell)$ defined by the recursive formula (31b). It is straightforward to see by direct differentiation of $Q(\mu; \kappa, \ell)$ that $Q^{(1)}(\mu; \kappa, \ell) = \ell Q(\mu; \kappa, \ell) / \sqrt{1 + \kappa^2 \mu^2}$ is given by (84) with $g_1(\mu; \kappa, \ell) = 1$.

The general validity of (84) for $n > 1$ is shown by induction. Assuming that (84) holds for n , using the product (Leibniz) rule for differentiation we obtain

$$Q^{(n+1)}(\mu; \kappa, \ell) = \frac{\ell^2 g_n(\mu; \kappa, \ell)}{(1 + \kappa^2 \mu^2)^n} Q(\mu; \kappa, \ell) - \frac{\ell \kappa^2 \mu (2n - 1) g_n(\mu; \kappa, \ell)}{(1 + \kappa^2 \mu^2)^{n+1/2}} Q(\mu; \kappa, \ell) \quad (85)$$

$$+ \frac{d g_n(\mu; \kappa, \ell)}{d \mu} \frac{\ell Q(\mu; \kappa, \ell)}{(1 + \kappa^2 \mu^2)^{n-1/2}}. \quad (86)$$

Substituting in (85), the expression derived from (31b):

$$\frac{d g_n(\mu; \kappa, \ell)}{d \mu} = \frac{g_{n+1}(\mu; \kappa, \ell) + \left((2n - 1) \kappa^2 \mu - \ell \sqrt{1 + \kappa^2 \mu^2} \right) g_n(\mu; \kappa, \ell)}{1 + \kappa^2 \mu^2},$$

we take

$$Q^{(n+1)}(\mu; \kappa, \ell) = \frac{\ell g_{n+1}(\mu; \kappa, \ell)}{(1 + \kappa^2 \mu^2)^{n+1/2}} Q(\mu; \kappa, \ell).$$

This concludes the proof. ■

APPENDIX E

HESSIAN OF THE NEGATIVE LOG-LIKELIHOOD FOR THE κ -LOGNORMAL DISTRIBUTION

This section presents the Hessian matrix of the negative log-likelihood for the κ -lognormal distribution. The Hessian is defined by means of the following partial derivatives with respect to $\beta = (\mu, \sigma, \kappa)$:

$$\mathbf{H} \triangleq \begin{pmatrix} \frac{\partial^2 \text{NLL}(\beta)}{\partial \mu^2} & \frac{\partial^2 \text{NLL}(\beta)}{\partial \mu \partial \sigma} & \frac{\partial^2 \text{NLL}(\beta)}{\partial \mu \partial \kappa} \\ \frac{\partial^2 \text{NLL}(\beta)}{\partial \sigma \partial \mu} & \frac{\partial^2 \text{NLL}(\beta)}{\partial \sigma^2} & \frac{\partial^2 \text{NLL}(\beta)}{\partial \sigma \partial \kappa} \\ \frac{\partial^2 \text{NLL}(\beta)}{\partial \kappa \partial \mu} & \frac{\partial^2 \text{NLL}(\beta)}{\partial \kappa \partial \sigma} & \frac{\partial^2 \text{NLL}(\beta)}{\partial \kappa^2} \end{pmatrix}. \quad (87)$$

Using (53) for the NLL gradient $\nabla_{\beta}\text{NLL}(\beta)$, we calculate $\mathbf{H} = \nabla_{\beta}\nabla_{\beta}\text{NLL}(\beta)$. After some algebra the Hessian \mathbf{H} is given by the following symmetric matrix

$$\mathbf{H} = \begin{pmatrix} \frac{1}{N\sigma^2} & \frac{2\sum_{i=1}^N(\ln_{\kappa}(x_i)-\mu)}{N\sigma^3} & -\frac{\sum_{i=1}^N\ln(x_i)s_{i,k}+\frac{\ln_{\kappa}(x_i)}{\kappa}}{N\sigma^2} \\ \times & \frac{3\sum_{i=1}^N(\ln_{\kappa}(x_i)-\mu)^2-N\sigma^2}{N\sigma^4} & -\frac{2\sum_{i=1}^N(\ln_{\kappa}(x_i)-\mu)\left(\ln(x_i)s_{i,k}-\frac{\ln_{\kappa}(x_i)}{\kappa}\right)}{N\sigma^3} \\ \times & \times & \frac{\partial^2\text{NLL}(\beta)}{\partial\kappa^2} \end{pmatrix}, \quad (88)$$

where $s_{i,k} \triangleq \frac{(x_i^{\kappa}+x_i^{-\kappa})}{2\kappa}$. The $H_{i,j}$ entries below the diagonal ($i > j$) are marked by \times . Due to the symmetry of the Hessian, it holds that $H_{i,j} = H_{j,i}$. Finally, the third diagonal entry of \mathbf{H} is given by

$$\begin{aligned} \frac{\partial^2\text{NLL}(\beta)}{\partial\kappa^2} &= \frac{1}{N\sigma^2} \sum_{i=1}^N \left(s_{i,k} \ln(x_i) - \frac{\ln_{\kappa}(x_i)}{\kappa} \right)^2 \\ &+ \frac{1}{N\sigma^2} \sum_{i=1}^N (\ln_{\kappa}(x_i) - \mu) \left(\ln^2(x_i) \ln_{\kappa}(x_i) - \frac{2\ln(x_i)}{\kappa} s_{i,k} + \frac{2\ln_{\kappa}(x_i)}{\kappa^2} \right) \\ &- \frac{1}{N} \sum_{i=1}^N \left[-\ln^2(x_i) + \ln^2(x_i) \frac{(\ln_{\kappa}(x_i))^2}{s_{i,k}^2} \right]. \end{aligned} \quad (89)$$

ACKNOWLEDGMENT

We would like to thank Prof. Jaime Gómez-Hernández, School of Civil Engineering, Technical University of Valencia (Spain), for providing the Berea permeability data used in this study, and Prof. Athanasios Liavas (School of Electrical and Computer Engineering, Technical University of Crete) for his helpful input.

REFERENCES

- [1] A. Papoulis and S. U. Pillai, *Probability Random Variables and Stochastic Processes*, 4th ed. Boston, USA: McGraw Hill, 2002.
- [2] G. Christakos, *Random Field Models in Earth Sciences*. San Diego: Academic Press, 1992.
- [3] J. P. Chilès and P. Delfiner, *Geostatistics: Modeling Spatial Uncertainty*, 2nd ed. New York, NY, USA: John Wiley & Sons, 2012.
- [4] C. E. Rasmussen and C. K. I. Williams, *Gaussian Processes for Machine Learning*. Cambridge, MA: MIT Press, 2006. [Online]. Available: www.GaussianProcess.org/gpml
- [5] S. De Iaco, D. T. Hristopulos, and G. Lin, “Geostatistics and machine learning,” *Math. Geosci.*, vol. 54, no. 3, pp. 459–465, 2022.
- [6] A. Andersson, “Mechanisms for log normal concentration distributions in the environment,” *Sci. Reports*, vol. 11, no. 1, p. 16418, 2021.
- [7] D. Sornette, *Critical Phenomena in Natural Sciences*. Berlin: Springer, 2004.
- [8] W. D. McComb, *The Physics of Fluid Turbulence*. Oxford, UK: Oxford University Press, 1990.
- [9] P. D. Ditlevsen, *Turbulence and Shell Models*. Cambridge, UK: Cambridge University Press, 2010.
- [10] R. Benzi and F. Toschi, “Lectures on turbulence,” *Phys. Reports*, vol. 1021, pp. 1–106, 2023.
- [11] B. Pearson and B. Fox-Kemper, “Log-normal turbulence dissipation in global ocean models,” *Phys. Rev. Lett.*, vol. 120, p. 094501, Feb 2018.
- [12] L. Meng, S. Mao, and J. Lin, “Heterogeneous elasticity drives ripening and controls bursting kinetics of transcriptional condensates,” *Proc. National Acad. Sci.*, vol. 121, no. 12, p. e2316610121, 2024.
- [13] A. Journel, “The lognormal approach to predicting local distributions of selective mining unit grades,” *J. Int. Assoc. for Math. Geol.*, vol. 12, no. 4, pp. 285–303, 1980.
- [14] D. Krige, *Lognormal-de Wijsian Geostatistics for Ore Evaluation*, 2nd ed. Johannesburg, South Africa: South African Institute of Mining and Metallurgy, 1981.
- [15] J. Rivoirard, C. Demange, X. Freulon, A. Lécureuil, and N. Bellot, “A top-cut model for deposits with heavy-tailed grade distribution,” *Math. Geosci.*, vol. 45, no. 8, pp. 967–982, 2013.
- [16] N. Cressie, “Block kriging for lognormal spatial processes,” *Math. Geol.*, vol. 38, no. 4, pp. 413–443, 2006.
- [17] G. Kondolf and A. Adhikari, “Weibull vs. lognormal distributions for fluvial gravels,” *J. Sediment. Res.*, vol. 70, no. 3, pp. 456–460, 2000.
- [18] S. El Adlouni, B. Bobée, and T. B. Ouarda, “On the tails of extreme event distributions in hydrology,” *J. Hydrol.*, vol. 355, no. 1–4, pp. 16–33, 2008.
- [19] B. Kedem and L. S. Chiu, “On the lognormality of rain rate,” *Proc. National Acad. Sci.*, vol. 84, no. 4, pp. 901–905, 1987.
- [20] C. Zhang, F. T. Manheim, J. Hinde, and J. N. Grossman, “Statistical characterization of a large geochemical database and effect of sample size,” *Appl. Geochem.*, vol. 20, no. 10, pp. 1857–1874, 2005.
- [21] J. Zhang, F. Liu, Y. Liu, H. Wu, W. Wu, and A. Zhou, “A study of accelerated life test of white OLED based on maximum likelihood estimation using lognormal distribution,” *IEEE Trans. on Electron Devices*, vol. 59, no. 12, pp. 3401–3404, 2012.
- [22] N. B. Mehta, J. Wu, A. F. Molisch, and J. Zhang, “Approximating a sum of random variables with a lognormal,” *IEEE Trans. on Wirel. Commun.*, vol. 6, no. 7, pp. 2690–2699, 2007.
- [23] F. Heliot, X. Chu, R. Hoshyar, and R. Tafazolli, “A tight closed-form approximation of the log-normal fading channel capacity,” *IEEE Trans. on Wirel. Commun.*, vol. 8, no. 6, pp. 2842–2847, 2009.
- [24] S. Enserink and M. P. Fitz, “Estimation of constrained capacity and outage probability in lognormal channels,” *IEEE Trans. on Veh. Technol.*, vol. 62, no. 1, pp. 399–404, 2013.
- [25] G. Dagan, “Higher-order correction of effective permeability of heterogeneous isotropic formations of lognormal conductivity distribution,” *Transp. Porous Media*, vol. 12, pp. 279–290, 1993.
- [26] X.-H. Wen and J. Gómez-Hernández, “Upscaling hydraulic conductivities in heterogeneous media: An overview,” *J. Hydrol.*, vol. 183, no. 1, pp. ix–xxxii, 1996.
- [27] D. T. Hristopulos, “Renormalization group methods in subsurface hydrology: overview and applications in hydraulic conductivity upscaling,” *Adv. Water Resour.*, vol. 26, no. 12, pp. 1279–1308, 2003.

- [28] E. Sudicky, W. Illman, I. Goltz, J. Adams, and R. McLaren, "Heterogeneity in hydraulic conductivity and its role on the macroscale transport of a solute plume: From measurements to a practical application of stochastic flow and transport theory," *Water Resour. Res.*, vol. 46, no. 1, p. W01508, 2010.
- [29] H. Zhou, L. Li, and J. Jaime Gómez-Hernández, "Three-dimensional hydraulic conductivity upscaling in groundwater modeling," *Comput. & Geosci.*, vol. 36, no. 10, pp. 1224–1235, 2010.
- [30] M. V. Kohlbecker, S. W. Wheatcraft, and M. M. Meerschaert, "Heavy-tailed log hydraulic conductivity distributions imply heavy-tailed log velocity distributions," *Water Resour. Res.*, vol. 42, no. 4, p. WR003815, 2006.
- [31] J. Söderlund, L. B. Kiss, G. A. Niklasson, and C. G. Granqvist, "Lognormal size distributions in particle growth processes without coagulation," *Phys. Rev. Lett.*, vol. 80, pp. 2386–2388, Mar 1998.
- [32] P. Coles and B. Jones, "A lognormal model for the cosmological mass distribution," *Mon. Notices Royal Astron. Soc.*, vol. 248, no. 1, pp. 1–13, 01 1991.
- [33] H. S. Xavier, F. B. Abdalla, and B. Joachimi, "Improving lognormal models for cosmological fields," *Mon. Notices Royal Astron. Soc.*, vol. 459, no. 4, pp. 3693–3710, 04 2016.
- [34] F. Tosone, M. C. Neyrinck, B. R. Granett, L. Guzzo, and N. Vittorio, "Beyond the lognormal approximation: a general simulation scheme," *Mon. Notices Royal Astron. Soc.*, vol. 498, no. 2, pp. 2663–2675, 09 2020.
- [35] R. M. Nadeau, W. Foxall, and T. V. McEvilly, "Clustering and periodic recurrence of microearthquakes on the San Andreas fault at Parkfield, California," *Science*, vol. 267, no. 6, pp. 503–507, 1995.
- [36] S. G. Abaimov, D. L. Turcotte, and J. B. Rundle, "Recurrence-time and frequency-slip statistics of slip events on the creeping section of the San Andreas fault in central California," *Geophys. J. Int.*, vol. 170, no. 3, pp. 1289–1299, 2007.
- [37] S. G. Abaimov, D. Turcotte, R. Shcherbakov, J. B. Rundle, G. Yakovlev, C. Goltz, and W. I. Newman, "Earthquakes: Recurrence and interoccurrence times," *Pure Appl. Geophys.*, vol. 165, pp. 777–795, 2008.
- [38] D. T. Hristopulos, M. Petrakis, and G. Kaniadakis, "Finite-size effects on return interval distributions for weakest-link-scaling systems," *Phys. Rev. E*, vol. 89, p. 052142, May 2014.
- [39] J. Ellassaiss-Schaap and K. Duisters, "Variability in the log domain and limitations to its approximation by the normal distribution," *CPT: Pharmacometrics & Syst. Pharmacol.*, vol. 9, no. 5, pp. 245–257, 2020.
- [40] G. Buzsáki and K. Mizuseki, "The log-dynamic brain: how skewed distributions affect network operations," *Nat. Rev. Neurosci.*, vol. 15, pp. 264–278, 2014.
- [41] F. Black and M. S. Scholes, "The pricing of options and corporate liabilities," *J. Political Econ.*, vol. 81, pp. 637–654, 1973.
- [42] R. C. Merton, "Theory of rational option pricing," *The Bell J. Econ. Manag. Sci.*, vol. 4, no. 1, pp. 141–183, 1973.
- [43] A. L. Koch, "The logarithm in biology 1. Mechanisms generating the log-normal distribution exactly," *J. Theor. Biol.*, vol. 12, no. 2, pp. 276–290, 1966.
- [44] M. Mitzenmacher, "A brief history of generative models for power law and lognormal distributions," *Internet Math.*, vol. 1, no. 2, pp. 226–251, 2004.
- [45] H. Mouri, "Log-normal distribution from a process that is not multiplicative but is additive," *Phys. Rev. E*, vol. 88, p. 042124, Oct 2013.
- [46] N. N. Taleb, "Statistical consequences of fat tails: Real world preasymptotics, epistemology, and applications," *arXiv preprint arXiv:2001.10488*, 2020.
- [47] N. L. Johnson, S. Kotz, and N. Balakrishnan, *Continuous Univariate Distributions*, 2nd ed. New York, NY: John Wiley & Sons, 1994, vol. 1.
- [48] A. Verster, D. de Waal, R. Schall, and C. Prins, "A truncated Pareto model to estimate the under recovery of large diamonds," *Math. Geosci.*, vol. 44, no. 1, pp. 91–100, 2012.
- [49] A. V. Teran, A. Bill, and R. B. Bergmann, "Time-evolution of grain size distributions in random nucleation and growth crystallization processes," *Phys. Rev. B*, vol. 81, p. 075319, Feb 2010.
- [50] J. Halley and P. Inchausti, "Lognormality in ecological time series," *Oikos*, vol. 99, no. 3, pp. 518–530, 2002.
- [51] A. L. Šizling, D. Storch, E. Šizlingová, J. Reif, and K. J. Gaston, "Species abundance distribution results from a spatial analogy of central limit theorem," *Proc. National Acad. Sci.*, vol. 106, no. 16, pp. 6691–6695, 2009.
- [52] S. Diamond and W. Dolch, "Generalized log-normal distribution of pore sizes in hydrated cement paste," *J. Colloid Interface Sci.*, vol. 38, no. 1, pp. 234–244, 1972.
- [53] A. M. Yaglom, *Correlation Theory of Stationary and Related Random Functions I*. New York: Springer Verlag, 1987.
- [54] D. T. Hristopulos, *Random Fields for Spatial Data Modeling: A Primer for Scientists and Engineers*. Dordrecht, the Netherlands: Springer/Nature, 2020.
- [55] G. Kaniadakis, "Non-linear kinetics underlying generalized statistics," *Phys. A*, vol. 296, pp. 405–425, 2001.
- [56] —, "H-theorem and generalized entropies within the framework of nonlinear kinetics," *Phys. Lett. A*, vol. 288, pp. 283–291, 2001.
- [57] —, "Statistical mechanics in the context of special relativity II," *Phys. Rev. E*, vol. 72, p. 036108, 2005.
- [58] —, "Maximum entropy principle and power-law tailed distributions," *Eur. Phys. J. B*, vol. 70, pp. 3–13, 2009.
- [59] —, "Theoretical foundations and mathematical formalism of the power-law tailed statistical distributions," *Entropy*, vol. 15, pp. 3983–4010, 2013.
- [60] G. E. P. Box and D. R. Cox, "An analysis of transformations," *J. Royal Stat. Soc. Ser. B (Methodological)*, vol. 26, no. 2, pp. 211–243, 1964.
- [61] D. T. Hristopulos and A. Baxevari, "Kaniadakis functions beyond statistical mechanics: weakest-link scaling, power-law tails, and modified lognormal distribution," *Entropy*, vol. 24, no. 10, p. 1362, 2022.
- [62] I. S. Gradshteyn and I. M. Ryzhik, *Table of Integrals, Series, and Products*, 7th ed. Boston: Academic Press, 2007.
- [63] K. S. Trivedi, *Probability and Statistics with Reliability, Queuing and Computer Science Applications*. Englewood Cliffs, NJ: Prentice Hall, 1982.
- [64] P. O'Connor and A. Kleyner, *Practical Reliability Engineering*. Chichester, West Sussex, UK: John Wiley & Sons, 2012.
- [65] D. Sornette and L. Knopoff, "The paradox of the expected time until the next earthquake," *Bull. Seismol. Soc. Am.*, vol. 87, no. 4, pp. 789–798, 1997.
- [66] A. Sweet, "On the hazard rate of the lognormal distribution," *IEEE Trans. on Reliab.*, vol. 39, no. 3, pp. 325–328, 1990.
- [67] E. Snelson, Z. Ghahramani, and C. Rasmussen, "Warped Gaussian processes," in *Advances in Neural Information Processing Systems*, S. Thrun, L. Saul, and B. Schölkopf, Eds., vol. 16. MIT Press, 2004, pp. 337–344.
- [68] V. D. Agou, A. Pavlides, and D. T. Hristopulos, "Spatial modeling of precipitation based on data-driven warping of Gaussian processes," *Entropy*, vol. 24, no. 3, p. 321, 2022.
- [69] Z. Ugray, L. Lasdon, J. Plummer, F. Glover, J. Kelly, and R. Martí, "Scatter search and local NLP solvers: A multistart framework for global optimization," *INFORMS J. on Comput.*, vol. 19, no. 3, pp. 328–340, 2007.
- [70] M. E. Johnson, *Multivariate Statistical Simulation*. New York: John Wiley, 1987.
- [71] N. J. Higham, "Computing real square roots of a real matrix," *Linear Algebr. Appl.*, vol. 88–89, pp. 405–430, 1987.
- [72] D. T. Hristopulos, "Non-separable covariance kernels for spatiotemporal Gaussian processes based on a hybrid spectral method and the harmonic oscillator," *IEEE Trans. on Inf. Theory*, vol. 70, no. 2, pp. 1268–1283, 2024.
- [73] Y. Li, Y. Zhang, Q. Xiao, and J. Wu, "Quasi-periodic Gaussian process modeling of pseudo-periodic signals," *IEEE Trans. on Signal Process.*, vol. 71, pp. 3548–3561, 2023.
- [74] A. Chorti and D. T. Hristopulos, "Nonparametric identification of anisotropic (elliptic) correlations in spatially distributed data sets," *IEEE Trans. on Signal Process.*, vol. 56, no. 10, pp. 4738–4751, 2008.
- [75] S. Krishna, B. Banerjee, T. Ramakrishnan, and G. Shivashankar, "Stochastic simulations of the origins and implications of long-tailed distributions in gene expression," *Proc. National Acad. Sci.*, vol. 102, no. 13, pp. 4771–4776, 2005.

- [76] M. Leitner, Z. Vörös, and M. P. Leubner, “Introducing log-kappa distributions for solar wind analysis,” *J. Geophys. Res. Space Phys.*, vol. 114, no. A12, p. A12104, 2009.
- [77] S. Nadarajah and J. Lyu, “New bivariate and multivariate log-normal distributions as models for insurance data,” *Results Appl. Math.*, vol. 14, p. 100246, 2022.
- [78] M. Abramowitz and I. A. Stegun, *Handbook of Mathematical Functions with Formulas, Graphs, and Mathematical Tables*, 10th ed., ser. National Bureau of Standards, Applied Mathematics. Washington, DC: US Government Printing Office, 1972, vol. 55.

Supplementary Information

S1. PROPERTIES OF κ -DEFORMED EXPONENTIAL AND LOGARITHM

This section focuses on mathematical properties of the κ -exponential and κ -logarithm.

Taylor series expansion of κ -exponential

The power-series expansion of $\exp_\kappa(y)$ around $y = 0$ is given by means of the following expression [1]:

$$\exp_\kappa(y) = \sum_{n=0}^{\infty} \xi_n(\kappa) \frac{y^n}{n!}, \text{ for } (\kappa y)^2 < 1, \quad (90)$$

where the κ -correction functions $\{\xi_n(\kappa)\}_{n=0}^{\infty}$ are polynomials of κ defined by the following recurrence relations

$$\xi_0(\kappa) = \xi_1(\kappa) = 1, \quad (91a)$$

$$\xi_n(\kappa) = \prod_{j=1}^{n-1} [1 - (2j - n)\kappa], \quad n > 1. \quad (91b)$$

The polynomials $\xi_n(\kappa)$ for the first seven orders $n = 0, \dots, 6$ are given by $\xi_0(\kappa) = \xi_1(\kappa) = \xi_2(\kappa) = 1$, $\xi_3(\kappa) = 1 - \kappa^2$, $\xi_4(\kappa) = 1 - 4\kappa^2$, $\xi_5(\kappa) = (1 - \kappa^2)(1 - 9\kappa^2)$, $\xi_6(\kappa) = (1 - 4\kappa^2)(1 - 16\kappa^2)$. The first three terms of the Taylor expansion (90) coincide with those of the ordinary exponential, i.e.,

$$\exp_\kappa(y) = 1 + y + \frac{y^2}{2} + (1 - \kappa^2) \frac{y^3}{3!} + \mathcal{O}(\kappa^2 y^4).$$

The Taylor expansion implies that for $y \rightarrow 0$ and $\kappa \rightarrow 0$ the κ -exponential function $\exp_\kappa(y)$ converges to the ordinary exponential. More precisely,

$$\exp_\kappa(y) = \exp(y) + \sum_{n=3}^{\infty} [\xi_n(\kappa) - 1] \frac{y^n}{n!} = \exp(y) + \mathcal{O}(\kappa^2 y^3). \quad (92)$$

The above is useful in perturbation analysis to express analytically the deviation between the κ -exponential and $\exp(x)$. In addition, based on the Taylor expansion (90), the sign of the leading corrections of $\exp_\kappa(y)$ with respect to $\exp(y)$ is negative.

Proposition 4 (Recurrence relations for κ -exponential corrections): Let $\xi'_n(\kappa) \triangleq 1 - \xi_n(\kappa)$ for $n \in \mathbb{N}$ and $\kappa > 0$ represent the difference between the power-series coefficients of the κ -exponential and those of the natural exponential. These corrections satisfy the recurrence relations

$$\xi'_0(\kappa) = \xi'_1(\kappa) = \xi'_2(\kappa) = 0, \quad (93a)$$

$$\xi'_{n+2}(\kappa) = \xi'_n(\kappa) + n^2 \kappa^2 [1 - \xi'_n(\kappa)], \text{ for } n \geq 0. \quad (93b)$$

Furthermore, the leading-order in κ^2 term of $\xi'_{n+2}(\kappa)$ is given by

$$L(\xi'_{n+2}(\kappa)) = \begin{cases} \kappa^2 [2^2 + 4^2 + \dots (2k)^2], & \text{if } n = 2k, \\ \kappa^2 [1^2 + 3^2 + \dots (2k+1)^2], & \text{if } n = 2k+1. \end{cases} \quad (93c)$$

Proof: Based on (91) it is straightforward to obtain the recursive relation

$$\frac{\xi_{n+2}(\kappa)}{\xi_n(\kappa)} = 1 - n^2 \kappa^2, \text{ for } n \geq 1. \quad (94)$$

The values of $\xi'_n(\kappa)$ for $n = 0, 1, 2$ in (93a) follow from the respective $\xi_n(\kappa)$. The recursive relation (93b) is obtained directly from (94). The above implies that $\xi'_n(\kappa) = c_n \kappa^2 + \mathcal{O}(\kappa^4)$ for all $n \geq 3$. By defining $L(\xi'_{n+2}(\kappa)) \triangleq c_n \kappa^2$, the recursive relation $L(\xi'_{n+2}(\kappa)) = L(\xi'_n(\kappa)) + n^2 \kappa^2$ follows from the above. Expanding the recursive terms, we obtain the series (93c) for the leading-order corrections.

Note: Similarly, second-order terms which contain contributions $\propto \kappa^4$ satisfy the recursive relation

$$L_2(\xi'_{n+2}(\kappa)) = L_2(\xi'_n(\kappa)) (1 + n^2 \kappa^2)$$

with $L_2(\xi'_n(\kappa)) = 0$ for $n = 0, 1, \dots, 4$, $L_2(\xi'_5(\kappa)) = -1^2 \cdot 3^2$, $L_2(\xi'_4(\kappa)) = -2^2 \cdot 4^2$, and so on. ■

Properties of κ -logarithm

a) *Integral relation:* The κ -logarithm satisfies the following equation [1]

$$\ln_{\kappa}(x) = \frac{1}{2} \int_{1/x}^x \frac{dt}{t^{\kappa+1}}, \quad (95)$$

which generalizes the symmetric integral representation of $\ln x$. In the standard integral representation of $\ln x$ the integration limits are 1 and x and the constant coefficient is 1 (instead of $1/2$).

b) *Representation involving logarithm and hyperbolic sine:* The κ -logarithm can be expressed using the natural logarithm and the hyperbolic sine as follows [1]:

$$\ln_{\kappa} x = \frac{1}{\kappa} \sinh(\kappa \ln x). \quad (96)$$

S2. COMPARING THE TAIL OF THE NORMAL AND LOGNORMAL DISTRIBUTIONS

In order to understand the upper tail difference between the lognormal and the normal distributions, we calculate extreme values assuming that both distributions have the same mean, μ_X , and variance, σ_X^2 . Thus, we select $\mu = 0$, $\sigma = 1.5$, we evaluate the lognormal mean, μ_X and variance, σ_X^2 , based on (16) and (17) respectively, and we use them in the normal distribution as well. Next, using the quantile function (19) for the lognormal and $Q_N(p) = \mu_X + \sigma_X \sqrt{2} \operatorname{erf}^{-1}(2p - 1)$ for the normal distributions and the lognormal median $\mu_{0.5} = \exp(\mu)$ based on (16), the ratios $x_{\max}/\mu_{0.5}$ are respectively given by

$$\frac{x_{\max}}{\mu_{0.5}} \triangleq \frac{Q_{\text{LN}}(p^*(N))}{Q_{\text{LN}}(0.5)} = \exp \left[\sqrt{2\sigma^2} \operatorname{erf}^{-1}(1 - 2/N) \right], \text{ lognormal} \quad (97a)$$

$$\frac{x_{\max}}{\mu_{0.5}} \triangleq \frac{Q_N(p^*(N))}{Q_N(0.5)} = \frac{\mu_X + \sigma_X \sqrt{2} \operatorname{erf}^{-1}(1 - 2/N)}{\mu_X}, \text{ normal}, \quad (97b)$$

where Q_{LN} and Q_N are the quantile functions of the lognormal and the normal distributions respectively.

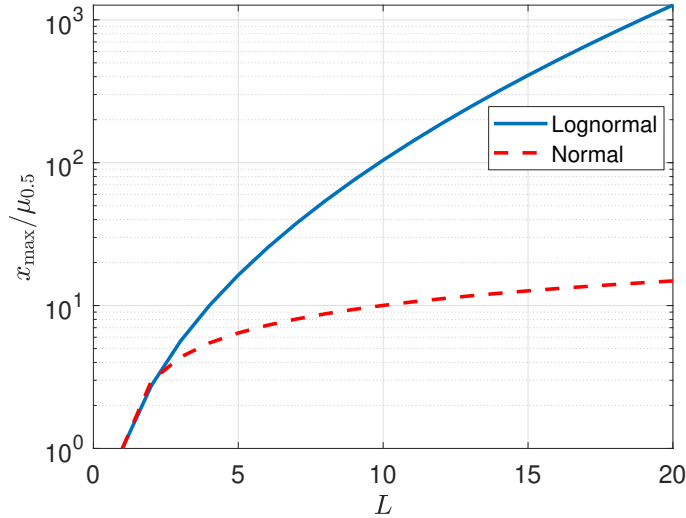


Fig. 21. Ratios $x_{\max}/\mu_{0.5}$ representing normalized typical extreme values for $N = 2^L$ independent random variables versus L for the lognormal (continuous lines) and the normal (broken line) distributions— $x_{\max} = Q(1 - \frac{1}{N})$ where $N = 2^L$ and $\mu_{0.5} = Q(0.5)$. Different L values correspond to probability levels between $p^*(2) = 0.5$ and $p^*(20) \approx 0.999999046$. The lognormal distribution refers to the exponential of a normal variable with $\mu = 0$ and $\sigma = 1.5$ (continuous line); the normal distribution has the same mean and variance as the lognormal, that is, $\mu_X = e^{2.25/2} \approx 3.08$ and $\sigma_X^2 = (e^{2.25} - 1)e^{2.25} \approx 80.53$ (broken line) based on (16) and (17).

We compare the ratios $x_{\max}/\mu_{0.5}$ versus L where $N = 2^L$ is the system size for a random variable X which follows (a) the normal and (b) the lognormal distribution with the same mean and variance. For the lognormal we assume $\mu = 0$ and $\sigma = 1.5$ leading to $\mu_X = \exp(\sigma^2/2) \approx 3.08$ and $\sigma_X^2 = \exp(\sigma^2) [\exp(\sigma^2) - 1] \approx 80.53$. Hence, $\mu_{0.5} = 1$ for the lognormal (due to $\mu = 0$) and $\mu_{0.5} = \exp(\sigma^2/2)$ for the normal. The curves of the normalized extreme values (97) shown in Fig. 21 reveal a steep increase of $x_{\max}/\mu_{0.5}$ with L for the lognormal. For $L = 20$, corresponding to a system size $N \approx 10^6$ (e.g., for a square grid with 10^3 nodes per side), $x_{\max}/\mu_{0.5} \approx 1.27 \times 10^3$, while the respective value for the normal distribution $x_{\max}/\mu_{0.5} \approx 14.88$, is about two orders of magnitude smaller. However, very large values of the ratio $x_{\max}/\mu_{0.5}$ are not suitable for all physical processes with skewed probability distributions.

S3. APPLICATION TO JURA MOUNTAIN HEAVY METAL DATASET

This section investigates the application of the κ -lognormal distribution to the Jura dataset. The latter contains heavy metal concentrations in the topsoil (units are mg/kg) measured at 259 locations in the Swiss Jura mountains [2], [3]. The seven metals include Cadmium (Cd), Copper (Cu), Lead (Pb), Cobalt (Co), Chromium (Cr), Nickel (Ni), and Zinc (Zn). The statistics of the data are shown in Table X.

TABLE X
SUMMARY STATISTICS FOR THE SEVEN METAL CONCENTRATIONS OF THE JURA DATASET.

Element	Mean	Median	Min	Max	Standard deviation	Skewness	Kurtosis
Cd	1.31	1.07	0.14	5.13	0.92	1.51	5.58
Cu	23.73	17.60	3.96	166.40	20.71	2.88	15.12
Pb	53.92	46.40	18.96	229.56	29.79	2.91	14.60
Co	9.30	9.76	1.55	17.72	3.58	-0.18	2.20
Cr	35.07	34.84	8.72	67.60	10.96	0.29	3.02
Ni	19.73	20.56	4.20	53.20	8.23	0.16	3.24
Zn	75.08	73.56	25.20	219.32	29.02	1.03	5.16

Most concentrations exhibit non-zero skewness and non-Gaussian ($\neq 3$) kurtosis coefficients (cf. Columns 7–8 in Table X). The logarithmic transformation is typically used for such data to reduce skewness before applying kriging or Gaussian process regression [3], [4]. This procedure is known as Gaussian anamorphosis in geostatistics [5], [6] and data warping in Gaussian process regression [7], [8].

In Table XI we list the κ -lognormal parameter estimates μ, σ, κ (derived by MLE) for the seven different concentrations. These are complemented by the NLL per site as well as the AIC and BIC values. The table also includes estimates of the lognormal parameters μ_0 and σ_0 as well as the respective NLL, AIC, and BIC values for comparison. Both AIC and BIC favor the κ -lognormal for Co, Cr, and Ni while the lognormal is preferred for Cd, Cu, Pb, Zn. For Cu and Pb the estimated κ is close to zero, indicating the proximity to the lognormal. For Cd the estimated κ is 0.43; nonetheless BIC favors the lognormal distribution, indicating that the deformed logarithm does not impart a strong advantage over the lognormal. For Co the estimated κ is slightly higher than one. The estimated distributions are all unimodal—confirmed by numerical evaluation of the roots of $p_1(z)$. Note that the κ -lognormal BIC values for Co, Cr, and Ni are clearly lower than the respective lognormal values. On the other hand, the difference between the BIC values of lognormal and κ -lognormal is considerably smaller for Cd, Cu, Pb and Zn (cases in which the lognormal is preferred).

TABLE XI
STATISTICS OF THE JURA HEAVY METAL DATASET (259 SAMPLING POINTS). COLUMNS 2-4 CONTAIN THE OPTIMAL κ -LOGNORMAL PARAMETERS. COLUMNS 5-7 DISPLAY RESPECTIVELY THE NEGATIVE LOG-LIKELIHOOD (NLL) PER SAMPLING LOCATION, AS WELL AS THE AIC AND BIC SELECTION CRITERIA. COLUMNS 8-9 CONTAIN THE OPTIMAL LOGNORMAL PARAMETERS, WHILE COLUMNS 10-12 THE NLL PER SITE, THE AIC AND BIC RESPECTIVELY. BOLD FONT INDICATES THE MODEL WITH THE LOWEST BIC (AIC FOLLOWS THE SAME PATTERN).

Element	κ -lognormal						Lognormal				
	μ	σ	κ	NLL	AIC	BIC	μ_0	σ_0	NLL ₀	AIC ₀	BIC ₀
Cd	0.03	0.74	0.43	1.11	579.37	590.04	0.04	2.90	1.11	578.38	585.49
Cu	2.90	0.70	$6.5 \cdot 10^{-4}$	3.97	2061.38	2072.05	3.89	2.14	3.97	2059.38	2066.50
Pb	3.89	0.42	$4.2 \cdot 10^{-4}$	4.44	2308.36	2319.03	3.50	2.87	4.44	2306.37	2313.48
Co	4.85	1.98	1.04	2.69	1397.81	1408.48	4.25	0.71	2.80	1454.77	1461.88
Cr	8.39	1.88	0.70	3.80	1975.91	1986.58	0.70	0.42	3.84	1995.60	2002.72
Ni	6.90	2.48	0.82	3.52	1828.56	1839.23	0.47	0.34	3.62	1877.68	1884.79
Zn	4.97	0.58	0.23	4.71	2445.59	2456.27	0.51	0.39	4.71	2445.25	2452.37

The histograms of the datasets are shown along with the fits to the optimal κ -lognormal and lognormal distributions (continuous lines) in Fig. 22. The tails of the κ -lognormal fit are evidently shorter than those of the lognormal for Co, Cr, and Ni concentrations. At the same time, the overall fit of the κ -lognormal to the histograms is better. On the other hand, for Cd, Cu, Pb and Zn there is no visible difference between the lognormal and κ -lognormal distributions. For Cu and Pb this is expected, since $\hat{\kappa} \approx 0$. For Cr the estimated κ is $\hat{\kappa} \approx 0.43$, but the NLL per site is practically the same for the lognormal and the κ -lognormal, indicating that both distributions provide an equally good fit to the data.

Certain comments are in order at this point: First, the equally good (visually) fit of both distributions to the Jura Cd data does not refute the fact that the κ -lognormal with $\kappa = 0.43$ has a shorter right tail than the lognormal. Thus, the κ -lognormal will assign lower probability to higher Cd concentrations than the lognormal. This pattern is also observed for Co and Ni and to a lesser extent for Zn and Cr as is evident in the respective Q-Q plots of Fig. 23: the horizontal axis, corresponding to the lognormal quantiles, has a considerably larger range than the vertical which corresponds to the κ -lognormal. The Q-Q plots in this case employ $N_Q = 500$ points.

Secondly, while the BIC and AIC selection criteria favor the lognormal if the latter is viewed as a two-parameter distribution, they cannot distinguish between the two distributions if the lognormal is viewed as a special case of the κ -lognormal for $\kappa = 0$.

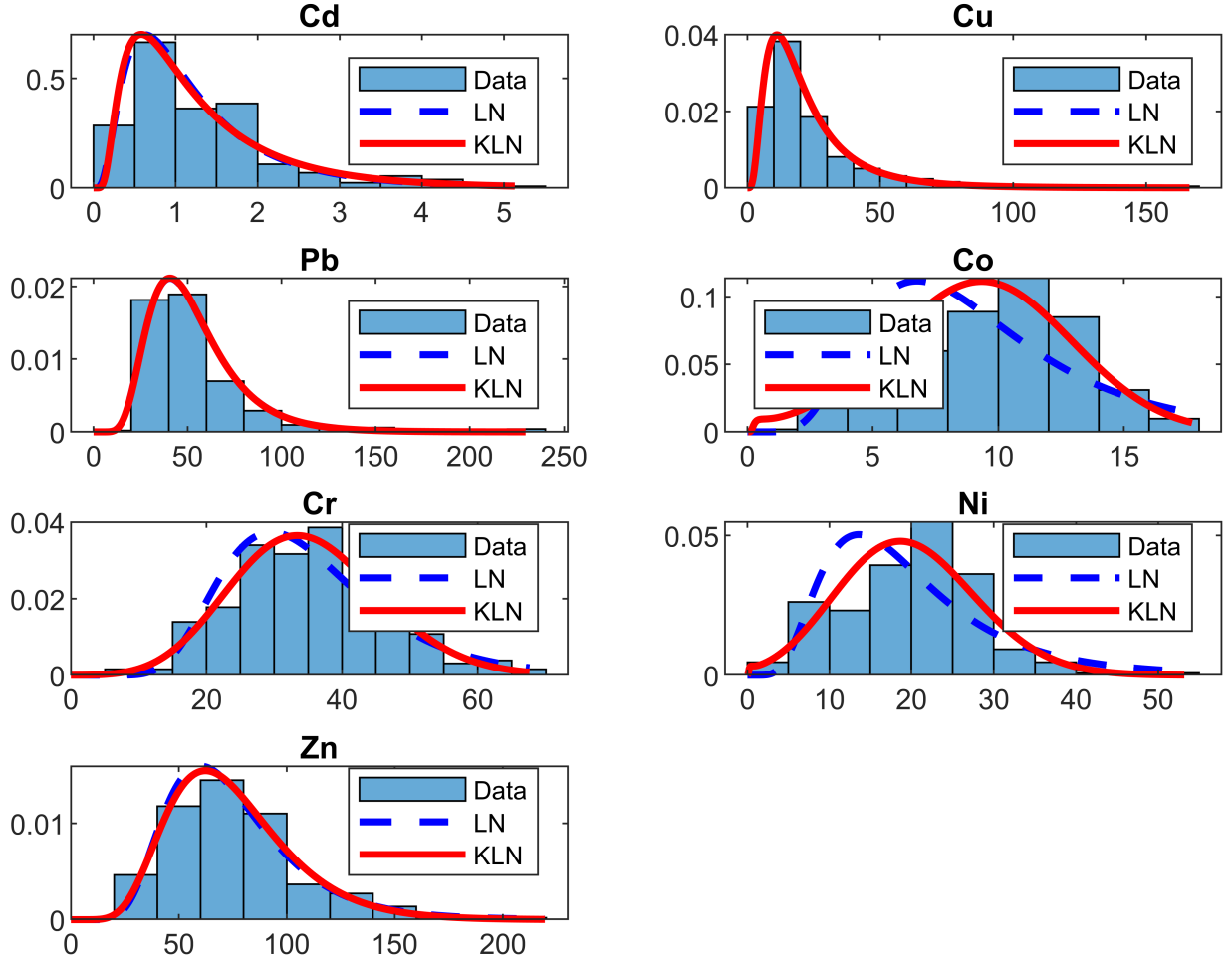


Fig. 22. Histograms of Jura heavy metal datasets (bins) with the optimal κ -lognormal (continuous red line) and lognormal (blue broken line) PDFs. The PDF curves are obtained using the MLE optimal parameters for the two distributions listed in Table XI.

Also note that for Co, Cr and Ni the long tail of the lognormal forces the mode of the PDF to lower values than the κ -lognormal. The latter, however, provides a better fit to the histogram peaks for these data, as evidenced in Fig. 22.

S4. APPLICATION TO BEREJA PERMEABILITY DATASET

This section focuses on the application of warped-GPR to the Bereja permeability dataset using a different covariance kernel for the latent Gaussian process.

We assume the latent Gaussian process has an anisotropic Matérn covariance kernel which is given by

$$C_Y(h) = \frac{\sigma^2 2^{1-\nu}}{\Gamma(\nu)} \left(\frac{\sqrt{2\nu} h}{\xi} \right)^\nu K_\nu \left(\frac{\sqrt{2\nu} h}{\xi} \right), \quad (98)$$

where $h \triangleq \sqrt{\mathbf{r}^\top \mathbf{M}^{-1} \mathbf{r}}$, ν is the smoothness index, $\Gamma(\cdot)$ is the Gamma function, and $K_\nu(\cdot)$ is the modified Bessel function of the second kind of order ν . Two training sets that comprise randomly selected 500 and 1100 points respectively are used. The initial value of the smoothness index is $\nu_0 = 1.5$.

The ML estimated parameters are shown in Table XII. For both training sets the ML estimated smoothness index is $\hat{\nu} = 0.5$, which resonates with the “rough” spatial profile of the permeability. The larger training set leads to smaller nugget variance σ_ϵ^2 , correlation scale ξ and anisotropy ratio ρ .

The cross-validation measures for both training sets are given in Table XIII. Only the statistics for the median-based predictor are listed since the mode-based predictor yields almost identical statistics (except for higher ME).

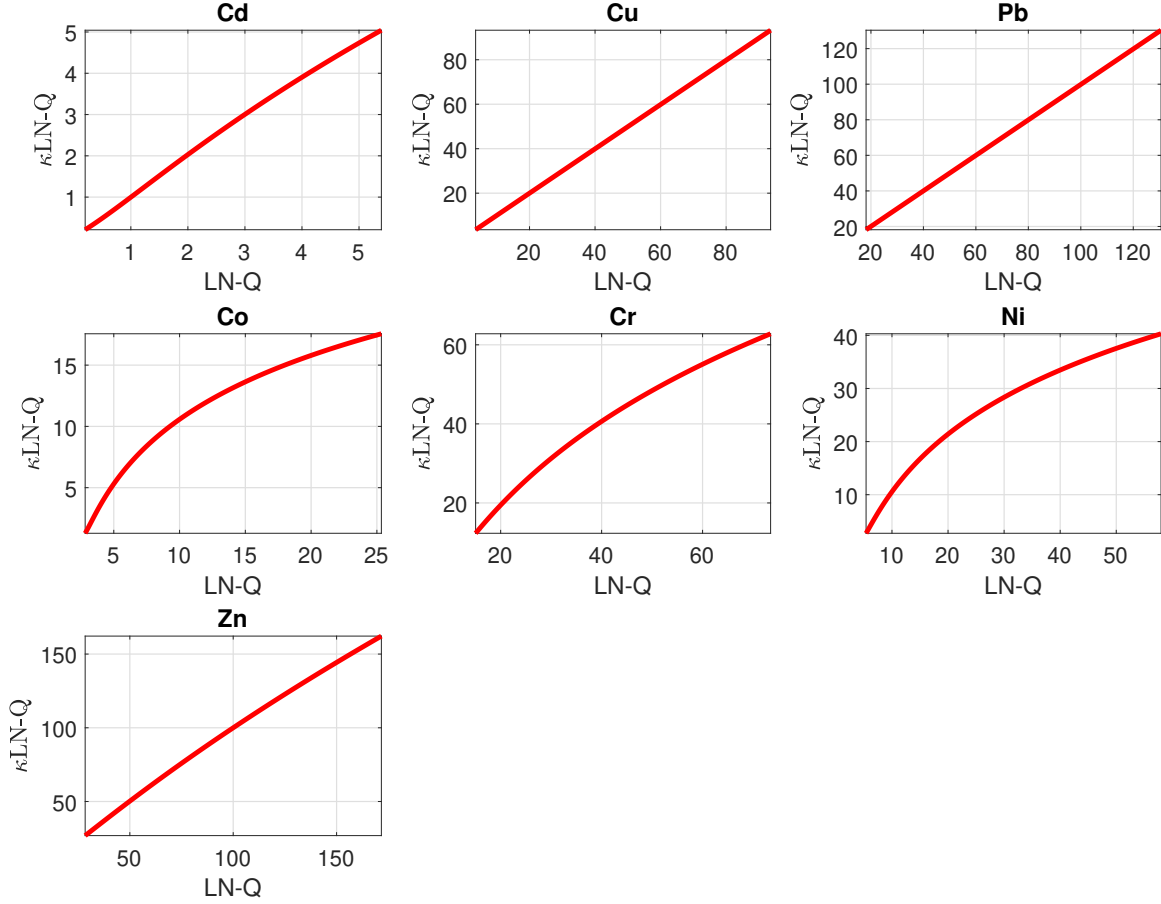


Fig. 23. Quantile-quantile plots of the lognormal distribution (horizontal axis) versus the κ -lognormal (vertical axis) based on the MLE parameters (determined by global optimization) for the seven metal concentrations of the Jura dataset.

TABLE XII

ML PARAMETER ESTIMATES FOR THE BEREJA PERMEABILITY DATASET. THE ML ESTIMATES ARE BASED ON TWO RANDOMLY SELECTED TRAINING SETS WITH $N_{tr} = 500, 1100$. THE MATÉRN SPATIAL COVARIANCE KERNEL (98) IS USED FOR THE LATENT GAUSSIAN PROCESS.

MLE estimates $N_{tr} = 500$	κ	μ	σ_ϵ^2	σ^2	ξ	ν	ρ	φ
	0.88	20.81	2.60	40.31	5.42	0.5	16.53	0.97
MLE estimates $N_{tr} = 1100$	κ	μ	σ_ϵ^2	σ^2	ξ	ν	ρ	φ
	0.88	21.24	1.84	34.64	3.39	0.5	10.32	0.95

TABLE XIII

CROSS-VALIDATION MEASURES FOR THE BEREJA PERMEABILITY DATASET OBTAINED FOR TWO RANDOMLY SELECTED TRAINING SETS WITH $N_{tr} = 500, 1100$. THE MEDIAN PREDICTOR IS BASED ON $\exp_\kappa(\mu_*)$ WHERE μ_* IS GIVEN BY (46), WHILE THE MODE PREDICTOR IS BASED ON (50). THE MATÉRN SPATIAL COVARIANCE KERNEL (98) IS USED FOR THE LATENT GAUSSIAN PROCESS.

$N_{tr} = 500$	ME	MAE	MARE	RMSE	RRMSE	R
Median predictor	0.55	6.65	0.12	8.67	0.16	0.83
$N_{tr} = 1100$	ME	MAE	MARE	RMSE	RRMSE	R
Median predictor	0.21	5.59	0.11	7.18	0.14	0.89

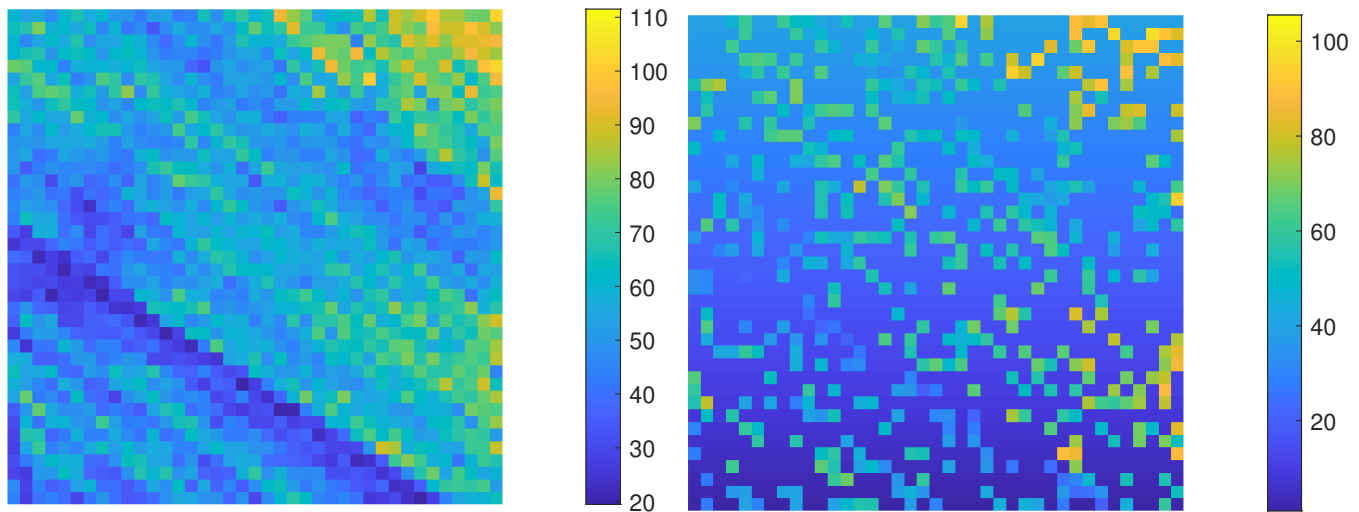


Fig. 24. **Left:** Berea permeability data. **Right:** Reconstructed permeability field using Matérn covariance kernel and a training set comprising 500 randomly selected values.

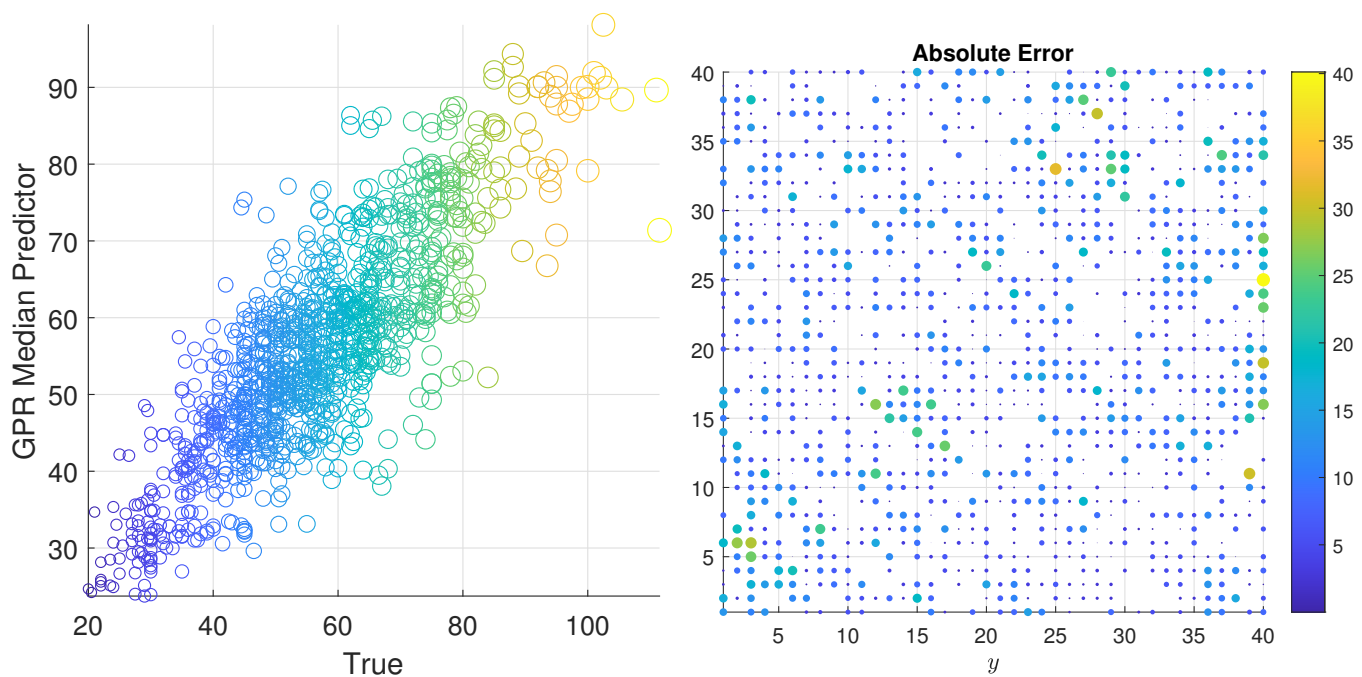


Fig. 25. **Left:** Scatter plot of test set permeability values versus the median-based warped-GPR predictions using the Matérn covariance kernel. **Right:** Spatial distribution of absolute values of prediction errors. Empty sites correspond to training set points. The training set comprises 500 randomly selected values.

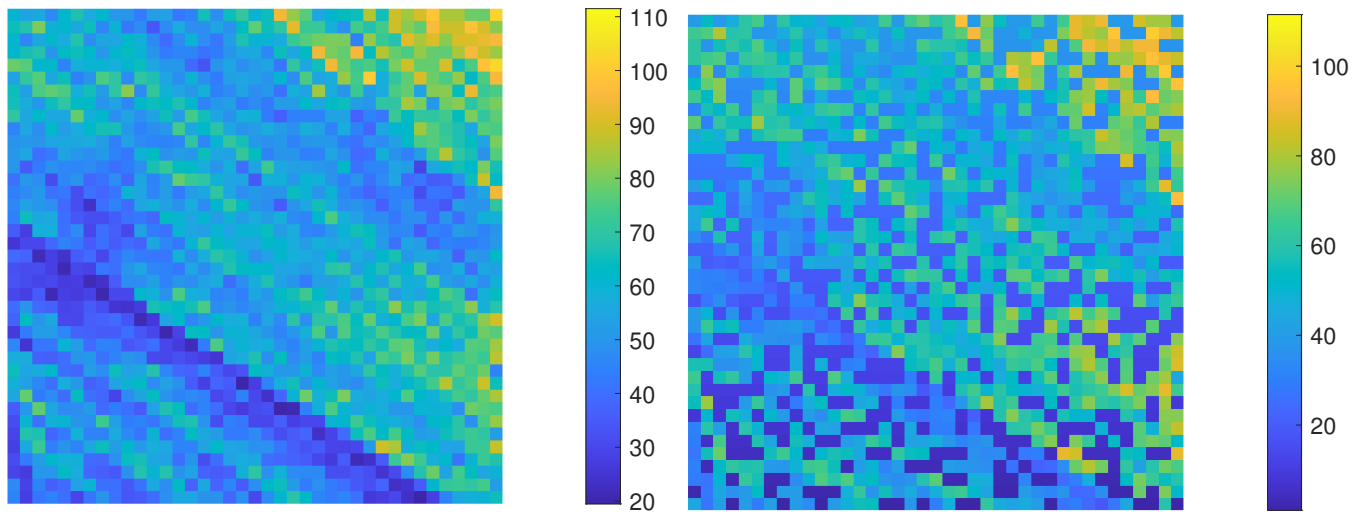


Fig. 26. **Left:** Berea permeability data. **Right:** Reconstructed permeability field using Matérn covariance kernel and a training set comprising 1100 randomly selected values.

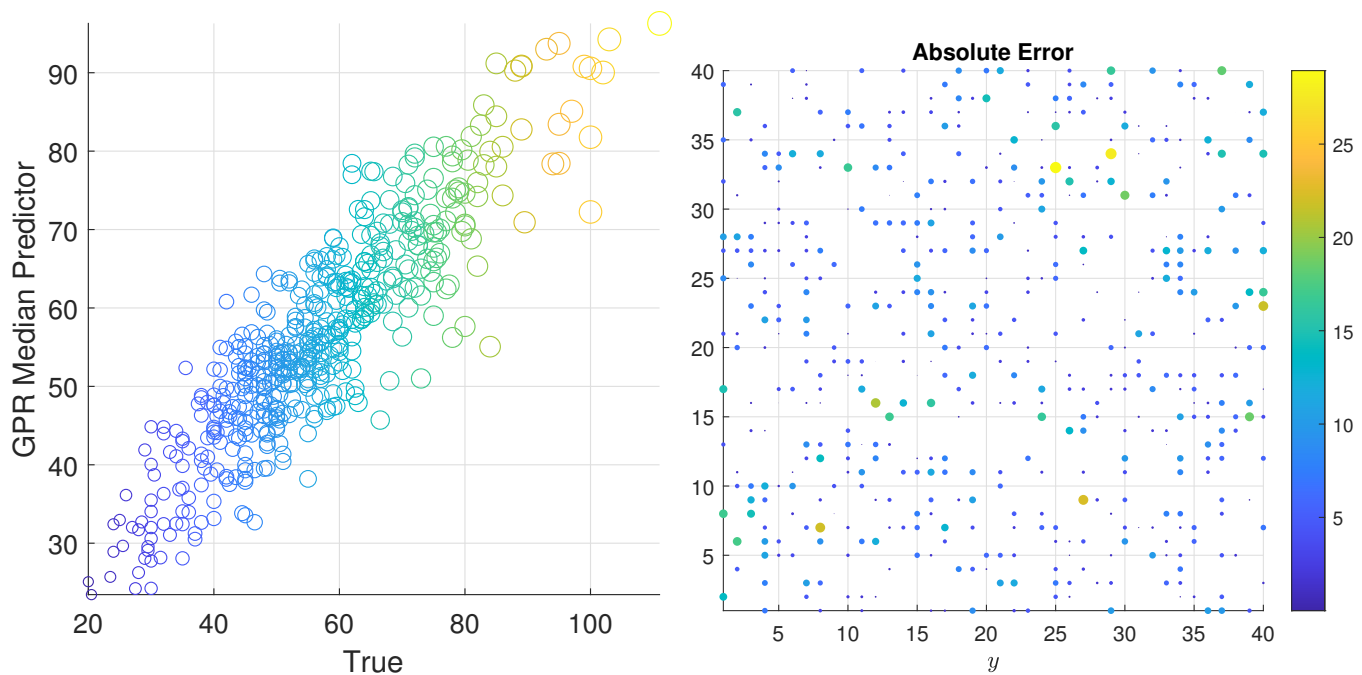


Fig. 27. **Left:** Scatter plot of test set permeability values versus the median-based warped-GPR predictions using the Matérn covariance kernel. **Right:** Spatial distribution of absolute values of prediction errors. Empty sites correspond to training set points. The training set comprises 1100 randomly selected values.

REFERENCES

- [1] G. Kaniadakis, “Theoretical foundations and mathematical formalism of the power-law tailed statistical distributions,” *Entropy*, vol. 15, pp. 3983–4010, 2013.
- [2] O. Atteia, J.-P. Dubois, and R. Webster, “Geostatistical analysis of soil contamination in the Swiss Jura,” *Environ. Pollut.*, vol. 86, no. 3, pp. 315–327, 1994.
- [3] P. Goovaerts, *Geostatistics for Natural Resources Evaluation*. Oxford University Press, 1997.
- [4] A. G. Wilson, D. A. Knowles, and Z. Ghahramani, “Gaussian process regression networks,” in *Proceedings of the 29th International Conference on Machine Learning*, ser. ICML’12, 2012, pp. 1139–1146.
- [5] J. P. Chilès and P. Delfiner, *Geostatistics: Modeling Spatial Uncertainty*, 2nd ed. New York, NY, USA: John Wiley & Sons, 2012.
- [6] D. T. Hristopulos, *Random Fields for Spatial Data Modeling: A Primer for Scientists and Engineers*. Dordrecht, the Netherlands: Springer/Nature, 2020.
- [7] E. Snelson, Z. Ghahramani, and C. Rasmussen, “Warped Gaussian processes,” in *Advances in Neural Information Processing Systems*, S. Thrun, L. Saul, and B. Schölkopf, Eds., vol. 16. MIT Press, 2004, pp. 337–344.
- [8] V. D. Agou, A. Pavlides, and D. T. Hristopulos, “Spatial modeling of precipitation based on data-driven warping of Gaussian processes,” *Entropy*, vol. 24, no. 3, p. 321, 2022.